Marcos Tonelli

Numerical investigation of the Ross Sea water masses using the Regional Ocean Modeling System – ROMS

Thesis submitted to the Oceanographic Institute of the University of São Paulo in partial fulfillment of the requirements for the degree of Doctor of Science in Oceanography. Program area – Physical Oceanography.

Advisor:

Dr. Ilana Wainer

São Paulo

2014

Numerical modeling is much more

than just pushing the button...

and I have barely scratched the surface.

To my beloved (and most patient) wife Denise.

Acknowledgement

To my super advisor Ilana Wainer, whose contagious enthusiasm kept me up and running, even when science didn't look that fun.

To my dear wife Denise, whose love and partnership made this journey much easier.

To my family for supporting me all the time.

To all of the TopBabes for the unconditional friendship. Especially to the wild "riders" who were always around.

To the OC^2 crew for the fun and the very nice programming tips.

To my dear friends Enrique and Virna for the priceless help.

To all the professors and employees of the Institute who helped me along the way.

To every one I missed here... it's 6 am and I have a displaced brain by now. Please forgive me.

Contents

Abstract

Dense water formation around Antarctica is recognized as a significant process that significantly impacts the global climate, since that's where the linkage between the upper and lower limbs of Global Thermohaline Circulation takes place. Assessing whether these processes may be affected by rapid climate changes and all the eventual feedbacks is crucial to fully understand the ocean heat transport and to provide quality future climate projections. Applying the Coordinated Ocean–Ice Reference (CORE) interannual forcing we have run a 60–year simulation (1948–2007) using ROMS with a new sea ice/ice shelf thermodynamics module. Another 100–year simulation forced with CORE normal year was previously run to provide stable starting fields. The normal year consists of single annual cycle of all the data that are representative of climatological conditions over decades and can be applied repeatedly for as many years of model integration as necessary. The 60–year forcing has interannually varying data from 1948 to 2007, which allows validation of model output with ocean observations. Both experiments employed a periodic circumpolar variable resolution grid reaching less than 5 km at the southern border. By applying the OMP water masses separating scheme, we were able to identify the main Ross Sea water masses: Antarctic Surface Water (AASW), Circumpolar Deep Water (CDW), Antarctic Bottom Water (AABW) and Shelf Water (SW), further separated into Ice Shelf Water (ISW) and High Salinity Shelf Water (HSSW). Results are consistent with previous observational studies (Bergamasco et al., 2002b; Orsi and Wiederwohl, 2009; Budillon et al., 2011). The interannual simulation indicates that the Southen Ocean is becoming warmer and less salty. The CDW poleward heat transport increased while shelf waters salinity as well as the AABW salinity

decreased during the simulation period, consistent with Johnson and Doney (2006), who have reported the export of less dense AABW. ROMS capability to represent ISW, HSSW and AABW is an important contribution to climate studies, since IPCC class models seem unable to provide reliable representations of such important processes which may lead to projections of more realistic scenarios. This is significantly improved in this study by including more explicit sea ice/ice shelf parameretization. ROMS is able to reproduce cryosphere–linked mechanisms of dense water formation around Antarctica.

Acronyms List

AABW Antarctic Bottom Water

AASW Antarctic Surface Water

ACC Antarctic Circumpolar Current

CAM3 Community Atmosphere Model 3.0

CCSM3 Community Climate System Model 3.0

CDO Climate Data Operator 1.3.0

CDW Circumpolar Deep Water

CLM3 Community Land Surface Model 3.0

COADS Comprehensive Ocean-Atmosphere Data Set

CSIM5 Community Sea Ice Model 5.0

HadISST Hadley Centre Sea Ice and Sea Surface Temperature

HSSW High Salinity Shelf Water

IPCC Intergovernmental Panel on Climate Change

ISW Ice Shelf Water

LSSW Low Salinity Shelf Water

MCDW Modified Circumpolar Deep Water

MOC Meridional Overturning Circulation

NASA National Aeronautics and Space Administration

NCAR National Center for Atmospheric Research

NCEP/NCAR National Centers for Environmental Prediction

NCL NCAR Command Language 5.1.1

NCVIEW NetCDF Data Viewer 1.93g

NetCDF Network Common Data Form

NOAA National Oceanic and Atmosphere Administration

NODC National Oceanographic Data Center

NWP Numerical Weather Prediction

POP Parallel Ocean Program

OMP Optimum Multiparameter Analysis

RG Ross Gyre

RIS Ross Sea Ice Shelf

RS Ross Sea

SAF Subantarctic Front

SAM Southern Annular Mode

SH Southern Hemisphere

SLP Sea Level Pressure

SODA Simple Ocean Data Assimilation

SO Southern Ocean

STF Subtropical Front

SWT Source Water Type

THC Thermohaline Circulation

UNEP United Nations Environment Program

WMO World Meteorological Organization

WOD2001 World Ocean Database 2001

WS Weddell Sea

List of Figures

1 Introduction

1.1 The role of the Southern Ocean on Climate

Scientific investigation of Climate has increased in numbers and complexity since Wallace Broecker first introduced the highly discussed "Global Warming" terminology. Although the scientific community will not even argue with skeptics who raise the flag for the so called "global warming swindle", the expression term used nowadays is Climate Change. Aiming to draw a comprehensive picture of Earth's climate evolution, science and politics have been working closely to put together intergovernmental efforts such as the Intergovernmental Panel on Climate Change (IPCC). Created in 1989 by World Meteorological Organization (WMO) and United Nations Environment Program (UNEP), the IPCC has as its primary goal to communicate to multi–nation governments a comprehensive scientific perspective of what is going on with the climate. Researchers from many countries work together to assess observed and modeled climatic data in order to understand and to communicate their findings to governments and the general society. The IPCC Assessment Report has just concluded its Fifth Edition and the bottom line is that, although there are several processes acting together to modulate the climate system, and in spite of the human activity impact, the ocean plays the most significant role regulating its oscillations in both short and long terms.

Manabe and Bryan (1969) and Bryan et al. (1975) used a coupled ocean–atmosphere climate model to show that very remote portions of the world ocean were intimately

connected together by a deep thermohaline circulation. Although they have used coarse grid resolution and a very general algorithm, they were able to trace cold, dense waters formed in the Norwegian Sea into the Southern Hemisphere, and trace waters found in the North Pacific and North Atlantic back to the coasts of Antarctica.

Due to much energy and momentum exchange with the lower atmospheric layers (Summerhayes et al., 1996; Wallace and Hobbs, 1977), the ocean redistributes incoming solar radiation from the tropics to the poles through a system defined by Broecker as the Global Conveyor Belt (Broecker, 1987). Broecker suggested that the heat flux around the globe was performed by a large scale oceanic current system with two limbs; an upper limb, that absorbs heat around the tropics and releases it back to the atmosphere at the poles, and a lower limb resulting from the cold water downwelling at the North Atlantic (Figure 1). Due to mass conservation, water from the lower limb flows along the ocean bottom to upwell again at the northern section of the Pacific and Indian oceans. Although this was a first approach to explain the global oceanic heat transport, if one take into account that 50% of the solar radiation at the top of the atmosphere end up stored in the ocean (Sulman, 1982), it gets clear that the ocean is indeed the great climate modulator on Earth.

Schmitz and McCartney (1993) and Colling (2001) discuss that Broecker's Conveyor Belt was actually a representation of the resulting effect from the interaction of many currents with different temperatures, creating a vertical circulation pattern that ventilates the ocean bottom: the Thermohaline Circulation (THC). Schmitz (1996) presented an update for the THC scheme (Figure 2). He highlights not only the water masses interaction to create the heat transport distribution pattern, but

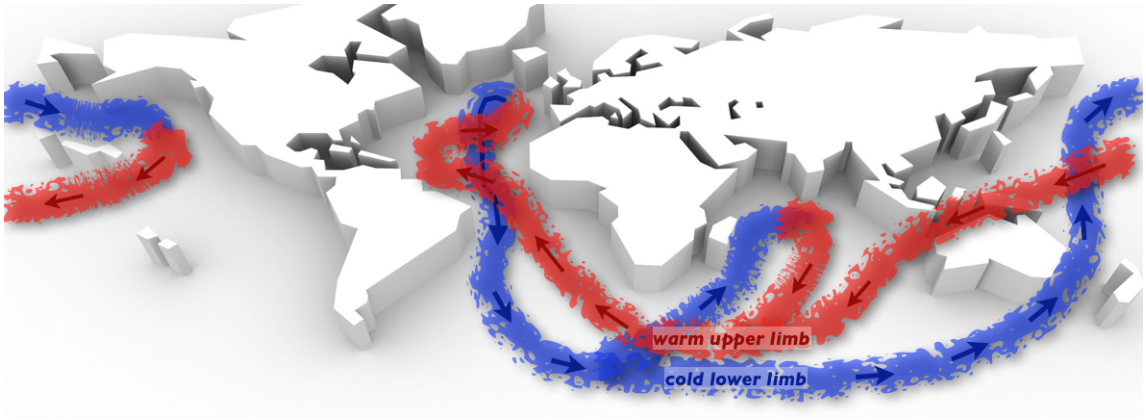

Figure 1: Representation of the Global Conveyor Belt as suggested by Broecker (1987) with a warm surface limb (red) that sinks at the Northern Atlantic Ocean connecting to the deeper cold limb (blue) to ventilate the global ocean bottom to later upwell at the Northern Indian and Pacific Oceans.

also the Antarctic Continent and the Southern Ocean (SO) key roles in the process. The complex picture replaces the Broecker diagram, since unique exchange processes and water transformation over the Antarctic continental shelf are responsible for the formation of the Antarctic Bottom Water (AABW); one of the main components of the THC's lower limb (Orsi et al., 2001, 2002). Finally, since the THC is driven not only by temperature and salinity gradients, but also by ocean-atmosphere momentum exchange, the more comprehensive term Meridional Overturning Circulation (MOC) was adopted by the scientific community and will be used hereafter.

The MOC impacts on the climate system go beyond the Earth's energy budget. It also affects the global cycle of carbon and nutrients. Besides heat, the sinking of SO surface waters carries oxygen and carbon dioxide into the ocean interior to spread throughout the global oceans, renewing oxygen levels in the deep layers and

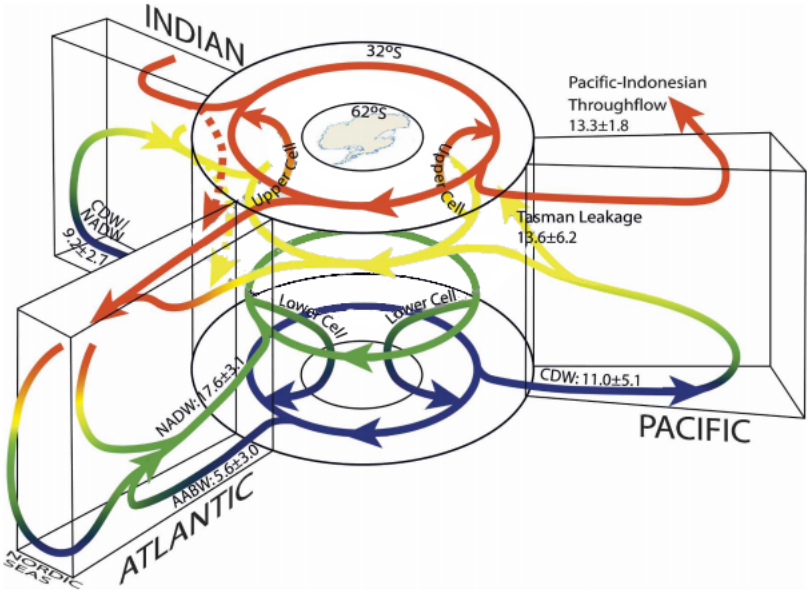

Figure 2: Schmitz (1996) Thermohaline Circulation update to Broecker (1987) scheme. Main water masses with estimated transport (Sv) are shown interacting along the major ocean basins at different levels, connected by the Southern Ocean. Colors indicate relative density range to vertical leveling: red–upper; yellow–intermediate; green–deep; blue–bottom. Dashed arrows indicate Indian–to–Atlantic westward exchange between Africa and the ACC. (Adapted from Lumpkin & Speer, 2006)

boosting the capacity of the Southern Hemisphere oceans to store heat and carbon. Thanks to the MOC's conveyor–like mechanism, the ocean has actually stored more than 85% of the total increase in heat stored by the Earth system over the second half of the 20th Century (most of this heat being trapped at the SO), preventing the energy excess to build up atmosphere warming or intensify melting of ice (Levitus et al., 2005). Rintoul et al. (2012b) discuss that integrated around the globe, the Southern Ocean stores more of the excess heat trapped by the Earth system than any other latitude band.

As for the carbon dioxide, Sabine et al. (2004) suggests that about 40% of the

total ocean inventory of anthropogenic CO_2 is found south of 30°S. This shows the efficiency with which the upper cell of the MOC transfers CO_2 full waters from the surface into the deep ocean. The sinking of intermediate and bottom waters removes anthropogenic carbon dioxide from the atmosphere and trap it in the ocean. Reciprocally, deep carbon–rich waters upwelling at high latitudes tend to release CO_2 back to the atmosphere so that wind-driven fluctuations of the MOC will eventually lead to changes in ocean uptake of CO_2 (Butler et al., 2007; Le Quéré et al., 2007; Verdy et al., 2007). These wind-driven variations of the MOC, in turn, are directly linked to atmospheric modes of oscillation such as Southern Annular Mode (SAM) (Lenton and Matear, 2007; Lovenduski et al., 2007).

Should one look at the biology and chemistry of the global ocean, deep SO overturning influence will be found. The upwelling of deep water returns nutrients to the surface ocean, where, associated with incoming solar radiation, they become available to be used by phytoplankton. But the upwelled nutrients are not fully consumed at the SO and get transported to lower latitudes within the intermediate and mode waters. Sarmiento et al. (2004) numerical investigations showed that setting the MOC's export of nutrients to zero leads to a 75% reduction of the primary production in the rest of the ocean. This primary production also plays an important role on the carbon dioxide sequester as organic material sinks from the surface ocean and decomposes in the deep sea (Tréguer and Jacques, 1993). Thus, by means of either biological or chemical mechanisms, the balance between the upwelling and downwelling limbs of the MOC will ultimately determine how much carbon dioxide is absorbed and stored by the ocean.

There is one component of the Climate System that plays a major part on mod-

ulating the Southern Ocean dynamics and the MOC, who is on the most up to date scientific investigations: the Cryosphere. Although it might seem evident that the cryosphere affects the SO, and therefore, the rest of the world, assessing this climate component within its own variability, its interactions with the Southern Ocean and further impacts, like sea level rise, is not an easy task. During the winter the freezing of the ocean surface forms sea ice covering about 16 million km^2, which is actually larger than the area of the Antarctic continent (Convey et al., 2009). Associated changes in sea ice extent or volume can lead to changes in many aspects: deep water mass formation rates, air-sea exchange of gases such as carbon dioxide, the trophic web from phytoplankton to superior animals and even the Earth' albedo on a planetary scale (Rintoul et al., 2012a). Warm waters advected to the inner continental shelves induce basal melting of ice shelves modifying high-latitude freshwater budget and stratification, finally altering the mass balance of the Antarctic ice sheet and the rate at which the very old glacial ice flows into the sea (Rignot et al., 2004).

Given the unmistakable worldwide influence of the Southern Ocean, changes in this peculiar environmental must be traced, assessed and unearthed. Changes in the ocean–cryosphere–atmosphere coupling mechanisms like MOC's heat transport–sea ice extent–ice shelf melting–freshwater balance will produce positive feedbacks that will enhance the climate changing scenario... and these changes are already underway (Turner, 2010).

citetgille02,gille08 estimated that the Southern Ocean is warming more quickly than the rest of the globe, while Jacobs et al. (2002) reported decreases in shelf water salinity and the surface salinity within the Ross Gyre along with a warming at depths of 300 meters north of the continental shelf. Curry et al. (2003) and Jacobs

et al. (2002) suggest that the freshening of upper layers of the Southern Ocean have resulted from a combination of factors, including sea ice melting and reduced production, basal melting and thinning of southeast Pacific ice shelves due to poleward warmer water advection crosswise the shelf break (Shepherd et al., 2004; Rignot et al., 2008), melting of the West Antarctic Ice Sheet and increased precipitation rates. These changes automatically draw one's attention to the potential impacts on the MOC, as they affect deep water formation around the SO. In fact many authors (e.g. Jacobs (2004, 2006); Aoki et al. (2005); Rintoul (2007)) have already reported the salinity/density decline on sinking waters near Antarctica, waters accountable for the formation of the AABW which is acknowledged to be the main component of MOC's lower limb and to drive the overturning circulation conveyor. Along the same line, the export of warmer AABW has been reported by (Johnson and Doney, 2006).

Sea level has also experienced changes. Sokolov and Rintoul (2009) assessed satellite data to report a widespread sea level rise on the Southern Ocean which is likely to impact the circumpolar circulation frontal system associated with the Antarctic Circumpolar Current (ACC). The ACC (which will be scrutinized later in the text – Figure 3) can be roughly described as a large current flowing around Antarctica who, due to the absence of land masses along the latitude band of the Drake Passage, connects the world ocean major basins. Sea level is usually higher to the northern border of the ACC, but the sea level rise reported by Sokolov and Rintoul (2009) indicates a southward shift of the current. From the biological side, Cubillos et al. (2007) found early indications that species whose distribution hinge on ACC's pathway are also shifting south.

Regarding sea ice, satellite data suggest that, although not statistically significant, the overall extent of Antarctic sea ice has slightly increased in recent decades (Zwally et al., 2002; Parkinson, 2004). This may represent a system adjustment to the fluctuating energy balance in the SO and regional changes must be carefully explored. Stammerjohn et al. (2008) reported changes in sea ice extent and the seasonality of advance/retreat in the Pacific sector of the SO, which according to Wilson and Norris (2001), produce substantial impacts on the marine ecosystem.

Still on the regional approach, the Antarctic Peninsula is subject to more significant impacts, due not only to its northern geographical projection and slender width but also for the western income of warm waters carried by ACC through the Drake Passage. The peninsula has warmed more rapidly than anywhere else in the Southern Hemisphere followed by responses reported in many studies. Meredith and King (2005) and Gille (2002, 2008) observed heightened ocean temperatures around the peninsula and Stammerjohn et al. (2008) reported the decrease in sea ice cover extent and duration during in the northern peninsula. The phytoplankton feedback followed the changes in the sea ice regime as Montes-Hugo et al. (2009) observed the primary production to decline in the northern and increased in the southern part of the waters west of the Antarctic Peninsula. Ducklow et al. (2007) reported shifts in penguin diets accompanied by changes in territorial behavior, as some species are moving further south of their original realms. Despite acknowledging that this intricated life structure is deeply affected by the SO's climate, the impact of changes in CO_2–related ocean chemistry on the Southern Ocean food web is largely unknown.

citetturner10 stand by the idea that changes in the SO's wind regime are likely to drive most of the changes that have been observed in recent decades around the

Antarctica, since ocean circulation, temperature distribution and sea ice dispersion and seasonality are deeply hinged on atmospheric circulation on the surface. These circulations patterns are established by distinct modes of variability. The dominant mode on the SO is the Southern Annular Mode (SAM), which refers winds that circles Antarctica from west to east and reaches from the stratosphere to the sea surface between 30 °S and 60 °S. A detailed definition of SAM is given later in the text. From observed data (Marshall, 2003; Thompson and Solomon, 2002) to climate model numerical investigations (Shindell et al., 1998), authors have reported changes in SAM with subsequent responses in different domains of the Southern Ocean system.

The evidences for the critical role played by the Southern Ocean in global budgets of heat, freshwater, carbon and nutrients cannot be neglected and, insomuch as the indications that the SO is changing seem to pile up, we can only hope that the science–politics understanding will thrive to enhance the quality of Antarctic research. Ocean observations and numerical experiments have been working together to draw a fine picture of the Antarctic Environment (Rintoul and Sokolov, 2001; Böning et al., 2008), but they will not always find a common ground as many uncertainties remain (Hallberg and Gnanadesikan, 2006; Toggweiler and Samuels, 1998).

2 Scientific Hypothesis – Rationale

The Southern Ocean and the Antarctic region as a whole are still rather remote places when it comes to scientific oceanographic sampling, particularly in the winter when it is ship–inaccessible due to great sea ice extent. But even during summertime some places are fairly difficult to sample, like the ice shelf cavities. An alternate way to investigate this environment is to use numerical models. However, Global Climate Models (GMCs) are unable to fully represent specific processes that allow the production and export of dense water from the SO (Kerr et al., 2009). The author suggests that the lack of some of the cryosphere components such as the ice shelves might be accountable for the incomplete representation.

A high–resolution numerical approach comprising the representation of the most important cryosphere components regarding the SO dynamics (sea ice and ice shelves) could lead to a better representation of the dense waters formation and export from Southern Ocean.

Taking that into account, we have employed the Regional Ocean Modeling System – ROMS with a thermodynamically active sea ice/ice shelf on a circumpolar hi–res grid in order: firstly, to assess whether this configuration might actually generate a more trustworthy representation of the SO dynamics; secondly, should we succeed, to estimate the variability of the dense water masses in the SO.

3 Objectives

3.1 Central Objective

To investigate the dense water formation and variability in the Ross Sea and the Weddell Sea from a numerical approach, using the Regional Ocean Modeling System – ROMS with thermodynamically active sea ice/ice shelf parameterization on a variable high resolution circumpolar grid.

3.2 Explicit Objectives

- To validate a Southern Ocean application of ROMS with the sea ice/ice shelf parameterization assessing the model capability to represent the main oceanographic features of the Southern Ocean:
    1. Temperature and salinity distribution patterns;
    2. Major water masses on the Ross Sea and the Weddell Sea;
- To evaluate ROMS capability to represent cryosphere–linked dense water formation processes from an inter-annual simulation (using annual simulation results as stable starting fields);
    1. To investigate inner shelf water formation in the Ross Sea and to estimate the variability of these water masses;
    2. To investigate the production and export of the Antarctic Bottom Water – AABW from the Ross Sea;

4 The Southern Ocean – Physical Background

4.1 The Southern Ocean and the Cryosphere

Presenting a straightforward definition for the Southern Ocean is somewhat difficult, since such definition will be built on processes and mechanisms that vary from each field of research. Although finding a common ground regarding SO's southern limit can be fairly simple (since it is south–limited by the Antarctic Continent), there is no singular definition of a northern boundary. From a broader perspective the SO may be referred as the whole oceanic area surrounding Antarctica (Figure 3), but again this would not be suitable for scientific purposes. The Antarctic Treaty suggested the 60 °S latitude to be this northern limit, but if one consider the oceanographic processes this boundary would easily reach 30 °S as that is the northernmost extent of the Subtropical Front (STF) (Sokolov and Rintoul, 2009).

In agreement with Orsi et al. (1995), the STF generally lies between 35 °S and 45 °S and marks the transition between warm and salty subtropical waters and cooler, fresher waters to the south. In the same fashion, Rintoul et al. (2012b) argues that it makes most sense to consider the Southern Ocean as encompassing those waters that participate in the circumpolar circulation around Antarctica to define the SO to include waters between the Antarctic continent and the STF. Although these waters display very specific physical-chemical features to distinguish them from lower latitudes waters, these attributes vary slowly along the flow path around Antarctica with small meridional gradients. To perform our numerical experiments

we have setup a circumpolar domain comprising the ocean between 30 °S and the Antarctic continent.

All in all, should one bear in mind the circumpolar geometry south of 55 °S, the global influence of the SO may be basically granted to the aspect neatly captured by Schmitz (1996) MOC depiction: the Drake Passage is the only continuous zonal oceanic band where ocean waters circle the Earth connecting the ocean basins and transferring climate anomalies between them (Figure 2; Rintoul et al. (2012b)). The lack of continental boundaries favors the establishment of a dynamical barrier for the north–south exchange of heat above the height of the shallowest bathymetry that supports the present glacial climate of Antarctica: the Antarctic Circumpolar Current (Sokolov and Rintoul, 2009).

The ACC in the most important dynamic feature of the Southern Ocean and consists of a westerly–driven clockwise geostrophic–balanced flux found approximately between 45 °–55 °S around Antarctica (Deacon, 1982; Trenberth et al., 1990). Carrying more water than any other current (147 Sv south of Australia (Rintoul and Sokolov, 2001) and 137 Sv close to South Africa and South America (Cunningham et al., 2003)), the ACC has a complex structure consisting of multiple narrow frontal jets: maximum sea level height and current speed gradients can be found in specific lines, as the jets keep the water masses properties that define the fronts.

Fronts typically represent sharp density or temperature gradients and can mediate air-sea heat exchange, with significant gradients at the fronts (O'Neill et al., 2005). Whitworth III (1980) identified the fronts from north to south as the Subantarctic Front (SAF), the Polar Front (PF), and the Southern ACC Front. But only SAF and the PF are in the foreground as they are continuous features of the

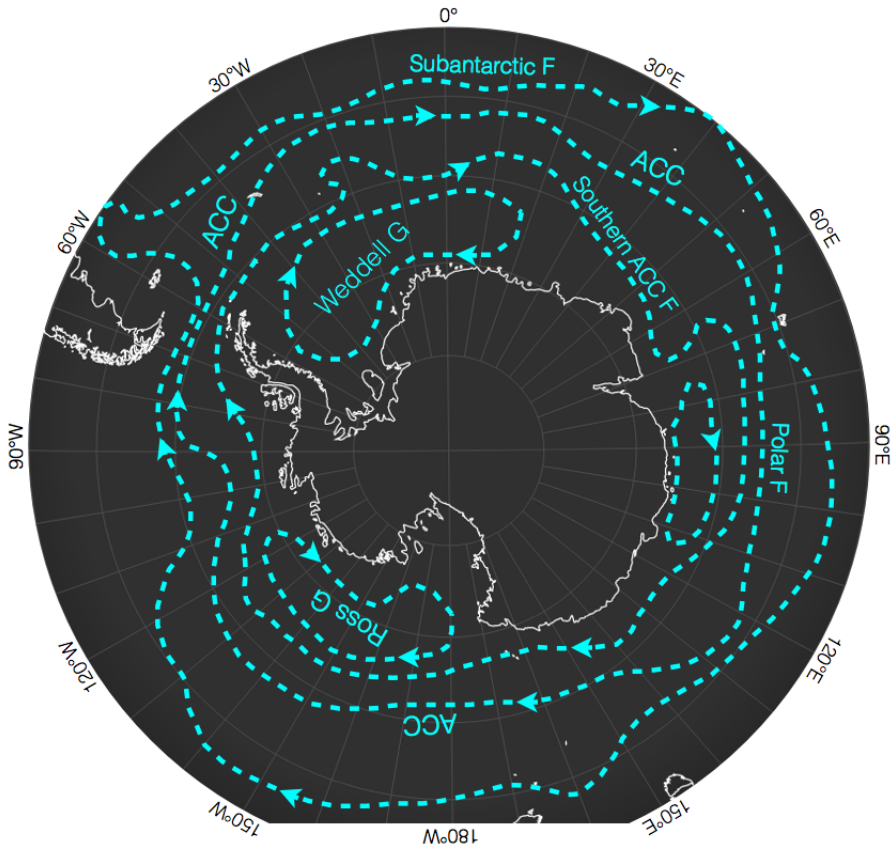

Figure 3: A schematic representation of the current systems in the Southern Ocean. The Antarctic Circumpolar Current (ACC) flows from west to east around Antarctica in two major branches, the Polar Front and Subantarctic Front. The Weddell and Ross gyres fill the deep basins between the Antarctic continent and the ACC. This clockwise gyres act as warm water source for the Weddell and Ross Seas as they branch off waters from ACC and advect them into the continental shelf.

ACC, with limbs that get closer and farther from each other along the whole path of the ACC (Figure 3; Orsi et al. (1995). The bands separating the fronts and the Antarctic continent are know as: Subantarctic Zone (SAZ), Polar Frontal Zone (PFZ), Antarctic Zone (AZ) and Continental Zone (CZ). Whitworth III (1980, 1983) discuss that the northernmost zone SAZ and the southernmost zones AZ and CZ, exhibit few seasonal differences on temperature–salinity relations below de surface

layers. Separating the SAF and the PF, the PFZ is a more variable region of transition between ZAS an AZ waters.

The eastward flow of the ACC is associated with a steep rise of isopycnals toward the south through the entire water column (Orsi et al., 1995) and topography controlled stationary eddies transport heat to the poles and momentum to deeper layers (Rintoul and Sokolov, 2001). Eddies resulting from the interaction between the meridional circulation and the ACC are responsible for the poleward mass transport (Karsten et al., 2002; Olbers et al., 2004). Therefore, the ACC's zonal flow and meridional circulation are strongly related and the SO's dynamic cannot be fully understood if these features are assessed separately (Budillon et al., 2002). In fact, water masses participating in the MOC will shoal dramatically southward as they flow crosswise the ACC, in a way that northern–born deep waters may enter the subpolar regime to mix laterally with Antarctic shelf waters (Figure 4; Orsi et al. (1995); Rintoul and Sokolov (2001). In places where the ACC main flow extends far enough from the Antarctic continent, large subpolar cyclonic cells of recirculating waters are established, where the two most prominent are the Weddell Gyre and the Ross Gyre (Figure 3; Deacon (1979); Rodman and Gordon (1982); Tchernia and Jeannin (1984); Reid (1997)).

Changes within the ACC regime are relevant due to its close association with the SO's dynamic. As reported by Gille (2002, 2008) the Southern Ocean warming is concentrated in the circumpolar band corresponding to the ACC. The author showed that most of the net heat content increase in the top 1000 m of the Southern Hemisphere oceans (south of 30 °S) occurred within the ACC. Sprintall (2003); Gille (2008); Morrow et al. (2008) suggest that the warming trend identified in the ACC

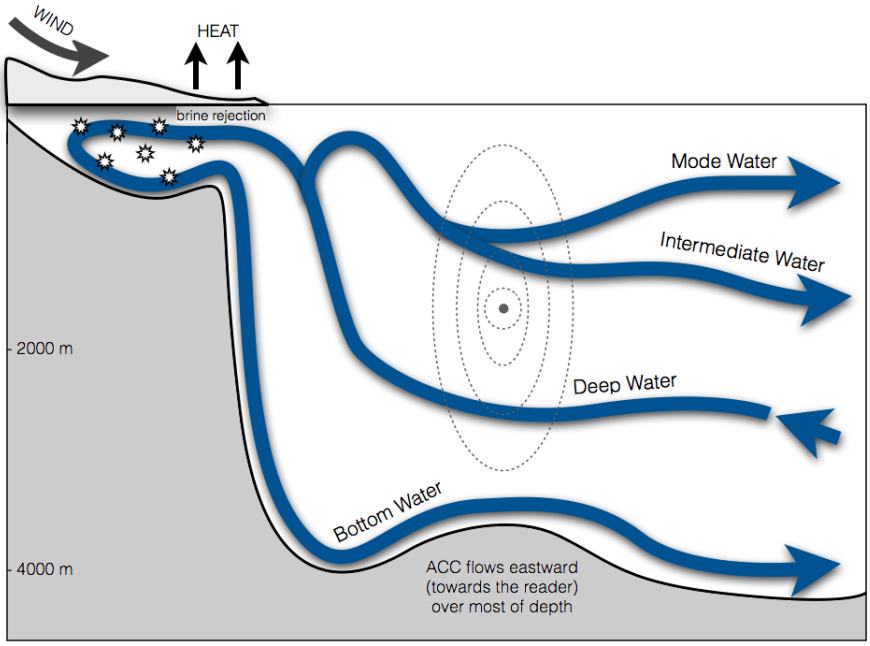

Figure 4: A schematic representation of the interaction between the Antarctic Circumpolar Current and the Southern Ocean overturning circulation. Two cells of the overturning are represented: deep northern–born water crossing the ACC to upwell to the surface of the SO. Part moves toward the Antarctic Continental Shelf to become denser (brine rejection and heat loss) and sink to form dense Antarctic Bottom Water; another portion moves north and sinks to depths of 500-–1,500 m on the northern border of the ACC as intermediate and mode waters.

region has been characterized as being consistent with displacing the ACC poleward by about 1 ° latitude every 35 years. Numerical experiments also indicate a poleward displacement of the ACC due to the contraction of the westerlies closer to the Antarctic continent as an adjustment of the atmospheric modes in response to a warming climate (Oke and England, 2004; Saenko et al., 2005; Yin, 2005; Fyfe and Saenko, 2006; Swart and Fyfe, 2012). However, Gille discusses that most climate models are run at relatively coarse spatial resolution and cannot capture the detailed frontal structure of the ACC or its response to wind, since they cannot represent

mesoscale eddies. The eddy–related problem regards the fact that at high latitudes the Rossby radius is comparatively small (Chelton et al., 1998), which means that the length scale in which oceanic flows are affected by Earth's rotation is rather small. Therefore, energetic eddies, that play an important role in the momentum balance, are of the order of several kilometers and generally smaller than a GCM grid cell.

Microwave SST satellite data provides evidence that changes in the mean latitude of the winds over the Southern Ocean lead changes in the mean latitude of the Polar Front (Dong et al., 2006). However, satellite altimeters, which have provided consistent time series of sea surface height (SSH) since the launches of ERS–1 in 1991 and TOPEX–Poseidon in 1992, are the most extensive modern data set that can be used to assess changes in the position of the ACC. Using the mean dynamic topography (MDT), which represents approximately 1% of the spatial variability in the mean SSH, oceanographic investigations have been able to characterize eddy–meanflow interactions (Hughes et al., 2001) and also the time–varying structure of the ACC fronts (Sallée et al., 2008; Sokolov and Rintoul, 2007, 2009). Branches of the ACC fronts appear to have trended 60 km southward during the first 15 years of the altimeter record, consistent with a long–term southward displacement of the fronts (Sokolov and Rintoul, 2009).

4.2 Aspects of High Latitude Atmosphere

The Southern Annular Mode (SAM) is the major mode of variability in the atmospheric circulation of the high southern latitudes (Gong and Wang, 1999; Thompson and Solomon, 2002; Turner et al., 2005) and refers to a large scale alternation of

atmospheric mass between the mid–latitudes (higher pressure) and high–latitudes (lower pressure) surface pressure. It is a circumpolar pattern of atmospheric mass displacement (Figure 6) in which the intensity and location of the gradient of air pressure between mid–latitudes and the Antarctic coast changes in a non–periodic way over a wide range of time scales from days to years. To assess SAM behavior, Gong and Wang (1999) define an objective index for SAM as the difference of normalized zonally mean sea level pressure between 40 °S and 65 °S. This definition is used in this work to compute SAM index from CORE interannual SLP forcing fields (Figure 5).

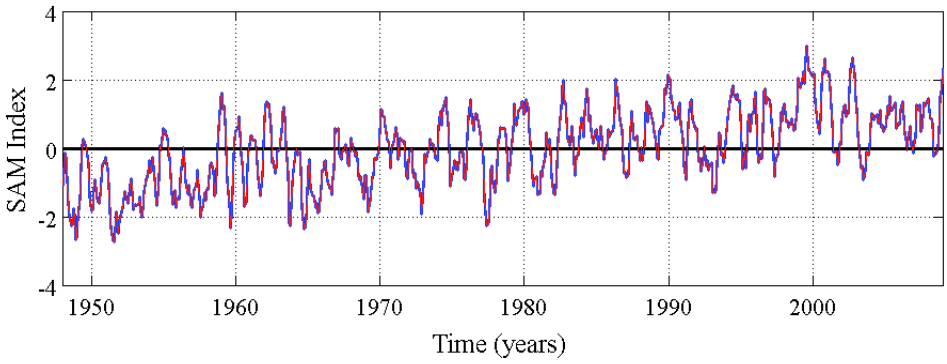

Figure 5: Southern Annular Mode Index computed as defined by Gong & Wang (1999): the difference between the normalized zonally mean SLP of 40 °S and 65 °S. Monthly Mean Sea Level Pressure data from CORE interannual forcing fields.

citetlimpasuvan00 carried numerical experiments to demonstrate that the structure and variability of the SAM results from the internal dynamics of the atmosphere and contributes a significant proportion of Southern Hemisphere climate variability (typically about 35%) from high–frequency to very low-frequency timescales.

citetthompson11 showed that over the past 50 years the SAM has oscillated to become more positive in the austral summer and autumn (as pressure dropped

around the coast of the Antarctic and increased at mid-latitudes) leading to stronger circumpolar westerly winds. Turner (2010) pointed that the strength of the westerly winds over the Southern Ocean has increased by 15—20% during the last 40 years, resulting in a 1-–2 ° poleward migration of the westerlies and contributing to the spatial variability in Antarctic temperature change (Marshall, 2007). More specifically, this leads to a significant warming trend in the northern Antarctic Peninsula and a slight cooling trend over the rest of the continent (Thompson and Solomon, 2002; Turner et al., 2005).

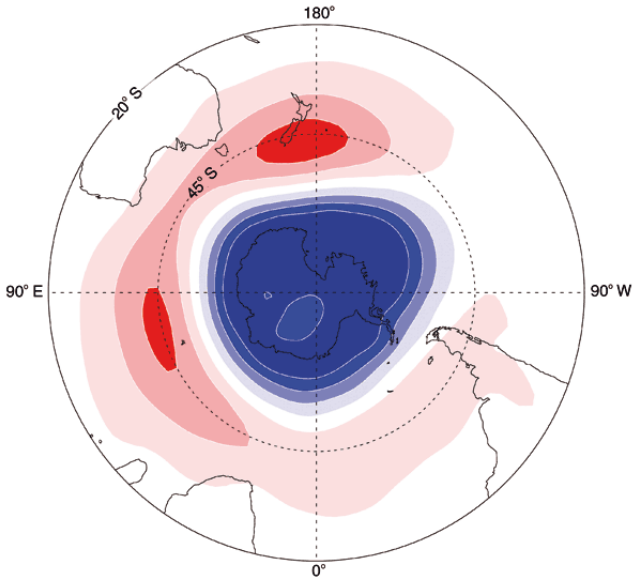

Figure 6: A simplified schematic representation of the Sea Level Pressure annular pattern of the SAM positive phase. The blue colors represent negative SLP anomalies and the red colors represent positive SLP anomalies. Adapted from horizon.atmos.colostate.edu/ao/Popular/index.html

The impact of the SAM on the ocean circulation is important. Mechanisms linking stronger winds to circumpolar ocean warming include a southward shift in the location of the ACC, increased heat flux into the ocean, and increased mesoscale

eddy activity (Marshall, 2003; Fyfe and Saenko, 2006; Fyfe et al., 2007; Gille, 2008; Hogg et al., 2008; Meredith and Hogg, 2006). Hall and Visbeck (2002) numerical investigations suggested that a positive phase of the SAM is associated with northward (southward) Ekman drift in the Southern Ocean (at 30 °S) leading to upwelling (downwelling) near the Antarctic continent (around 45 °S) (Figure 7). These oceanic responses may be directly related to MOC changes to explain patterns of observed oceanic temperature change in the Southern Ocean described by Gille (2002) and Gille (2008). Hughes et al. (2003) showed that SAM variability produces a sea level response around Antarctica , also seen by its modulation of the ACC flow through the Drake Passage (Meredith and Hogg, 2006).

The tendency for the westerly wind pattern to strengthen and contract closer to the Antarctic continent is likely caused by a reduction in ozone in the stratosphere (Thompson and Solomon, 2002), but climate models suggest that increases in greenhouse gases will, in the future, drive similar changes in Southern Ocean winds (Shindell et al., 1998; Marshall, 2003).

These changes may eventually bring about changes to the atmospheric energy balance. Simmonds (2003) reported a decrease in the annual and seasonal numbers of cyclones south of 40 °S. They suggested that due to SAM oscillations, except for the Amundsen Bellingshausen Sea, there are now fewer but more intense cyclones in the Antarctic coastal zone between 60 ° and 70 °S.

Variability in the ice cover in this region is linked to changes in SAM. Between 1974 and 1976, the large Weddell Sea Polynya was created by the injection of relatively warm deep water into the surface layer due to sustained deep–ocean convection during negative SAM, but since the late–1970s SAM has been mainly positive, re-

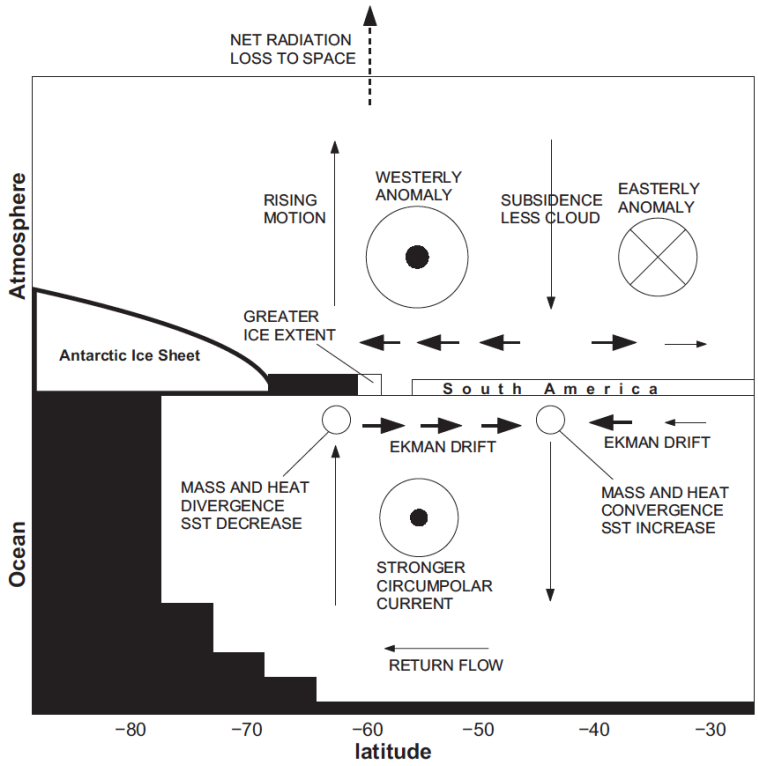

Figure 7: A representation of the changes in the atmosphere and ocean associated with variations in the Southern Annular Mode (SAM), the primary mode of variability of the Southern Hemisphere atmosphere. A strengthening of the winds drives stronger upwelling on the southern side of the Southern Ocean and stronger downwelling on the northern side. The stronger winds also tend to drive sea ice farther offshore. Extracted from Hall & Visbeck (2002).

sulting in warmer and wetter condition forestalling any reoccurrence of the Weddell Sea Polynya (Gordon et al., 2007). A more positive SAM was reported by Raphael (2003) as a feed back to diminished sea ice. On the other hand, Marshall et al. (2006) suggested that increased SST around the Antarctic continent would warm the atmosphere and increase geopotential height thus leading to a more negative phase of SAM.

4.3 Ice covered Antarctic

The cryosphere components found in the Antarctic environmental are largely responsible for most of the regional dynamics. Throughout almost the entire year, the Antarctic continent is surrounded by a zone of frozen seawater 1 or 2 m thick (Lythe et al., 2001a). By September, Antarctic sea ice covers an area of 19 – 20 x 10^6 km^2 spreading the thin first year sea ice close to 60 °S around most of the continent and even farther 55 °S at the Weddell Sea section of the Southern Ocean. A huge amount of this ice will eventually melt during the austral summer shrinking to approximately 3 x 10^6 km^2 in March, i.e. less than 20% of its maximum annual extent (Figure 8). But even the thin ice can impact the Antarctic climate. A 10 cm thick layer will strongly reduce the air-sea exchange of moisture and gases, lessening the air-sea heat transfer by 90% (Rintoul et al., 2012a). The widespread of thin ice will also affect the albedo of the ocean. While the ice–free surface of the ocean can absorb about 90% of the incident solar radiation, depending on the thickness and snow cover, the ice surface can reflect a similar amount of this radiation, insulating cold waters underneath. However, the positive feedback takes place when the sea–ice retreats; an ice–free ocean with reduced albedo absorbs radiation that warms the water and leads to further sea ice melting (Rintoul et al., 2012a).

Sea ice variability is subject to atmospheric and ocean dynamics. While warm waters may cause the sea ice to melt, the additional freshwater increases the stability of the surface layer and affects air-sea exchange, water mass formation and the depth of the mixed layer. Surface winds are able to move the floating ice modulating its spacial distribution (Venegas and Drinkwater, 2001). As the wind blows over the sea ice, it can push the surface ice cover, creating vast open water pools surrounded by

sea ice known as polynias. These polynias usually occur on coastal regions and are frequently found in the Ross Sea (RS) and the Weddell Sea (WS) (GORDON and COMISO, 1988). However, polynias can be formed farther north on oceanic regions due to the upwelling of warm waters who will melt the sea ice from the bottom (Fahrbach et al., 1994). Zwally and Gloersen (1977) reported the occurrence of a massive oceanic polynia in the Weddell Sea that persisted throughout 3 years (1974–1976) and was as big as the State of California in the United States; the Weddell Polynia.

Sea ice formation and heat loss to the atmosphere are directly affected by the wind regime and the opening of coastal polynias (Ball, 1957; Bromwich and Kurtz, 1984; Kurtz and Bromwich, 1985). Although the polynias may constantly change in size and shape, the rates by which they are formed may alter shelf waters salinity. As sea ice is pushed offshore from its formation zone by strong katabatic winds, the contact with the atmosphere will cause the ocean to lose heat boosting the ice production, which is followed by the brine rejection that increase local salinity. Increased salinity along with lower surface water temperature due to heat loss are accountable for the formation of dense waters over the continental shelves in the Weddell and Ross Seas (Fahrbach et al., 1994; Barber and Crane, 1995).

Another cryosphere component are the ice shelves. Ice shelves are the floating fringe–like part of the continental Ice Sheet that have reached the ocean (Thomas, 1973). The ice shelves inhibit the flow of the ice sheet into the ocean as they impart forces on grounded glaciers and ice streams, acting, as defined by Rintoul et al. (2012a), as a “buttress” to hold the ice sheet back. An example of its impact was the dramatic acceleration of the flow of glaciers into the ocean triggered by the collapse

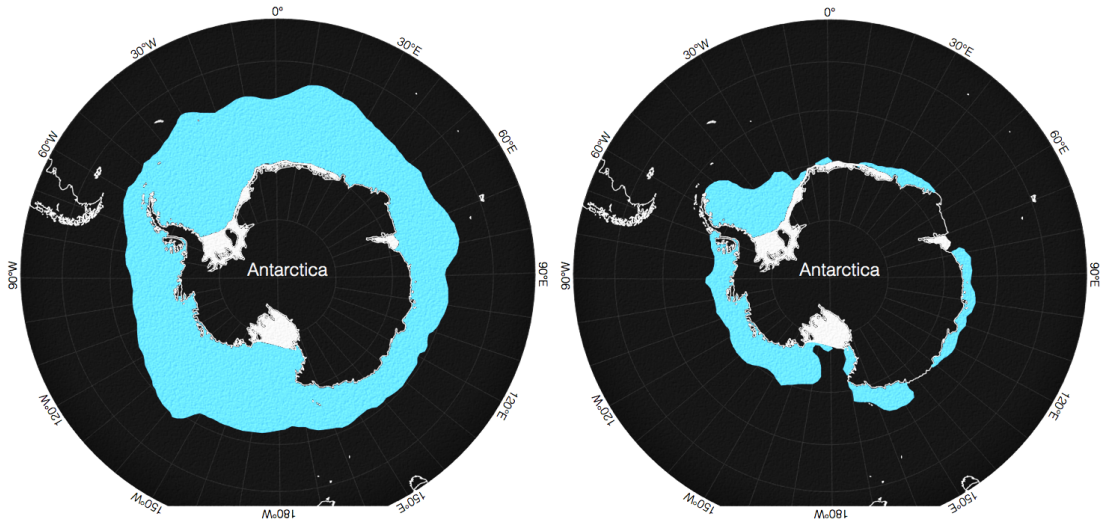

Figure 8: Maps of average sea ice extent in the Antarctic winter (September – left panel) and summer (February – right panel). They represent average sea ice extent from 1979 to 2002/2003, based on ESMR–Nimbus–5 satellite observations.

of the massive Larsen–B ice shelf (Rignot et al., 2004; Pritchard and Vaughan, 2007). The IPCC AR4 discusses that present estimates of the rate of future sea–level rise may be too conservative, since the ice sheets respond so promptly to changes in the ice shelves.

The definition of where the ice shelf begins and the ice sheet ends can be mapped by means of surface roughness optical imagery, to establish the transition between the grounded and the floating ice known as the grounding line (Turner et al., 2009). Rignot et al. (2008) have linked the increase in the basal melt rate and the retreat of grounding lines to warmer ocean temperatures. In line with Rignot and Jacobs (2002), a 1 °C increase in ocean temperatures increases basal melt rates by about 10 m yr^{-1}. Changes in the continental ice in Antarctica depend on the variability of the adjacent ocean.

As discussed by Rintoul et al. (2012a), ice shelves are just beginning to be added

to climate models, but the ice balance depends strongly on oceanic properties and circulation not well–represented in present models. To reduce the uncertainty in future estimates of sea–level rise, long–term observations of the ocean near and beneath ice shelves are crucial for testing and improving these models, in order to provide an improved understanding of ocean–ice shelf interaction.

4.4 Regional Oceanography

From the oceanographic perspective the dominant feature of the Southern Ocean dynamics is the Antarctic Circumpolar Current. As discussed before, the ACC connects the three major oceanic basins due to the lack of continental barriers along the latitude band of the Drake Passage carrying a massive amount of water (~120 SV; Carmack (1977); Whitworth and Nowlin (1987); Locarnini (1994); Rintoul et al. (2012b)). As it flows around the Antarctic continent, the ACC not only provides a dynamical barrier separating oceanographic regimes north of the Subantarctic Front from the ones south of the Polar Front, but more important, the ACC dominates the southerly circulation taking place in its poleward side (Orsi et al., 1995; Orsi, 1999). Throughout its clockwise incursion, the ACC carriers the most voluminous water mass in the SO known as the Circumpolar Deep Water (CDW) (Budillon et al., 2003; Orsi and Wiederwohl, 2009). The CDW is identified by a thick salty warm water at mid–depths with low oxygen. The CDW is the main heat source for the ocean south of the Polar Front. Above the CDW, the Antarctic Surface Water (AASW) extends with uniform properties from the PF to the continental margins of Antarctica, where shelf waters are found at near freezing temperatures (Figure 9, Worthington (1981); Orsi et al. (1995); Budillon et al. (2003); Orsi and Wiederwohl

(2009)).

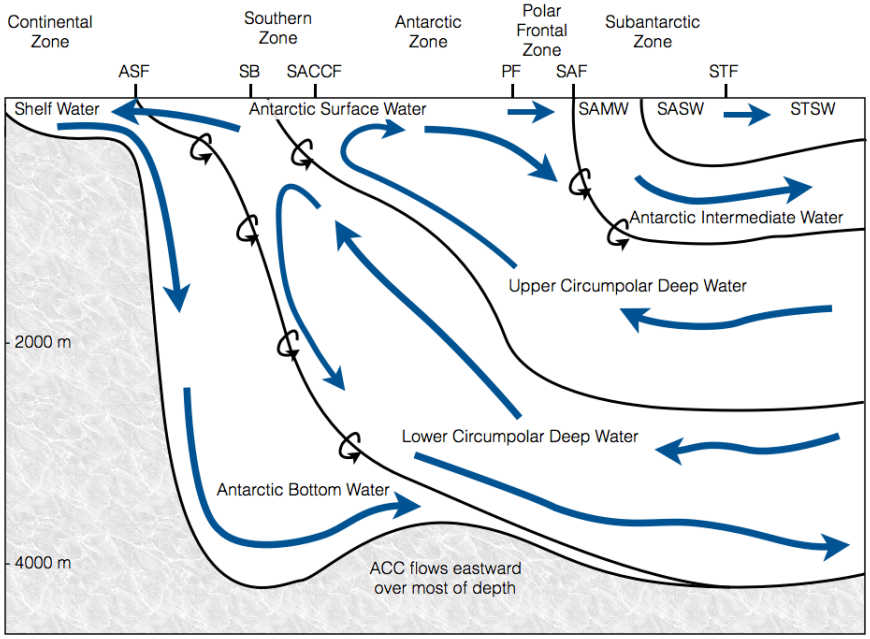

Figure 9: A schematic meridional section in the Southern Ocean showing the water masses, meridional circulation, fronts, and most zones. Acronyms: Continental Shelf Water (CSW), Antarctic Surface Water (AASW), Subantarctic Mode Water (SAMW), Subantarctic Surface Water (SASW), Subtropical Surface Water (STSW), Antarctic Slope Front (ASF), Southern Boundary (SB), Southern ACC Front (SACCF), Polar Front (PF), Subantarctic Front (SAF), and Subtropical Front (STF). After Talley et al. (2011).

Below the AASW, the CDW flows from the deep layers and upwells along the southward shoaling isopycnals of the ACC (Speer et al., 2000). It may be distributed into two distinct classes: a lighter CDW known as Upper CDW (UCDW) and a denser one called Lower CDW (LCDW). The UCDW is characterized by low oxygen and high nutrient concentrations. As it shoals toward the south, UCDW reaches the upper–ocean mixed layer within the ACC and returns northward near the surface (Deacon, 1984). The LDCW, in turn, is characterized by high salinities

and is dense enough to flow underneath AASW to enter the system of cyclonic gyres and westward–flowing slope frontal jets of the subpolar regime, often spreading on the Antarctic continental shelves. There, LCDW mixes with Antarctic surface waters and water masses found over the Antarctic continental shelves to form denser water, resulting in the formation of Antarctic Bottom Water (AABW), that sinks downslope to the ocean bottom (Foster and Carmack, 1976; Jacobs et al., 1970). The production and northward export of AABW eventually fill most of the World Ocean bottom layers, ventilating deep global ocean (Orsi et al., 2002) as an integral component of the southern closure of the MOC lower cell (Figure 2; Lumpkin and Speer (2007)).

The AABW formation is considered to happen at three regions around Antarctica: western RS, western WS and Adélie Land close to the Mertz Glacier. Kerr et al. (2012) analyzed numerical results from the Ocean Circulation and Climate Advanced Modelling (OCCAM) model (Coward and De Cuevas, 2005) and estimated the AABW production of ~11 Sv at the northwestern Weddell Sea and ~1 Sv at the Ross Sea. But because of the shelf break high complexity, local water mixing and advection processes are not yet fully understood (Rintoul, 1998; Baines and Condie, 1998; Gordon, 1998; Orsi, 1999; Bindoff et al., 2000; Foldvik et al., 2004; Ivanov et al., 2004). Continental slope water formation is believed to happen in three phases (Bergamasco et al., 2003): first, the dense water formation over the continental shelf due to convection from surface cooling and brine rejection; second, the geostrophic adjustment as the newly formed water flows towards shelf break, where a frontal system is formed and an enhanced slope–flow appears due to baroclinic instability; third, the canyon channeled water sinking due to gravity and bottom

stress (Huthnance, 1995; Shapiro and Hill, 1997; Bergamasco et al., 2004; Cenedese et al., 2004; Gordon et al., 2004).

AABW production relies upon the interaction between the CDW warm deep waters and the cold dense shelf waters at the Antarctic continental margins. The continental shelves around Antarctica are generally narrow, except for the Ross Sea and the Weddell Sea, whose shelves extent for over 400 km and depths reaching 400 m (Carmack, 1990). Continental margins have irregular depressions, canyons and massive ice shelves that play an important part in the formation and export of dense shelf waters near the freezing point (Orsi et al., 1995; Williams et al., 2008). However, these extensive continental shelves are located where the poleward extent of the ACC is not close to the Antarctic continent, but rather far. The advection of ACC warm waters to the shelf break region is performed by large scale cyclonic gyres that fill the gap between the ACC and the Antarctic continent, named after their geographic location: the Ross Gyre and the Weddell Gyre.

Between the southern borders of ACC and the Antarctic shelf break, these clockwise gyres constitute the detailed pathway for transport to, from, and along the continental margin (Figure 3; Whitworth III et al. (1998); Johnson (2008); Muench et al. (2009)). The gyres are quite often well represented by numerical models and can usually be identified as dome–shaped structures surrounded by downward sloping masses of equal density that extend towards the coastal west–moving Slope Current in the south and towards the east–moving ACC in the north (Dinniman et al., 2007; Turner et al., 2009). Transport estimates in the gyres vary locally: Fahrbach et al. (1994) reported a 30 ± 10 Sv transport of the Weddell Gyre in the Weddell Sea, whereas Klatt et al. (2005) estimates came to 56 ± 8 Sv across the Greenwich Merid-

ian. The Ross Gyre, in turn, transports 40 Sv across longitude 150 °W (McCartney and Donohue, 2007).

On the southern limits of the gyres, the Antarctic Slope Current (ASC) can be referred as the combination of all the westward currents flowing around Antarctica: the Antarctic Coastal Current (ACoC), the ASC itself and the southern branch of polar gyres. The ACoC (a.k.a. East Wind Drift) is the southernmost current in the world that flows parallel to the Antarctic coastline and is mainly westwards (Deacon, 1937). Although Heywood et al. (2004) suggested the ACoC to be circumpolar, the Antarctic Peninsula strongly blocks its westward flow. In parallel to the ACoC, a strong density front (Antarctic Slope Front – ASF) extends continuously from 120 °W near the Amundsen Sea westwards to 55 °W at the tip of the Antarctic Peninsula, mainly attributed to coastal downwelling caused by the prevailing easterly winds there (Sverdrup, 1953; Whitworth III et al., 1998). In line with Whitworth III et al. (1998), there is a parallel westward surface–intensified flow north of the ACoC (found further south over the continental shelf), referred as the Antarctic Slope Current. However, in regions where the continental shelf is narrow the ACoC and the topographically controlled ASC are sometimes hard to differentiate, what justifies grouping the entire southern westward flow into an all–encompassing ASC (Heywood et al., 1998).

The subpolar regime complex dynamics controls the ocean–cryosphere–atmosphere interaction in the inner domains of the Southern Ocean and drives the water masses formation and export from the Ross Sea and the Weddell Sea, whose dynamics are individually scrutinized next.

4.4.1 The Ross Sea

Placed between Cape Adare (170 °E) and Cape Colbeck (156 °W), thecontinental shelf of the Ross Sea comprises a triangular area of about 5 x 10^5 km^2 and mean depth of 500 m, excluding the far southern portion covered by the Ross Sea Ice Shelf (RIS) which also extends to approximately 5 x 10^5 km^2. The RIS is a 250 m–thick ice cover that reaches half of the continental shelf and under which water flows freely in the ice cavity. Irregular topography is featured by shallow elevated banks and depressions reaching 1200 m deep that behave as reservoirs of the salty and dense waters, since they are deeper than the continental shelf. These banks and depressions display a SSW–NNE orientation crisscrossing NW-–SE oriented continental shelf break, which corresponds to the 700 m isobath linking the area in front of Cape Adare to Cape Colbeck (Figure 10). These channel–like depressions perform the important task to deliver dense waters from the inner continental shelf to the shelf break region and down the continental slope where water mixing takes place. They are also preferred pathways for warm water masses flowing onto the continental shelf. Three channels are in the foreground conveying shelf waters to ASF region: the Drygalski Trough (DT) in the western RS; the Joides Trough (JT), between DT and the Pannell Bank; and the Glomar–Challenger Trough (GCT) in the centraleastern RS (Figure 10; Jacobs and Comiso (1989); Budillon et al. (2003, 2011)).

The oceanographic domain of the Ross Sea extents from the very grounding line of the Ross Sea Ice Shelf (under which waters flow freely to interact with the bottom of the ice shelf) until the northernmost extent of the Ross Gyre, which happen to occur at the Southern ACC Front region. Cape Adare (170 °E) marks the western

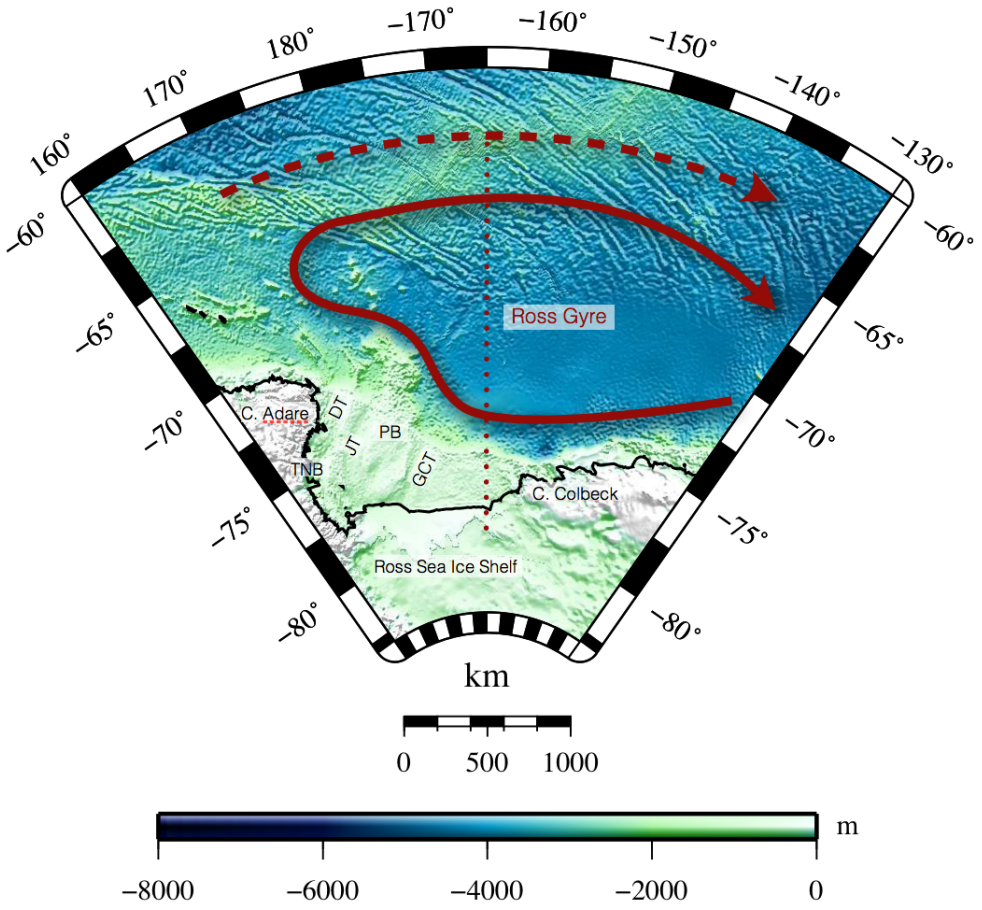

Figure 10: Ross Sea topography showing the channels primarily related to cross–shelf break water mass transport (Drygalski Trough – DT, Joides Trough – JT and Glomar–Challenger Trough – GCT), Pennell Bank rise – PB, Terra Nova Bay – TNB, and the Ross Sea Ice Shelf (RIS; south of ~78° S). Full arrow represents the Ross Gyre cyclonic circulation and the dashed arrow represents the eastward flow of ACC. Dotted line represents the cross–section analyzed for model validation.

limit and the eastern boundary is determined by the meridional extent of the RG around 120 °W (Budillon, 2007). As the Ross Gyre interacts with the southern border of the ACC, it branches off part of the voluminous CDW and advects a thick salty water layer with low oxygen to the shelf break region (Worthington, 1981; Budillon et al., 2003; Orsi and Wiederwohl, 2009). Within the Ross Gyre (RG),

CDW flows along the shelf break, vertically placing itself between the Antarctic Surface Water (AASW) and AABW (Carmack, 1977; Whitworth and Nowlin, 1987; Locarnini, 1994; Orsi et al., 1995; Orsi, 1999). At some particular points, the CDW enters the continental shelf (preferably through the cross–shelf break channels; DT, JT and GCT), and interacts with the colder and fresher AASW to become Modified Circumpolar Deep Water (MCDW), which can be identified by a subsurface maximum temperature and minimum dissolved oxygen. CDW is the only water mass to provide heat to the inner continental shelf of the RS (Jacobs et al., 1985; Locarnini, 1994; Jacobs and Giulivi, 1998, 1999; Gouretski, 1999; Budillon et al., 1999, 2003; Orsi and Wiederwohl, 2009).

The water mass distribution for the RS may be divided into two regimes: the oceanic regime dominated by the Ross Gyre and the shelf regime where the shelf waters (SW) formation takes place. The continental shelf break and shelf slope constitute the transition zone where most of the mixing between the CDW (MCDW) and SWs occur (Kurtz and Bromwich, 1983, 1985; Orsi and Wiederwohl, 2009).

The Antarctic Surface Water (AASW) is observed mainly in the mixed layer (20—100 m) of the oceanic regime, but gradually deepens toward the coast, reaching nearly 400 m along the upper continental slope east of the Ross Sea (Tonelli et al., 2012). It is formed by means of mixing between upwelled MCDW and colder underlying waters. Since it occupies the surface layers, AASW is extremely variable throughout the year, being influenced by atmospheric conditions, ice melting and formation, and precipitation. Typical properties for AASW are θ < -1.5 °C and salinity < 34.4 (Bromwich and Kurtz, 1984; Jacobs et al., 1985; Orsi and Wiederwohl, 2009). During large melting events, the freshwater advection further decreases

the AASW salinity to < 33, generating a very stable upper mixed layer. These events can be followed by phytoplankton blooms due to the release of nutrient and micro–elements of meteoric origin that have been entrapped in the pack ice during winter (Grotti et al., 2001).

The CDW is captured by the cyclonic RG as a warm ($\theta > 1.5\,^{o}$C) and saltier than 34.7 tongue. When it gets to the shelf slope, it is carried westward along the ASF below the AASW, now as MCDW ($0.5\,^{o}\text{C} < \theta < 0.95\,^{o}$C and $34.57 < S < 34.68$). As it flows along the shelf break, MCDW properties are progressively attenuated and a prominent poleward inflow of oceanic waters ($\theta >$ -1.2 ^{o}C and $S > 34.50$) from the mouth of the GCT is established (Stover, 2006; Orsi and Wiederwohl, 2009).

The shelf regime is characterized by a lateral east–west salinity gradient. The Terra Nova Bay Polynia (TNB) is located in the western side of the Ross Sea, which recurrence affects the physical features of the water column, as continual formation and removal of new ice increases seawater salinity (Kurtz and Bromwich, 1983, 1985; Jacobs et al., 1985; Van Woert, 1999). This region has been identified as the formation site of the High Salinity Shelf Water (HSSW). The very dense HSSW ($S >$ 34.80) formed in the TNB spreads close to the bottom, following the axis of the DT in both north and south directions (Jacobs et al., 1985; Van Woert, 1999; Budillon and Spezie, 2000; Fusco et al., 2002). The northern branch flows to the shelf break to interact with MCDW and to form deep and bottom waters to be exported from the RS. The southerly branch of HSSW flows towards the western RIS where a slightly less salty HSSW ($S > 34.76$) is formed by recurrence of the RIS Polynia. From there, both HSSW varieties move southward beneath the RIS to interact with the basal ice generating the Ice Shelf Water by means of basal melting (Jacobs et al.,

1970; Gordon and Tchernia, 1972; Rodman and Gordon, 1982; Budillon et al., 1999). Establishing the salinity gradient pattern to the eastern RS, the Low Salinity Shelf Water (LSSW; S $<$ 34.62) is formed due to the interaction between AASW and colder waters in the subsurface layers (Jacobs et al., 1985; Locarnini, 1994; Russo et al., 1999).

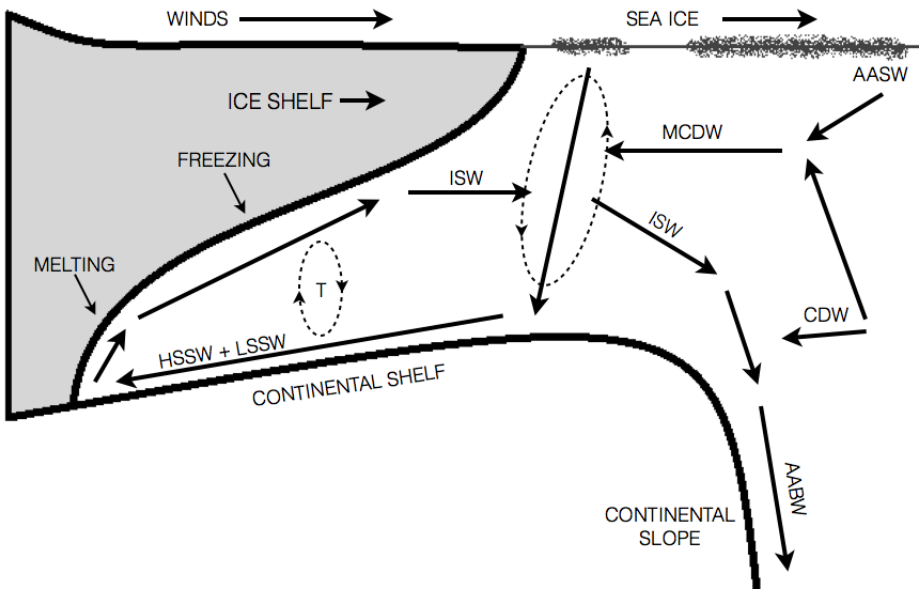

Figure 11: Vertical circulation scheme under the Ross Sea Ice Shelf. HSSW and LSSW interact with the bottom of the ice shelf to form the ISW by means of basal melting. ISW flows north connecting the sub–RIS domain with the shelf slope where complex mixing results in the formation of AABW. "T" represents the tidal influence and larger revolving cell represents the convection associated with sea ice formation (Based on Smethie & Jacobs, 2005)

The southern branch of HSSW flows southward under the RIS to interact with the eastern–originated LSSW, where the cooling and melting at different depths forms the Ice Shelf Water (ISW), characterized by a temperature (θ $<$ -1.93 °C) lower than the freezing point at the surface pressure. ISW exits the RIS cavity near the Greenwich meridian and is primarily found on the central continental shelf of

the Ross Sea (Figure 11; Budillon et al. (2002); Jacobs et al. (1985); Smethie Jr and Jacobs (2005), from where it moves northward toward the shelf break along the GCT to give a further contribution to the AABW formation (Jacobs et al., 1985; Budillon et al., 2011)). ISW is, therefore, responsible for connecting the RIS and the continental slope (Dinniman et al., 2007; Orsi and Wiederwohl, 2009).

There are two largest sources of AABW leaving the Ross Sea: the DT (western Ross Sea) and the GCT (central Ross Sea), corresponding to the pathways of the main outflows of HSSW and ISW, respectively. Cold shelf water (SW) flowing north along the GCT is, therefore, relatively unmodified by the time it reaches the shelf break, so that almost pure SW is fairly frequently found over the continental slope. In this sector of the Ross Sea, the AABW is slightly different, being fresher and colder, than the AABW formed by the HSSW at the western shelf break (Budillon et al., 2011). In contrast, tidal advection bringing the ASF inshore of the shelf break near the DT allows mixing to occur directly between the HSSW and the warmest CDW, before the dense shelf water begins to descend the slope (Budillon et al., 2011; Smethie Jr and Jacobs, 2005; Bergamasco et al., 2003).

4.4.2 The Weddell Sea

The Weddell Sea is in many ways similar to the Ross Sea; it has an extensive continental shelf with a large ice shelf, a cyclonic gyre (Weddell Gyre) which rules the local oceanographic dynamics, and significant water mixing at the shelf slope that will link the upper and lower limbs of the MOC by means of the production of AABW (Orsi et al., 1993; Fahrbach et al., 1994; Fahrbach et al., 1995; Rintoul et al., 2012b).

The southern limit of the WS is given by the Filchner–Ronne Ice Shelf (FRIS).

With a total area of about 4.1 x 10^5 km^2, the FRIS is the second largest ice shelf in the world, only smaller than the Ross Sea Ice Shelf. It is the combination of two massive ice shelves separated by Berkner Island; the Filchner ice shelf in the eastern side of Berkner Island and the much larger Ronne ice shelf in the western side of the island (Figure 12; Hellmer (2004)). To the west, the WS is boundaried by the Antarctic Peninsula (Carmack and Foster, 1975). The northern and eastern boundaries definitions are more oceanographic–dependent, since they are given by the Weddell Gyre extent. The northernmost extent of the WG coincides with the Southern ACC Front roughly around 62 °S. To the east, the gyre reaches 20 °E where, similar to the Ross Gyre, it captures warm waters carried eastward by ACC: Upper CDW (UCDW; $\theta > 1.5$ °C and $34.5 < S < 34.7$) and Lower CDW (LCDW; $S > 34.7$; Orsi et al. (1993); Orsi et al. (1995). Both varieties are transported westward along the southern branch of the gyre, gradually cooling and freshening as it entrains ambient waters, and is referred to as Warm Deep Water (WDW) due to its ambient characteristics. West of 30 °W, WDW interacts with the dense shelf waters off the FRIS (Whitworth III et al., 1998) and AABW formation occurs (Carmack, 1977; Orsi et al., 1993; Orsi, 1999; Hellmer and Beckmann, 2001; Naveira Garabato et al., 2002; Schodlok et al., 2002).

When the WDW approaches the continental slope, it penetrates onto the continental shelf in certain locations, preferably through topographic depressions, often in modified form. There, the WDW mixes with cold shelf waters that are made saline by brine rejection during sea ice formation, creating dense water plumes that spill off the shelf and entrain further deep as they descend (Killworth, 1977; Carmack and Foster, 1975; Foldvik et al., 2004; Wilchinsky et al., 2010). Interaction of shelf

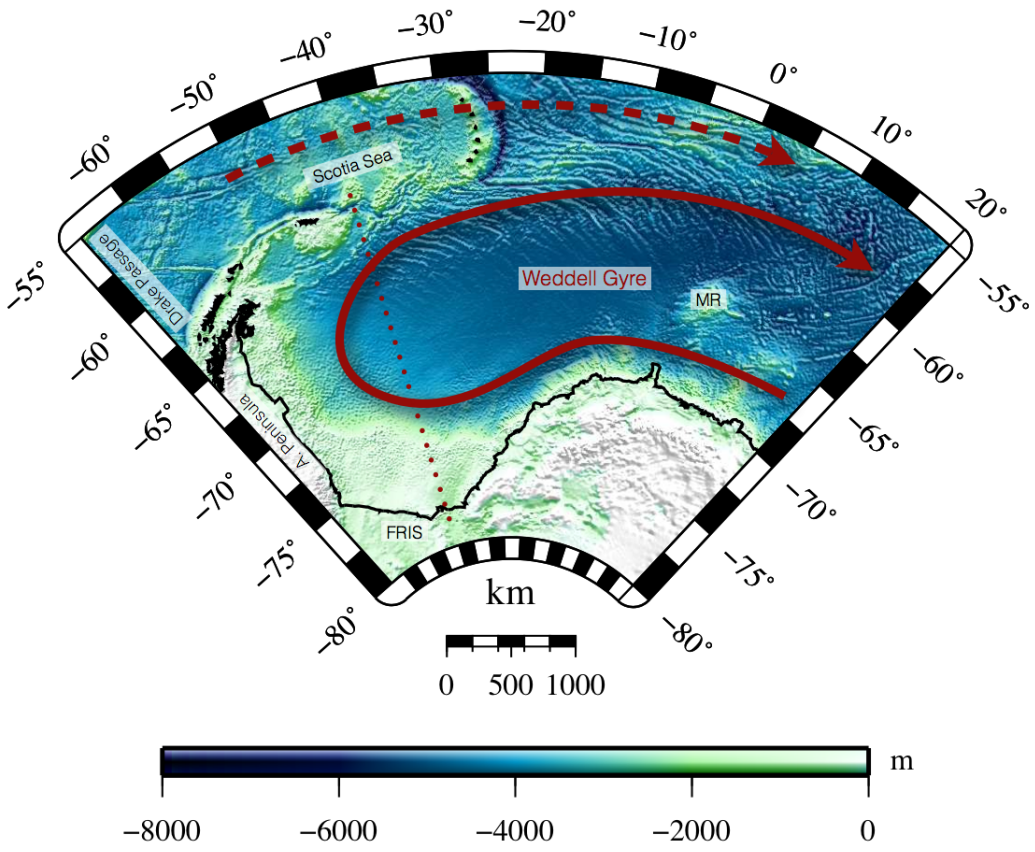

Figure 12: Weddell Sea main features: the Antarctica Peninsula and the Drake Passage in the western limit, Scotia Sea, Maud Rise – MR, Filchner–Ronne Ice Shelf (FRIS; south of ~75 °S). Full arrow represents the Weddell Gyre cyclonic circulation and the dashed arrow represents the eastward flow of ACC. Dotted line represents the cross–section analyzed for model validation.

waters with the bottom of the FRIS is also important in setting the properties of some of the shelf waters, with temperatures below the surface freezing point made possible by the pressure at which the interaction occurs (Nicholls et al., 2009). The WS continental shelf exhibits an east–west salinity gradient very much alike the one observed in the Ross Sea shelf. The eastern shelf is dominated by the Low Salinity Shelf Water (LSSW; θ < -1.6 °C and S < 34.44), whose salinity, under the influence of ACoC, acts as a deterrent to the bottom waters formation (Gill, 1973; Fahrbach

et al., 1994). To the west, salty waters spread along the bottom of the shelf as the High Salinity Shelf Water (HSSW; θ < -1.6 °C and S > 34.55) is formed due to brine rejection from sea ice formation (Carmack and Foster, 1975; Foldvik et al., 2004; Nicholls et al., 2009).

The recurrence of polynias at the edge of the Ronne ice shelf (western WS) trigger the HSSW formation, that is then carried by the local circulation to the ice shelf cavity. As HSSW transports heat underneath FRIS, it leads to basal melting that results in the formation of the very cold Ice Shelf Water (ISW; $\theta \approx$ -1.9 °C). Finally, ISW is channeled outward the FRIS domain onto the shelf slope (as shown in Figure 11), to mix with WDW and form the Weddell Sea Deep Water (WSDW) and the Weddell Sea Bottom Water (WSBW). These water masses will produce the WS variety of AABW (Killworth, 1977; Wilchinsky et al., 2010; Fahrbach et al., 2011; Hellmer et al., 2012). WSBW, formed primarily near the FRIS edge (Nicholls et al., 2009), produces the coldest and densest AABW exported from the Weddell Sea (θ < -0.7 °C), which is too dense to flow over the topographic barriers and end up trapped between these seabed elevations and the continental slope. The lighter WSDW (0 °C > θ > -0.7 °C) is primarily produced directly by mixing between dense shelf waters and WDW. However, it may be indirectly formed by slow diapycnal upwelling of WSBW within the Weddell gyre (Naveira Garabato et al., 2002; Foldvik et al., 2004; Gordon et al., 2004; Nicholls et al., 2009).

5 Methods

5.1 The Regional Ocean Model System – ROMS

The model used in this study is the Regional Ocean Model System – ROMS – which is a free–surface, terrain–following, hydrostatic primitive equations ocean model (Song and Haidvogel, 1994; Haidvogel et al., 1991, 2008). As discussed in Haidvogel et al. (2008), the computational kernel in ROMS utilizes consistent temporal averaging of the barotropic mode to guarantee both exact conservation and constancy preservation properties for tracers and therefore more accurately resolves barotropic processes, while preventing aliasing of unresolved barotropic signals into the slow baroclinic motions. More details can be found in section 3 of Haidvogel et al. (2008) and Shchepetkin and McWilliams (2005).

Two topographic surfaces are defined for this model configuration: the bottom of the water column and, where necessary, the depth of the portion of the ice shelf thickness that is below the mean sea level. Bottom topography was constructed combining ETOPO5 (NGDC, 1988) and BEDMAP in which sea floor topography is derived from the Smith and Sandwell (1997), ETOPO2 and ETOPO5 (NGDC, 1988). Ice shelf thickness was obtained from the BEDMAP gridded digital model of ice thickness (Lythe et al., 2001b). Both surfaces were smoothed with a modified Shapiro filter which was designed to selectively smooth areas where the changes in the ice thickness or bottom bathymetry are large with respect to the total depth (Wilkin and Hedstrom, 1998). It should be noted that perhaps too much smoothing

was applied. In particular at the Amery ice shelf.

A periodic circumpolar domain between 83 °S and 50 °S with variable horizontal resolution was constructed. Resolution gradually increases from ~50km at the northern boundary to ~4.8 km at the southern boudary (Figure 13). In the vertical, 40 terrain–following levels with higher resolution near surface and bottom are used. In this configuration, the model domain contains 309 x 720 grid cells and 40 vertical levels. This grid allows for an efficient and computationally time–effective modeling framework with a higher resolution in the areas of interest.

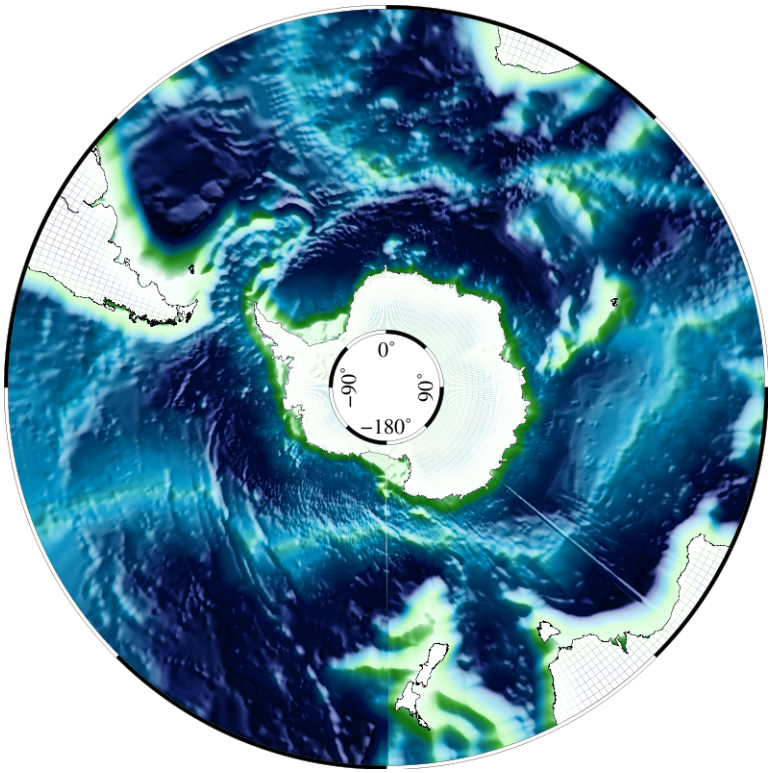

Figure 13: Model simulation domain. It consists of a periodic circumpolar domain between 83 °S and 50 °S with variable horizontal resolution, which gradually increases from ~50 km at the northern boundary to ~4 km at the southern boudary.

For the 3D momentum advection a 4^{th} order centered scheme is applied in the horizontal and in the vertical. For tracers, a 3^{rd} order upstream horizontal and a 4^{th}

order centered vertical advection schemes are applied. Biharmonic horizontal mixing of momentum and tracers is used in which the viscosity and diffusivity depend on the grid spacing. Quadratic bottom stress, with a coefficient of 3.0×10^{-3} was applied as a body force over the bottom layer. The vertical momentum and tracer mixing were handled using the KPP mixing scheme. For computational efficiency, ROMS uses a split–explicit time–stepping scheme in which external (barotropic) and internal (baroclinic) modes are computed separately. The external and internal time step were set to 0.75 and 30 minutes, respectively in compliance with the Courant, Friedrichs and Lewy (CFL) criterion.

A dynamic–thermodynamic sea–ice module is coupled to the ocean model, having both of them the same grid (Arakawa–C) and time step and sharing the same parallel coding structure (Budgell, 2005). The sea–ice dynamics is based on elastic–viscous–plastic (EVP) rheology (Hunke, 2001). The sea–ice thermodynamics follows Mellor and Kantha (1989). Two ice layers and a single snow layer are used in the sea–ice module to solve the heat conduction equation. The salt flux underneath the sea–ice is a function of the basal melting or freezing which is controlled by the difference between the water–sea–ice heat flux and the sea–ice–atmosphere conductive heat flux.

In addition to sea–ice, an ice shelf parameterization is included in order to consider the ice shelf impacts on ocean circulation and water mass formation. The thickness and extent of the ice shelf do not change along the simulations. Under the ice shelves, the upper boundary is no longer at sea level but conforms to the ice shelf base. Below the ice shelves, the atmospheric contributions to the momentum and buoyancy fluxes are set to zero. The heat and salt fluxes are calculated as described

in Dinniman et al. (2007) with the modification that the heat and salt transfer coefficients are functions of the friction velocity (Holland and Jenkins, 1999).

Two topographic surfaces must be defined for this model configuration: the bottom of the water column and, where necessary, the depth below mean sea level of the ice shelf thickness. Bottom topography was constructed combining ETOPO5 (National Geophysical Data Center - NGDC 1988) and BEDMAP in which sea floor topography is derived from the Smith and Sandwell (1997), ETOPO2 and ETOPO5 (NGDC 1988). Ice shelf thickness was obtained from the BEDMAP gridded digital model of ice thickness (Lythe et al., 2001b). Both surfaces were smoothed with a modified Shapiro filter which was designed to selectively smooth areas where the changes in the ice thickness or bottom bathymetry are large with respect to the total depth (Wilkin and Hedstrom, 1998).

The model is initialized with the temperature and salinity fields from the January Levitus World Ocean Data 1998 climatology. Under the ice shelf, specified vertical profiles of temperature and salinity were prescribed as initial conditions. This avoids instabilities produced by the excessive gravity waves at the beginning of the simulation. At the open northern boundary, the model uses the free–surface Chapman condition, the 2D momentum Flather condition and the 3D momentum and tracer radiation condition. Temperature and salinity from Levitus 1998 climatology are prescribed as lateral boundary conditions at the open northern boundary.

The atmospheric forcing for the first experiment corresponds to the Normal Year Forcing Version 2.0 – COREv2 – (Large and Yeager, 2009). The Normal Year Forcing consists of a single annual cycle of all the data needed to force an ocean model. These data are representative of climatological conditions over decades and can be applied

repeatedly for as many years of model integration as necessary (Large and Yeager, 2009; Griffies et al., 2009). It includes a 6–hourly 10 m winds, sea level pressure, 10 m specific humidity and 10m air temperature; the daily solar shortwave radiation flux and downwelling longwave radiation flux and the monthly precipitation. The air–sea interaction boundary layer is based on the bulk parameterization of Fairall et al. (2003). It was adapted from the Coupled Ocean–Atmosphere Response Experiment (COARE) algorithm for the computation of surface fluxes of momentum, sensible heat and latent heat. Surface salinity is relaxed to Levitus climatology with a time scale of 180 days.

In this study, the Normal Year Forcing was used on the first 100–year spin–up run. The annual simulation was used not only to warm up the model and provide stable starting fields for the interannual simulation, but also to validate the application setup. The interannual run was initialized with the last 10–year mean ocean fields from the annual simulation and forced with the interannual full 60–year cycle (1948–2007). The overall setup was kept from the previous simulation.

5.1.1 Common Ocean–Ice Reference Experiments – CORE

As described by Large and Yeager (2004) all aspects of the bulk forcing methodology are developed for two model configurations; a stand–alone Ocean General Circulation Model (OGCM) and an OGCM coupled to a Sea–Ice Model (SIM). The air–sea–ice surface boundary conditions are computed from the prognostic model surface temperatures, combined with the specified near surface atmospheric state (wind, temperature and humidity), downwelling radiation, precipitation and continental runoff. In the former, observed sea–ice concentration and specified ice–ocean fluxes effectively replace the SIM, and eliminate the need for air–ice fluxes. In both

cases, some restoring to observed sea surface temperature and/or salinity is possible.

A complete collection of forcing data sets is chosen on the basis of global coverage, spatial resolution, frequency duration and, to some extent, the needs and behavior of the ocean and sea–ice components of the Communty Climate System Model/NCAR. The global NCEP/NCAR reanalysis gives the atmospheric state, the recent ISCCP–FP product provides the radiation fields, the precipitation is a blend of multiple products, the continental runoff is derived from continental water budgets and climatological river discharge, the sea–ice concentration comes from the National Snow and Ice Data Center, historical SST is a reconstruction that has been made compatible with sea–ice concentration, and ocean salinity is non–standard at high latitudes. Other data sets are used to determine objective corrections to the forcing data sets, with the major factors a general increase in the wind speed, a reduction in the near surface humidity and a reduction in the solar insolation between 60 °S and 40 °N. Further adjustments to high latitude air–temperatures and downwelling longwave radiation are needed to improve water mass formation and sea–ice simulations. The corrected/adjusted forcing is used in conjunction with observed SST to produce an observationally based air–sea flux climatology over 60 years (1948–2007). A necessary achievement of the exercise is to lower the global air–sea heat flux over 17 years (1984–2000) from 31 W/m^2 heating to a more reasonable 1 W/m^2. A freshwater imbalance of 3.4 $mg/s/m^2$ is overcompensated by increased evaporation, so an overall increase in precipitation is used to give a nearly balanced (-0.1 $mg/s/m^2$) global mean budget.

The products based on 17–year mean fluxes include, global maps of the climatological heat, freshwater and momentum (wind stress) fluxes and their components,

zonal averages of the fluxes and flux components, the implied northward transports of heat and freshwater in each ocean basin. The climatological seasonal cycle is examined with the first and second annual harmonics of net heat flux, net freshwater flux, zonal wind stress, and meridional wind stress. Annual mean fluxes are zonally averaged over the three ocean basins in order to display interannual variability over 60 years (1948–2007), which is then related to the observed variability of several large scale climate indices. Global and basin averages of annual average heat flux reveal decadal variability, with persistently warming heat fluxes from about 1975 to 1990, and numerous cooling years both before and after.

Finally, as an alternative to forcing with a full 60–year cycle and its interannual variability, a "Normal" Year Forcing (NYF) was developed. It consists of single annual cycles of all the data needed to force an OGCM and SIM. For a given SST it produces comparable fluxes as the full cycle, provided the same corrections are applied. NYF is constructed so that it can be repeated over and over without initiating spurious transients, while still retaining seasonal and propagating synoptic (weather) variability.

5.2 Optimum Multiparameter Analysis – OMP

To investigate the water masses formation from the simulations results we have chosen the Optimum Multiparameter Analysis (OMP). It was introduced by Tomczak (1981) as a alternate option to expand the classic triangle mixing from TS diagrams. Many improvements were done until Tomczak and Large (1989) presented the term *Optimum Multiparameter Analysis*. OMP uses conservative and non–conservative sea water parameters to solve a linear system of mixing equations

(Equation 1, Tomczak and Large (1989); Tomczak et al. (1994); Tomczak (1999).

Tomczak and Large (1989), You and Tomczak (1993) and Hinrichsen and Tomczak (1993) showed that OMP can be successfully applied for mixing and ocean circulations where all hydrographic properties can be considered conservative. To expand it to non–conservative properties Karstensen and Tomczak (1997, 1998) introduced the Redfield ratios (Redfield et al., 1963), which allowed the correction of non-conservative terms for larger scale approaches.

$$\begin{cases} x_1\theta_1 + x_2\theta_2 + x_3\theta_3 + x_4\theta_4 + 0 = \theta_{Obs} + R_\theta \\ x_1S_1 + x_2S_2 + x_3S_3 + x_4S_4 + 0 = S_{Obs} + R_S \\ x_1O_1 + x_2O_2 + x_3O_3 + x_4O_4 - \Delta O = O_{Obs} + R_O \\ x_1N_1 + x_2N_2 + x_3N_3 + x_4N_4 + \Delta N = N_{Obs} + R_N \\ x_1P_1 + x_2P_2 + x_3P_3 + x_4P_4 + \Delta P = P_{Obs} + R_P \\ x_1Si_1 + x_2Si_2 + x_3Si_3 + x_4Si_4 + \Delta Si = Si_{Obs} + R_{Si} \\ x_1 + x_2 + x_3 + x_4 + 0 = 1 + R_{CMass} \end{cases} \quad (1)$$

OMP is based on a linear mixing model, where every property of one water mass is subjected to the same mixing processes and present the same turbulent mixing coefficients, allowing the spacial distribution of the water mass through the linear system of equations.

Water mass is a volume of water that, under atmospheric impact during a certain amount of time, is formed in a particular region of the ocean (Tomczak, 1999), where it gains physical properties that will only be changed by mixing processes, and can therefore be considered an physical entity occupying a finite volume in the ocean (Tomczak and Large, 1989).

Each water mass has mixing resulting physical properties from its formation site so that it may be represented by a water type: an ensemble of properties (such as thermohaline indexes) that represent a homogeneous water. When a water type presents the formation site properties it may be referred as a Source Water Type (SWT) (Tomczak et al., 1994).

OMP tries to estimates the contribution of a SWT in a water sample that represents an original water mass, with no mixing. Every water sample must be linear combinations of SWTs, with well known properties. OMP solves a linear mixing equation system, where the SWTs work as variables and the hydrographic properties as system parameters (Poole and Tomczak, 1999).

OMP estimates the best collection of contributions from all SWTs for each sample, allowing the spacial distribution of water masses. Two method restrains must be taken into account: the sum of every SWTs contribution must be 100% (mass conservation) and there can not be negative contributions, since the smallest contribution must be zero.

5.3 Analytical Description

The linear mixing equations can be represented in a matrix form. SWT parameters represent matrix G, SWTs contributions represented by a vector x, observed properties represented by vector B and the residuals by a vector R. Thus, we have: $\mathsf{Gx} = \mathsf{B} + \mathsf{R}$. Assuming a four SWTs mixing and a collection of properties (temperature, salinity, oxygen, phosphate, nitrate e silicate), we have the following matrix notation:

$$\begin{bmatrix} \theta_1 & \theta_2 & \theta_3 & \theta_4 & 0 \\ S_1 & S_2 & S_3 & S_4 & 0 \\ O_1 & O_2 & O_3 & O_4 & -rO/P \\ P_1 & P_2 & P_3 & P_4 & 1 \\ N_1 & N_2 & N_3 & N_4 & -rO/P \\ Si_1 & Si_2 & Si_3 & Si_4 & -rO/Si \\ 1 & 1 & 1 & 1 & 0 \end{bmatrix} \begin{bmatrix} x_1 \\ x_2 \\ x_3 \\ x_4 \\ \Delta P \end{bmatrix} = \begin{bmatrix} \theta_{Obs} \\ S_{Obs} \\ O_{Obs} \\ P_{Obs} \\ N_{Obs} \\ Si_{Obs} \\ 1 \end{bmatrix} + \begin{bmatrix} R_\theta \\ R_S \\ R_O \\ R_P \\ R_N \\ R_{Si} \\ R_{CMass} \end{bmatrix} \quad (2)$$

Equation 2, the last line in G represents the mass conservation and each column (j=1-4) represents the SWTs properties (Tj, Sj,Oj,Pj, Nj, Sij). Terms: rO/P, rN/P, rSi/P indicate the Redfield ratios and ΔP represents the changes in concentration due to biogeochemical reaction. OMP solves the equation b minimizing the residuals subjected to certain conditions (Equation 5.3), usually by the least square method (Emery and Thomson, 1998; Tomczak and Large, 1989; Mackas et al., 1987).

$$R^T R = (Gx - B)^T W^T W (Gx - B) = \sum_{i=1}^{m} W_i^2 \left(\sum_{i=1}^{n} G_i x_j - B_i \right)^2 \quad (3)$$

Equation 5.3 presents a crucial term for the system to be solve precisely: matrix W. W will weight the system, since data may have different quality levels. This way, each parameter is weighted to represent a water mass. To determine the weights in W one must look at the variance in G, as each parameter impacts the results differently and the water mass contribution. W is obtained by Equation 5.3, where σi is the parameter variance i between the SWTs in G and δi is the maximum variance between the parameters in the water mass source region.

$$W_i = \frac{\sigma_i^2}{\delta_{i(max)}} \tag{4}$$

It is also important to normalize the data in G, making them adimensional and thus, comparable. Normalized matrix G'_{ij} comes from Equation 5, where the difference between each value in G_{ij} and the line mean $\overline{G_i}$ (6) is divided by the standard deviation δ_i (7). In the same fashion, vector B is also normalized (Equation 8).

$$G'_{ij} = \left(G_{ij} - \overline{G_i}\right) \delta_i \tag{5}$$

$$\overline{G_i} = \frac{1}{n} \sum_{j=1}^{n} G_{ij} \tag{6}$$

$$\delta_i = \sqrt{\frac{1}{n} \sum_{j=1}^{n} \left(G_{ij} - \overline{G_i}\right)^2} \tag{7}$$

$$B'_i = \left(B_i - \overline{G_i}\right) / \delta_i \tag{8}$$

Finally, there is the Redfield ratios normalization through Equation 8, that results from G' divided by G and multiplied by the Redfield itself:

$$r'_{tracer/P} = \frac{(G'_i)_{max} - (G'_i)_{min}}{(G_j)_{max} - (G_j)_{min}} r_{tracer/P} \tag{9}$$

Once normalized, the equations allow an objective evaluation of the solution quality. Low residuals suggest that the samples are well represented by the SWT

collection. The upper limit in residuals (5%) of mass conservation can be used to remove regions poorly represented by SWTs (Budillon et al., 2003).

6 Results

6.1 Model Validation

To evaluate the model stability, kinetic energy and potential energy were monitored along the entire simulation. Figure 14 displays the model normalized energy evolution during the first 30 years of simulation. Although the model had already stabilized after 30 years of simulation, the water column was not yet in good agreement with the observed structure in the Southern Ocean. The model was run for additional 70 years in order to comprise two climatological cycles (33 years), which allowed the thermohaline structure to adjust.

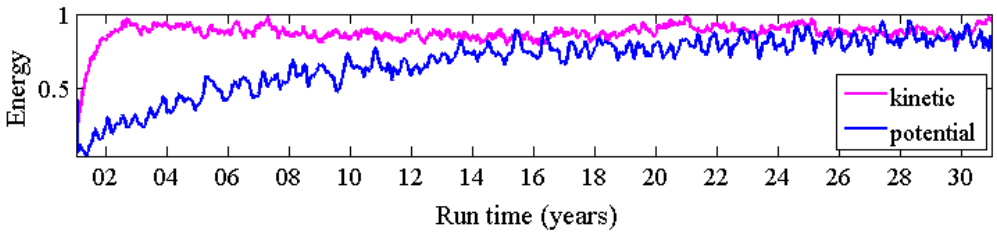

Figure 14: Normalized energy evolution (kinetic and potential) for the annual simulation. It took about 30 years to the model to stabilize, but additional it was run for 70 years in order to produce a more realistic representation of the thermohaline structure in the Southern Ocean.

To assess ROMS capability to realistically represent the main cryosphere–linked oceanographic processes with thermodynamically active sea ice/ice shelf, the last 10–year mean temperature and salinity data from the 100–year annual cycle run were

analyzed on two cross sections: one in the Ross Sea along the 165 °W longitude and the other in the Weddell Sea along the 40 °W longitude (Figure 10 and Figure 12, respectively).

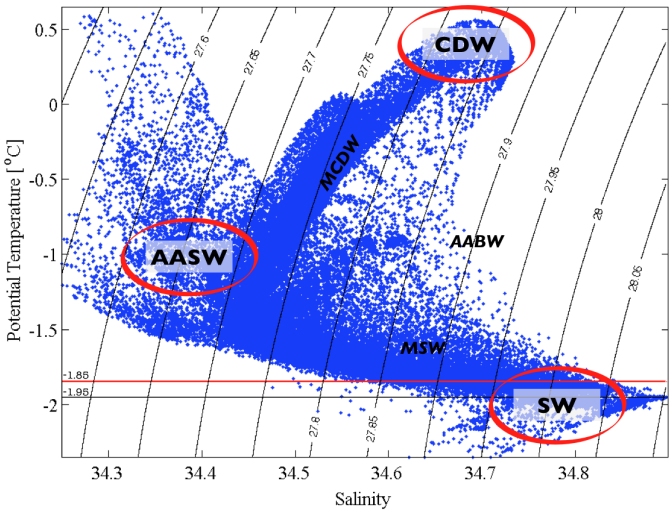

Figure 15: Scattered θ−S diagram created with the simulation results showing the main Ross Sea water Masses. AASW: Antarctic Surface Water, CDW: Circumpolar Deep Water, MCDW: Modified Circumpolar Water, AABW: Antarctic Bottom Water, MSW: Modified Shelf Water, SW: Shelf Water.

We build the scattered θ–S diagram (Figure 15) with data from the RS 165 °W cross–section (Figure 10) in order to validate against observed data of Orsi and Wiederwohl (2009) and to check the water column structure represented by the model. The overall structure quite similar to Orsi and Wiederwohl (2009), where the warm CDW, fresh AASW and the cold and salty SW can be identified. As for most of numerical models, some biases are expected, no matter how good the simulation may be. In that sense, we must point that although the scattered θ–S displays the same triangular–shaped distribution as for Orsi and Wiederwohl (2009), the temperature field structure appears to be slightly different. Orsi and Wiederwohl

(2009) suggest the CDW to be between 1.0 °C and 1.5 °C temperature range, while our results show CDW between 0 °C and 0.5 °C in agreement with Bergamasco et al. (2002b). One might discuss that this difference may be related to the region sampled, since Orsi and Wiederwohl (2009)'s θ–S scatter plot represents the entire Ross Sea and ours represents only the RS 165 °W cross–section. However, the RS cross–section coincides with the region where CDW enters the Ross Sea within the Ross Gyre and, although some interaction with cold AASW above is to expect, this 1.0 °C difference may be slightly overestimated and would rather represent the formation of MCDW (Stover, 2006; Orsi and Wiederwohl, 2009). Nevertheless, these results are consistent with Assmann et al. (2003) numerical experiments where MCDW is centered at the 27.80 kgm^{-3} density layer, while our results show MCDW between the 27.75 and 27.80 kgm^{-3} density layers.

The scattered θ–S diagram obtained with the simulation results was used to obtain the SWTs for the OMP analysis (Table 1). Three water masses properties values were chosen considering both the observed data values and the intrinsic model bias in order to assess whether this numerical simulation was able to fully represent the water column structure for this sector of the Ross Sea. The OMP analysis results show water masses contribution maps (%) for AASW, CDW and SW (Figure 16 upper panel, Figure 16 middle panel, Figure 16 lower panel, respectively).

The AASW (Figure 16 upper panel) occupies the surface layers along most of the cross–section extent with salinity ranging from 34.30 to 34.45 and temperature centered at –1.0 ° C, consistent with Orsi and Wiederwohl (2009). Higher contribution values ($> 90\%$) will not show deeper than 200 m, except for the region near the shelf break where AASW reaches 500 m. Some AASW contribution is found in the upper

Table 1: Water Types derived from the Ross Sea θ−S diagram

Water Mass	Salinity	Temperature
AASW	34.37	–1.0
CDW	34.68	0.5
SW	34.78	<–1.85

layers over the continental shelf and close to the ice shelf, where sea ice formation will impact to transform it into SW to be the densest water mass around Antarctica (Orsi and Wiederwohl, 2009). The saltier MCDW originated by the CDW that makes its way into the continental shelf is also part of this process. The MCDW was not individually assessed in this work due to OMP numerical constraints, but an important interaction between AASW and CDW close to the shelf break may also be seen on OMP results (Figure 16 upper panel and Figure 16 middle panel).

As described by Worthington (1981) the CDW (Figure 16 middle panel) appears as the most voluminous water mass, identified as a thick layer between the upper and colder AASW and the saltier AABW. As CDW is branched from ACC and carried southward by the Antarctic Coastal Current between 160 °W 165 °W (Orsi and Wiederwohl, 2009), it is found at intermediate layers from northern limit of the cross–section 65°S to the continental slope at 75 °S where its incursion seems to be blocked by AASW near the shelf break. 34.68 salinity values are consistent with observational data, even though the model has represented CDW at least half degree colder (0.5 °C) than Orsi and Wiederwohl (2009) results around 1.0 °C. Small CDW contribution values at the bottom layers is probably related to the presence of AABW, although this water mass was not separated in this investigation. As

described by several authors (Jacobs et al., 1985; Budillon et al., 2002; Smethie Jr and Jacobs, 2005; Budillon et al., 2011), AABW results from the interaction between the CDW (MCDW) and dense shelf waters. Figure 16 lower panel shows the contribution of the SW, which displays some (~30%) contribution of this water mass at the bottom layers away from the continental slope.

Following Orsi and Wiederwohl (2009), we have established the upper limit of the SW (Figure 16 lower panel) as the sudden scatter reduction at -1.85 °C, here centered at the 28.00 kgm^{-3}. Here the SW seems to be more restrained to the salinity range of 34.65 – 34.90 compared to the S>34.50 suggested by Orsi and Wiederwohl (2009), what makes these consistent results. The densest SW is a feature of the RS continental shelf and has its distribution pretty much constrained by the topography. OMP results show the SW spreading along the bottom layers of the shelf and clearly trapped by the risen shelf break. The SW (Figure 16 lower panel) occupies the bottom layers over the continental shelf and deepens towards the base of the ice shelf. Observational studies such as Budillon et al. (2003) point that the ISW spreads along the deep layers of the shelf, but over a thin layer of HSSW, which agrees with the believed formation process for the ISW. They discuss that from the 400 m depth to the bottom of the continental shelf there is essentially a mixture of HSSW and ISW that reach to shelf break to take part in the formation of the AABW. As suggested by Jacobs (2004) the ISW is defined as being colder than the sea water freezing point (at surface) with its formation occurring by means of melting at the RIS base. Although the ice shelf used in this simulation is static in time, its thermodynamic is enough to reproduce such melting processes. However, for the model validation, SW was not separated into regional components (HSSW,

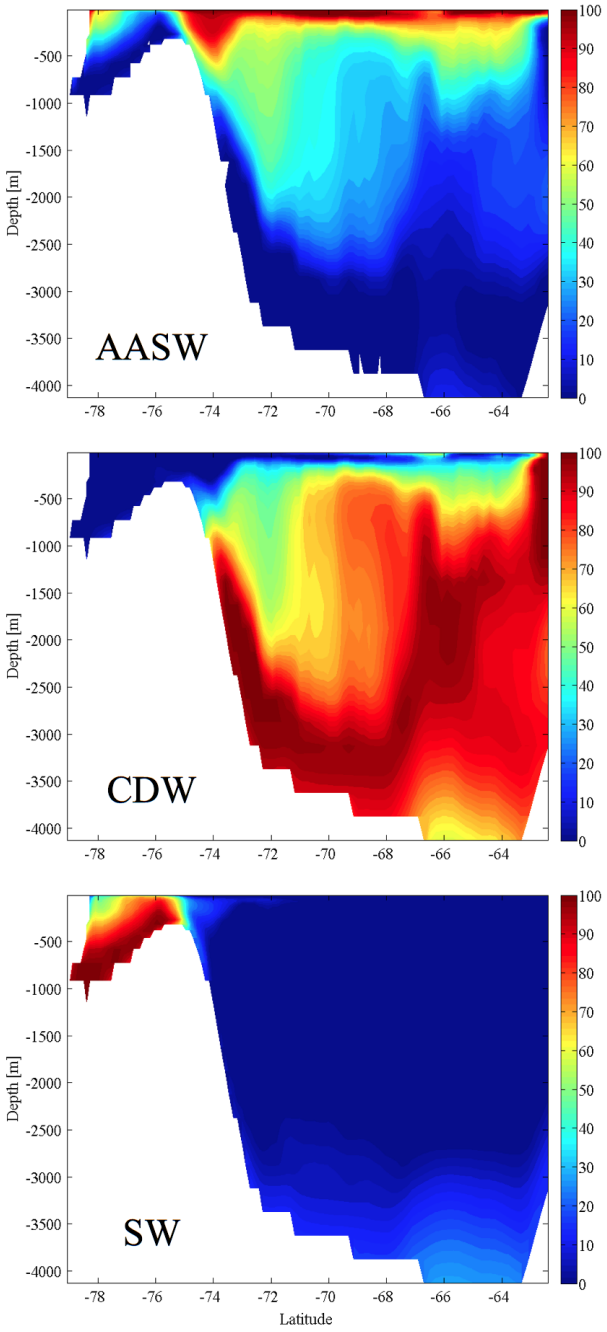

Figure 16: Water masses contribution (%) from OMP analysis along the 165°W cross–section in the Ross Sea. Upper panel shows Antarctic Surface Water (AASW); middle panel shows Circumpolar Deep Water (CDW); lower panel show the Shelf Water (SW).

LSSW and ISW). As discussed by many authors (Budillon et al., 2003; Holland et al., 2003; Muench et al., 2009; Orsi and Wiederwohl, 2009), the formation and export of the SW and its components occurs in pulses related to the polynias recurrence.

Another feature to be noticed is the very light contribution of the SW on the oceanic basin at 4000 m depth, where the AABW takes place. Since the AABW results from the interaction of the SW and the CDW near the shelf break, these results suggest that the model may be reproducing important processes such as the AABW formation.

The same procedure was adopted to assess the water masses representation in the Weddell Sea. Data from the WS 40 °W cross–section (Figure 12) to build the scattered θ–S plot (Figure 17) in order to validate against observed data of (Nicholls et al., 2009) and to evaluate the water column structure represented by the model. The results are consistent with the observations and the main water masses were reproduced with some deviations. The CDW appears as a warm ($\theta \approx 1.5\,^{\circ}C$) and salty ($34.8 < S < 34.9$) water on the top corner of the triangular distribution of the θ–S diagram (Figure 17). The θ–S plot presented by Nicholls et al. (2009) used data from CTD profiles south of 70 ºS and shows Warm Deep Water (WDW) ($\theta \approx 0.5\,^{\circ}C$ and $34.6 < S < 34.7$) on the warmer portion of the diagram. The CDW is converted into fresher and colder WDW (both shown together on the θ–S plot) as it flows along the continental slope within the Weddell Gyre (Whitworth III et al., 1998). The difference is to expect, since the cross–section analyzed here has extends until 60°S (comprising the oceanic regime dominated by CDW), while the data used by Nicholls et al. (2009) were restricted to the continental shelf and shelf slope, and therefore, only WDW would show.

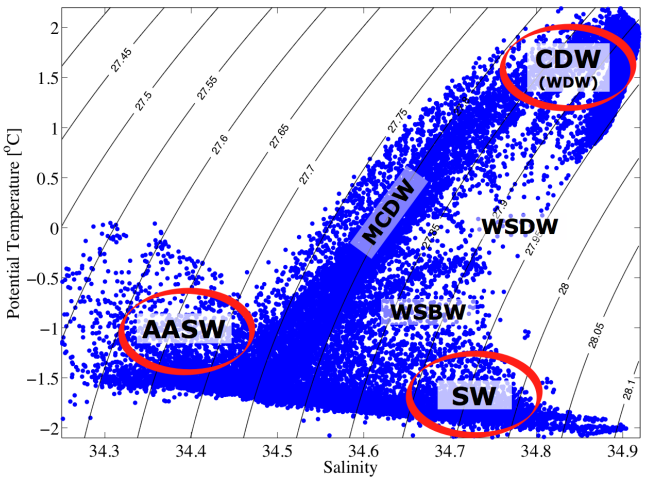

Figure 17: Scattered θ−S diagram created with the simulation results showing the main Weddell Sea water Masses. AASW: Antarctic Surface Water, CDW: Circumpolar Deep Water/WDW: Warm Deep Water, MCDW: Modified Circumpolar Water, SW: Shelf Water, WSDW: Weddell Sea Deep Water, WSBW: Weddell Sea Bottom Water.

The θ–S signature of the Weddell Sea Deep Water (WSDW) is not observed in the θ–S diagram, which should be slightly colder than the WDW (Nicholls et al., 2009). However, this may also be related to the region sampled, since WSDW is mainly formed in the western part of the WS (Nicholls et al., 2009) and the 40 °W cross–section is placed in the eastern part of the WS. The Weddell Sea Bottom Water (WSBW), in turn, displays good agreement with the observations (θ ≈ -1.0 °C and S ≈ 34.7), and is found to be only a little saltier (≈ 0.1) than the results by Nicholls et al. (2009). The Antarctic Surface Water (AASW) is represented by the model with a narrower salinity range ($34.3 < S < 34.45$) against the observations wider distribution ($34.0 < S < 34.4$), and ≈0.5 °C colder (θ ≈ -1.0 °C) against (θ ≈ -0.5 °C) by Nicholls et al. (2009). Finally the cold dense Shelf Water (SW) shows good agreement with the observations (θ ≈ -1.7 °C and $34.6 < S < 34.8$), suggesting

that the model is reproduces the ocean–ice interaction under the FRIS. Table 2 shows the SWTs used to run the OMP analysis to separate the WS water masses.

Table 2: Water Types derived from the Weddell Sea $\theta - S$ diagram

Water Mass	Salinity	Temperature
AASW	34.40	–1.0
CDW	34.8	1.5
SW	34.73	$<$–1.75

Although some differences can be found between the regional varieties of the water masses, the overall distribution of the water masses in the Weddell Sea is pretty similar to the Ross Sea. The AASW spreads along the surface for the entire cross–section (Figure 18 upper panel). Close to the shelf break some AASW contribution can be found in deeper layers, down to 400 m, where it may take part on water mixing (Whitworth III et al., 1998). Similar to the RS, some AASW is found over the inner continental shelf where it participates on the shelf waters formation (Orsi et al., 1993). Figure 18 middle panel shows the CDW contribution along the cross–section, where the water mass appears as previously described: a thick layer of warm salty water placed between 1000 m and 3000 m depth bordering the continental slope. This represents the CDW branched off the ACC by the Weddell Gyre that advects heat to the WS continental shelf (Carmack, 1977; Orsi, 1999; Naveira Garabato et al., 2002). The CDW contribution at the northern part of the cross–section is related to the northern outflow branch of the Weddell Gyre. Figure 18 middle panel also depicts some CDW contribution at the bottom layers between the continental slope and the Scotia Ridge, which suggests its participation on the AABW formation

(Whitworth III et al., 1998).

Finally, SW appears partially trapped by the continental shelf topography (Figure 18 lower panel). Although the time averaging of the date was expected to mask some of the regional dynamics, some SW is found on the edge of the shelf break as if it was about to flow downward the shelf slope. This is consistent with the suggested mechanism of AABW formation (Carmack, 1977; Whitworth III et al., 1998; Naveira Garabato et al., 2002; Nicholls et al., 2009) and is corroborated by the SW contribution found in the ocean bottom adjacent to the continental slope.

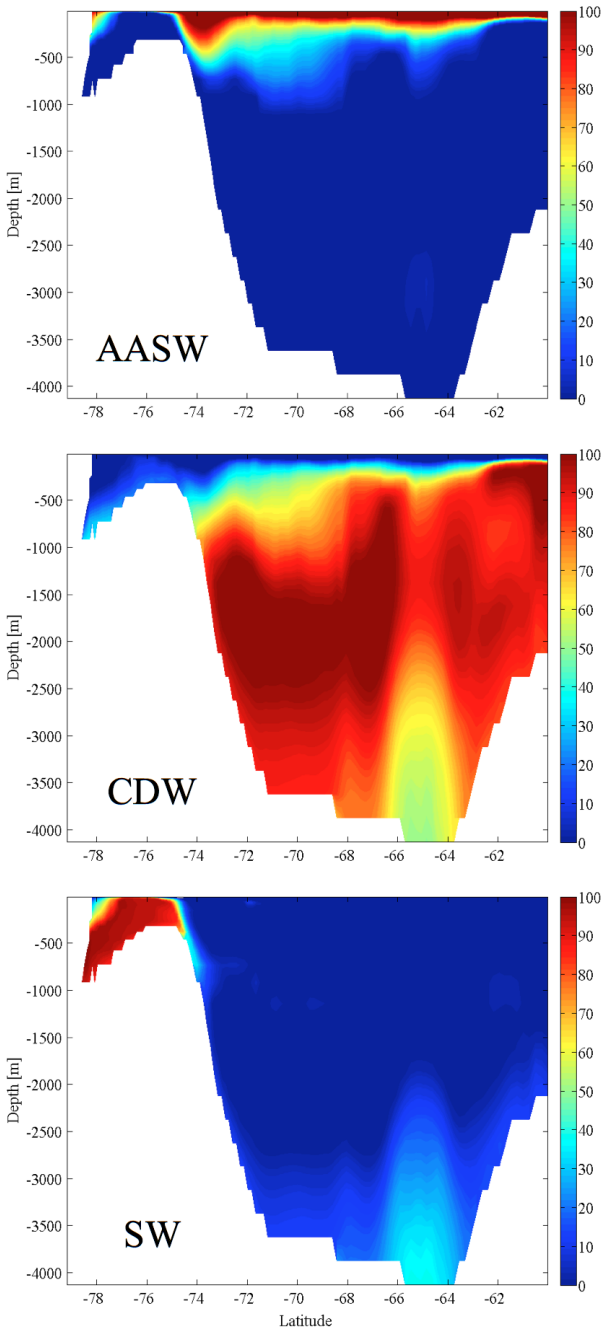

Figure 18: Water masses contribution (%) from OMP analysis along the 40°W cross–section in the Weddell Sea. Upper panel shows Antarctic Surface Water (AASW); middle panel shows Circumpolar Deep Water (CDW); lower panel show the Shelf Water (SW).

6.2 Interannual Simulation

6.2.1 Ross Sea Water Masses

As described by many authors (e.g. Budillon et al. (2011); Smethie Jr and Jacobs (2005); Bergamasco et al. (2003)), the primary pathways for dense water export from the Ross Sea are the cross–shelf topographic channels: the Drygalski Trough (DT) in the western RS; the Joides Trough (JT), between DT and the Pannell Bank; and the Glomar–Challenger Trough (GCT) in the centraleastern RS (Figure 10). To assess the RS shelf waters representation and variability for the interannual simulation, we have analyzed temperature and salinity data referring to 3 cross–sections (S1, S2 and S3) following the topographic channels as shown in Figure 22. The first two cross–sections (S1 and S2) are placed close to the formation site of the High Salinity Shelf Water (HSSW) that will either interact with the Modified Circumpolar Deep Water (MCDW) at the shelf break region or flow southward underneath the ice shelf to produce the Ice Shelf Water (ISW). The extensive S3 cross–section covers the shelf and the oceanic domain of the Ross Sea, extending from the ice shelf cavity (where the formation of the ISW takes place), across the shelf slope region (where important water mixing occurs), onto the deep basin where the newly formed Antarctic Bottom Water (AABW) spreads northward. The S3 cross–section was analyzed in two separate segments regarding the oceanographic regimes in the RS; the southern segment covering the shelf area and the continental shelf break, and the northern segment covering the shelf slope

and deep ocean region.

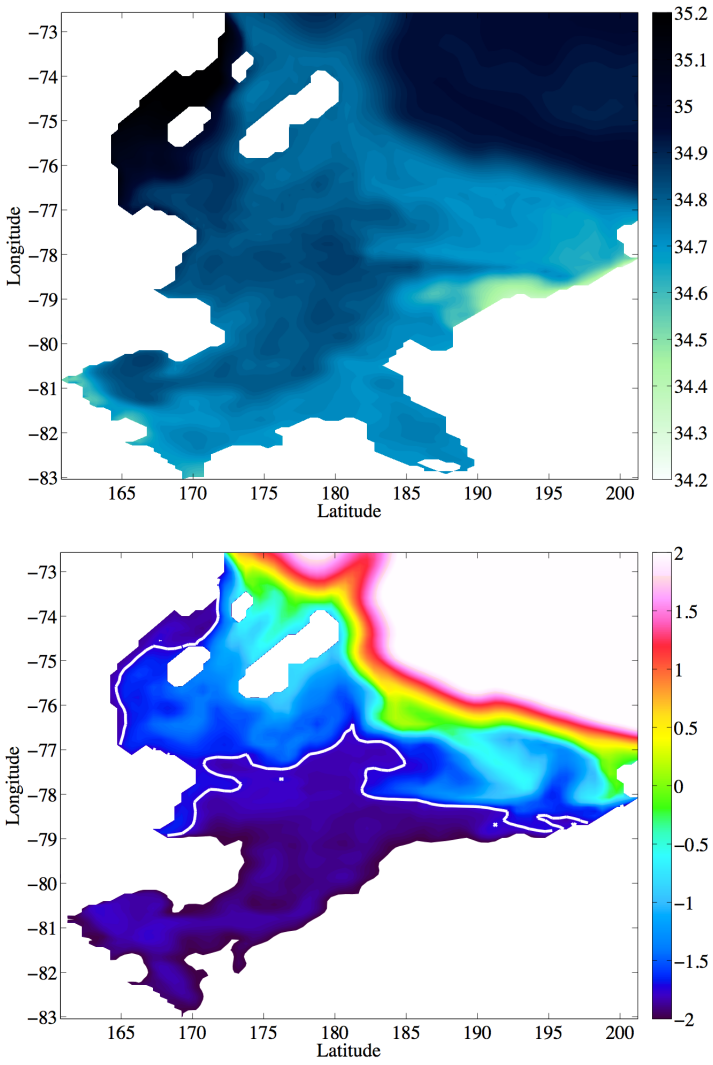

Figure 19: Bottom salinity (upper panel) and bottom temperature (bottom panel) over the Ross Sea continental shelf. The white line represents the model water freezing temperature (-1.9°C), which restrains the Ice Shelf Water domain.

Figure 19 upper panel shows the time–averaged bottom salinity of the Ross Sea. First thing to be noticed is the east–west salinity gradient which is a very important feature of the RS (Jacobs et al., 1985). The salty waters at the western RS highlight the source region of the High Salinity Shelf Water (HSSW), while the relatively fresher waters at the eastern RS represents the Low Salinity Shelf Water (LSSW)

formation site (Locarnini, 1994; Jacobs et al., 1985; Budillon and Spezie, 2000; Fusco et al., 2002). As for the bottom temperature, Figure 19 bottom panel displays the temperature gradient between the ice cavity and the shelf slope. The supercooled water widely spread south of 78°S represents the Ice Shelf Water (ISW), which is characterized by temperatures lower than the freezing point (Budillon et al., 2002; Smethie and Jacobs, 2005). Most of the ISW spread under the Ross Ice Shelf on the central continental shelf of the RS, from where it moves northward toward the shelf slope along the GCT to take part in the formation of the AABW (Dinniman et al., 2007; Orsi and Wiederwohl, 2009; Budillon et al., 2011).

With respect to water masses variability, the model data were analyzed as decadal means referred to the last five decades of the XX^{th} century and the first decade of the XXI^{st} century. The decadal mean data were used to create the θ–S diagrams for the entire Ross Sea for each decade: 1950, 1960, 1970, 1980, 1990 and 2000 (Figure 20). Assessing these diagrams, we were able to recognize some changes in the thermohaline structure of the RS. The first explicit changes are related to do Circumpolar Deep Water.

Throughout the 60 years of simulation, CDW became warmer ~1 °C with no significant changes in salinity. This is consistent with Gille (2002) who has reported an warming trend on the Southern Ocean, spanning from 0.01°C/year to 0.03°C/year in the Pacific sector. Although one might argue that Gille (2002) results would not reach south of 55°S, the CDW warming in the numerical results are still consistent with the observed temperature trends. Bearing in mind the origin of the CDW, which is branched off the ACC by the northern limb of the Ross Gyre and transported to the shelf slope region (Orsi and Wiederwohl, 2009), this water mass is the

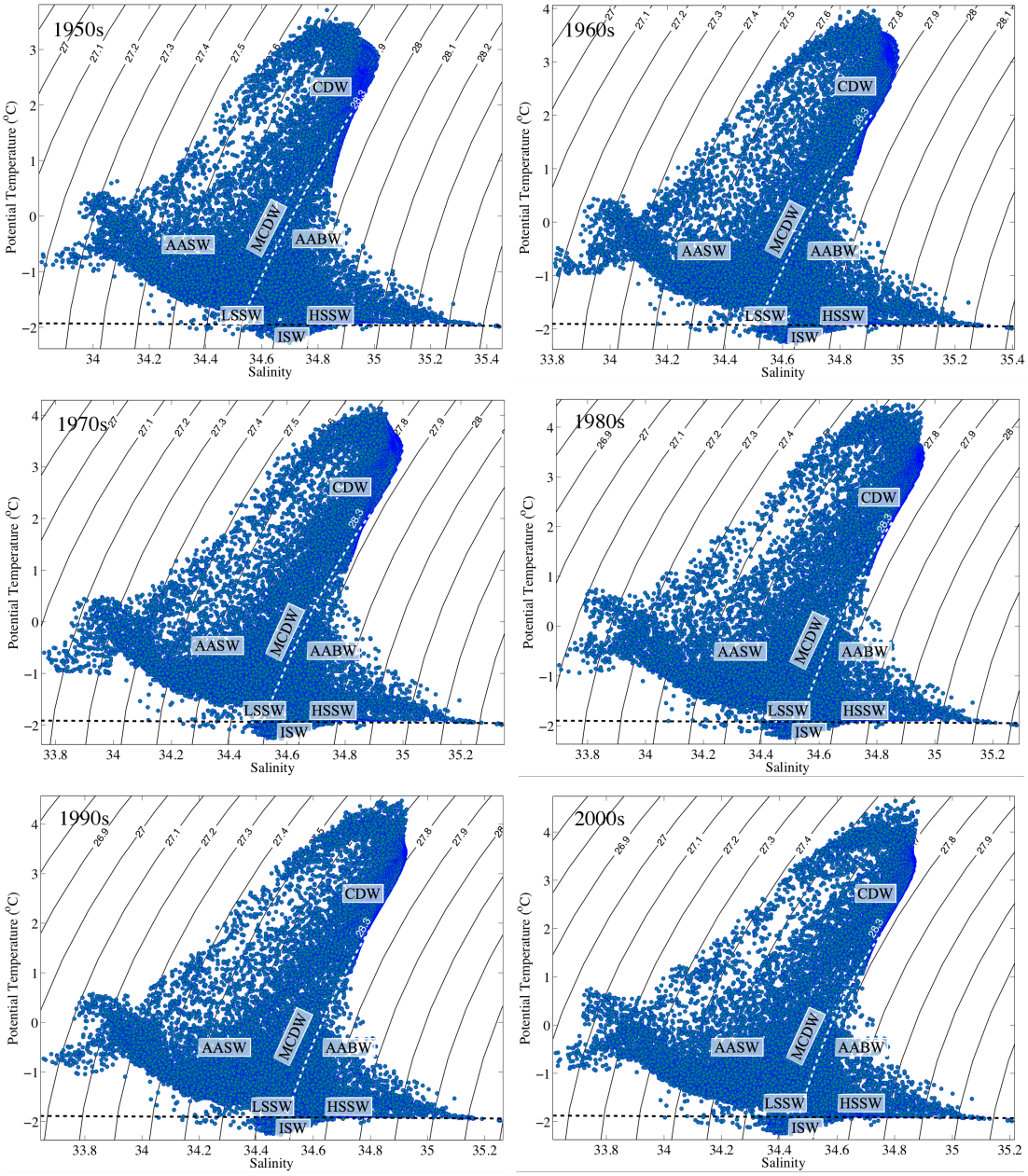

Figure 20: *θ−S diagrams for the entire Ross Sea for the six decades: 1950, 1960, 1970, 1980, 1990 and 2000 (left to right and top to bottom). The white dashed line represents the* $\gamma^n = 28.3\ kg.m^{-3}$ *surface as the upper limit of the AABW and the black dashed line represents the surface freezing point of seawater.*

ultimate heat source for the Ross Sea continental shelf (Stover, 2006). Ergo, any warming on the northern limits of the RS is expected to occur within the southern

limb of the RG as well, and beyond that, is rather relevant to the water masses formation at the shelf slope region.

Changes were also found for the other main water masses of the Ross Sea. The Antarctic Surface Water exhibits no significant warming trend, however, a freshening of about 0.1 is observed. In the same fashion, the Shelf Water and the Antarctic Bottom Water display a freshening of ~0.2 and no relevant warming. This is consistent with Jacobs et al. (2002) who have observed a substantial decrease in shelf water salinity over the past four decades in the Ross Sea of about 0.09 at the surface layers, ~0.1 at mid layers (~400 m depth) and about 0.13 at depths of 900 m, from the 1950s to the 2000s. According to Jacobs et al. (2002), the shelf water is vertically stabilized by salinities that increase with depth, but the entire water mass has shifted toward lower values since the 1950s.

As more heat is transported into the continental shelf but no relevant warming is observed in the shelf waters, the energy balance must be affecting the cryosphere components. Two cryosphere–linked processes might lead to this scenario: first, warmer waters on the continental shelf would enhance basal melting under the ice shelf producing less salty waters; second, warmer waters would inhibit the sea ice formation and the consequent brine rejection, also leading to the freshening of the shelf waters. Since the ice shelf parameterization used in this investigation is thermodynamically active, but static in time with no mass exchange, we believe that the waning in the sea ice formation should be credited for the salinity decrease in the shelf waters.

From the decadal means, we are not able to assure whether an ice coverage decline would be more related to the weakened sea ice formation or the increase in

the amount of ice that fails to survive the summer. Either way, the water column thermohaline structure will respond to the waning of the sea ice coverage. To assess this hypothesis, we have analyzed the Ice Fraction (the fraction of the model grid cell covered by sea ice) along the 6 decades in the western and the eastern parts of the RS. As presented in Figure 21, the western portion of the Ross Sea has experienced a smooth decline in the ice fraction of almost 10% starting from 99% coverage in the beginning of the simulation until 90% coverage in the 2000 decade mean. Although this ice coverage decrease might impact the brine release to the water column, it was still not strong enough to hinder the production of the HSSW, therefore preserve the characteristic east–west salinity gradient at the bottom of the RS continental shelf as displayed in Figure 19. The eastern Ross Sea, however, is subject to a more significant influence of the CDW heat influx. Throughout the 6 decades of simulation the ice fraction in the eastern RS dropped from around 77% in the 1950s to 50% by 2000.

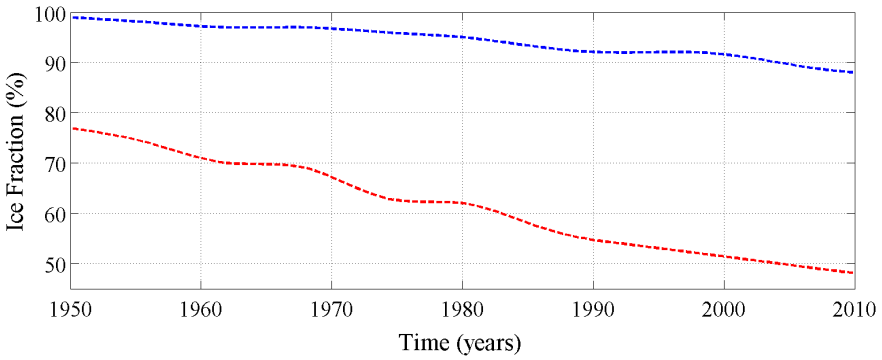

Figure 21: Sea ice fraction evolution throughout the 60–year interannual simulation. Blue represents the western Ross Sea ice coverage and red represents the eastern Ross Sea ice coverage.

6.2.2 Ross Sea Water Masses Variability

The Ross Sea water masses variability is analyzed through decadal means of temperature and salinity data from the interannual simulation along the three cross–sections presented in Figure 22: S1, S2 and S3. These data were first used to create vertical sections of temperature and salinity to create θ–S diagrams for each decade along S1, S2 and S3 Figure 23.

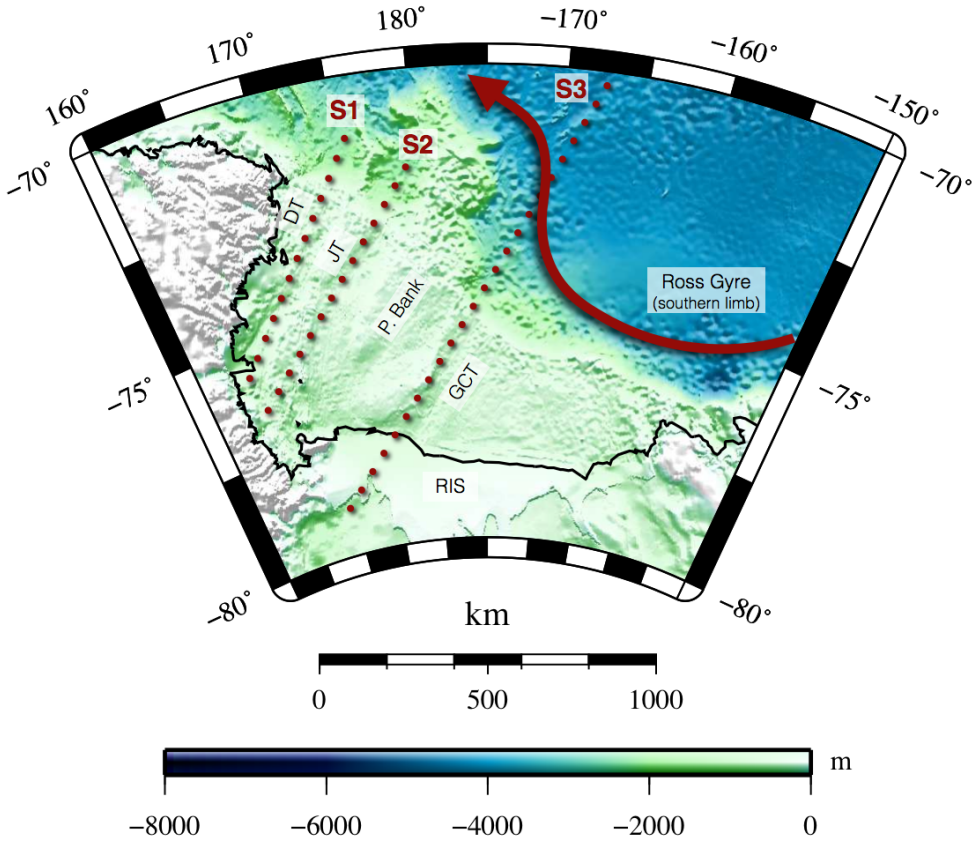

Figure 22: Ross Sea cross–shelf topographic channels (Drygalski Trough – DT, Joides Trough – JT and Glomar–Challenger Trough – GCT), Pennell Bank rise – PB, and the Ross Sea Ice Shelf – RIS. Full arrow represents the southern limb of the Ross Gyre. Dotted lines following the topographic channels represent the cross–sections analyzed for water masses investigation: S1, S2 and S3.

From the θ–S diagrams we have extracted the SWTs for the water masses inves-

tigation. Table 3 displays the θ and S interval span covered to perform the OMP analysis for each water mass. The separation scheme was run several times for each decade and for each cross–section with slight variations of the SWTs within 10% of the θ–S interval range. The decadal averaged contribution was considered for S1, S2 and S3 separately. The SWTs for the shelf waters were extracted from θ– S diagrams created with data from each cross–section. Figure 23 shows the 1950s θ– S diagrams for S1, S2 and S3 on the left and the 2000s θ– S diagrams on the right. The side–by–side comparison of the first and last decades highlights the evolution of the water column properties, in particular, the warming trend of the MCDW and overall freshening trend.

Figure 24 shows the spacial contribution (%) of the AASW, the MCDW and the HSSW water masses along the S1 cross–section for the first (1950) and the last (2000) decades of the simulation. The vertical distribution is consistent with observations. As described by Orsi and Wiederwohl (2009), the AABW occupies mainly the mixed layer (down to 100 m depth) with values of θ ∼ -1.5 °C and salinity $<$ 34.40 (Figure 20), quite similar to properties reported by Bromwich and Kurtz (1984) and Jacobs et al. (1985). Although it is not clear in the OMP results, the AASW has changed during the 6 decades. The water mass salinity decreased from 34.48 in the 1950s to 34.30 in the 2000s along the S1 cross–section.

The MCDW derives from the warm and salty CDW that is captured by the cyclonic Ross Gyre. As it reaches the shelf slope flowing westward, CDW becomes MCDW, whose properties are progressively attenuated, becoming less salty and colder. As described by Stover (2006) the MCDW is able to penetrate the continental shelf through the cross–shelf break topographic depressions. As the S1 section

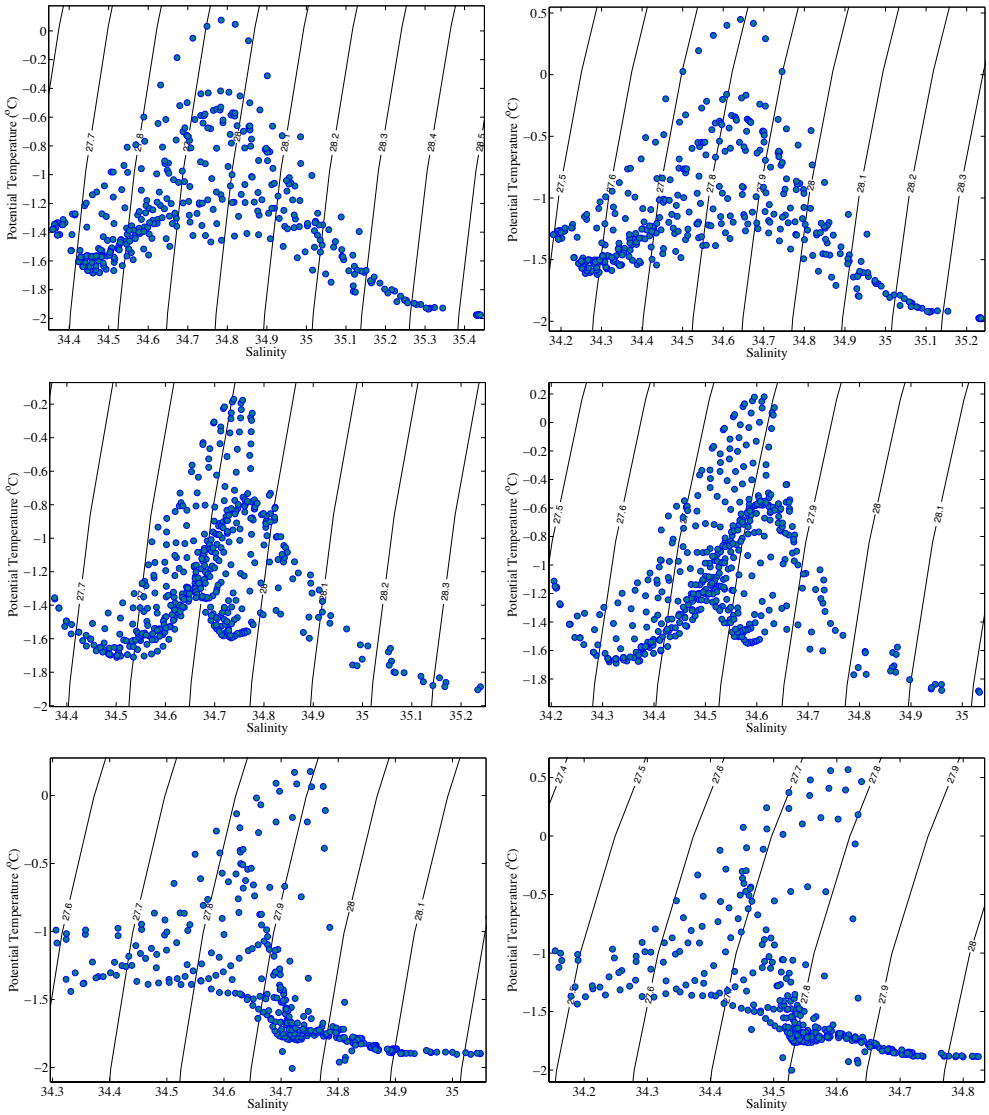

Figure 23: *θ–S diagrams for the shelf cross–section S1 (top panels), S2 (mid panels) and S3 southern segment (bottom panels). The left panels represent the 1950s data and the right panels represent the 2000s data.*

follows the Drygalsky Trough, we are able to perceive this water mass intrusion, which appears here as a fairly cold (θ ~ -0.65°C) and salty (S ~ 34.78) water. The MCDW properties vary during the 6 decades to become 0.15 less salty and ~ -0.3°C warmer by 2000. Since S1 is the westernmost cross–section in the RS, the MCDW variety found here has experienced more interactions with shelf slope waters and,

Table 3: Water Types derived from scattered θ−S diagrams of the S1, S2 and S3 cross–sections. Slash separated values refer to the water mass property variation during the simulation period.

Cross–section	Water Mass	Salinity	Temperature
S1	AASW	34.48 / 34.32	–1.5
	MCDW	34.78 / 34.63	–0.65 / –0.35
	HSSW	35.20 / 34.95	–1.8
S2	AASW	34.50 / 34.32	–1.55
	MCDW	34.78 / 34.63	–0.75 / –0.48
	HSSW	35.05 / 34.85	–1.8
S3 – south	AASW	34.42 / 34.28	–1.2
	MCDW	34.70 / 34.58	–0.0 / 0.5
	ISW	34.85 / 34.70	< -1.85
S3 – north	AASW	34.30 / 34.25	–0.5 / –0.3
	CDW	34.90 / 34.85	2.5 / 3.2
	AABW	34.80 / 34.63	–0.4 / –0.3

therefore, warming trend is not as intense as for the eastern RS.

The HSSW is also very well represented in this simulation. Formed in the western Ross Sea by means of brine rejection due to sea ice formation, the HSSW appears as a very dense ($\theta \sim$ -1.8°C and S ~ 34.80; Figure 20) water mass spreading along the bottom of the continental shelf, consistent with previous studies (Van Woert, 1999; Budillon and Spezie, 2000). At the bottom some HSSW flows towards the shelf slope and some flows south towards underneath the RIS to produce the ISW (Orsi and Wiederwohl, 2009), which is assessed in S3. Again, we cannot notice any

relevant variation in HSSW vertical distribution from the OMP results. However, although the local variety of the HSSW has kept the cold signature throughout the simulation, it also became less salty, dropping from ~ 35.20 in the 1950s to ~ 34.95 by 2000.

The water masses distribution for the S2 cross–section (Figure 25) are similar to the pattern found in the S1 section. The AASW is observed in the mixed layer and limited to 100 m detph. It is slightly saltier and colder than in S1 (S ~ 34.5 and θ ~ -1.55ºC). The AASW experiences a decrease of about 0.18, reaching S ~ 34.32 at the end of the simulation. MCDW is a bit colder than the one found along S1 (θ ~ -0.75ºC and S ~ 34.78). Since the Joides Trough exhibits a deeper shelf break, MCDW is able to penetrate further south with a more prominent contribution when compare

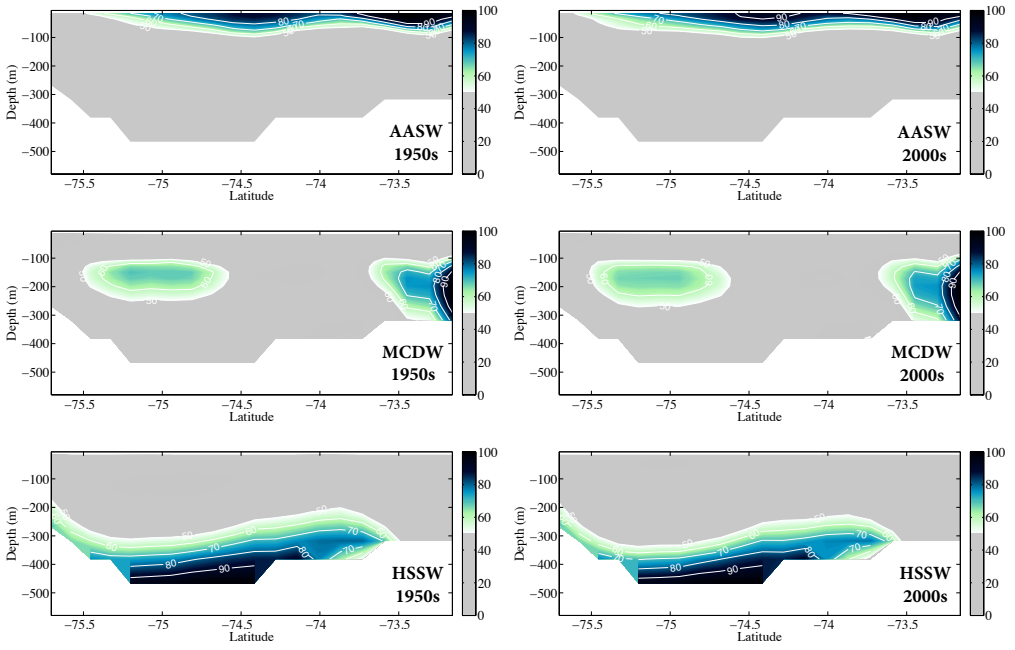

Figure 24: Water masses contribution (%) along the S1 section. The left panels refer to the 1950s and the right panel refer to the 2000s. Top panels display the AASW contribution, mid panels display the MCDW contribution, and bottom panels display the HSSW contribution.

to the Drygalsky Trough. Finally, the HSSW appears at the southern portion of the section, trapped by the topography. The HSSW here has been channeled eastward from the western RS and is slightly fresher than is S1 counterpart (~ 35). The HSSW salinity decreases to 34.85 during the simulation period.

The S3 cross–section displays a very interesting water mass distribution. Starting with the southern segment (Figure 26), we are able to observe the AASW at the surface layers, relatively warmer and fresher (θ ~ -1.2°C and S ~ 34.42) than the western AASW. This has direct bearing with the central location of the S3 following the Glomar–Challenger Trough (GCT), which makes AASW subject to the impact of the recently formed MCDW. During the simulation, the AASW along S3 experiences an important decrease in salinity from 34.42 in the 1950s to 34.28 in the 2000s.

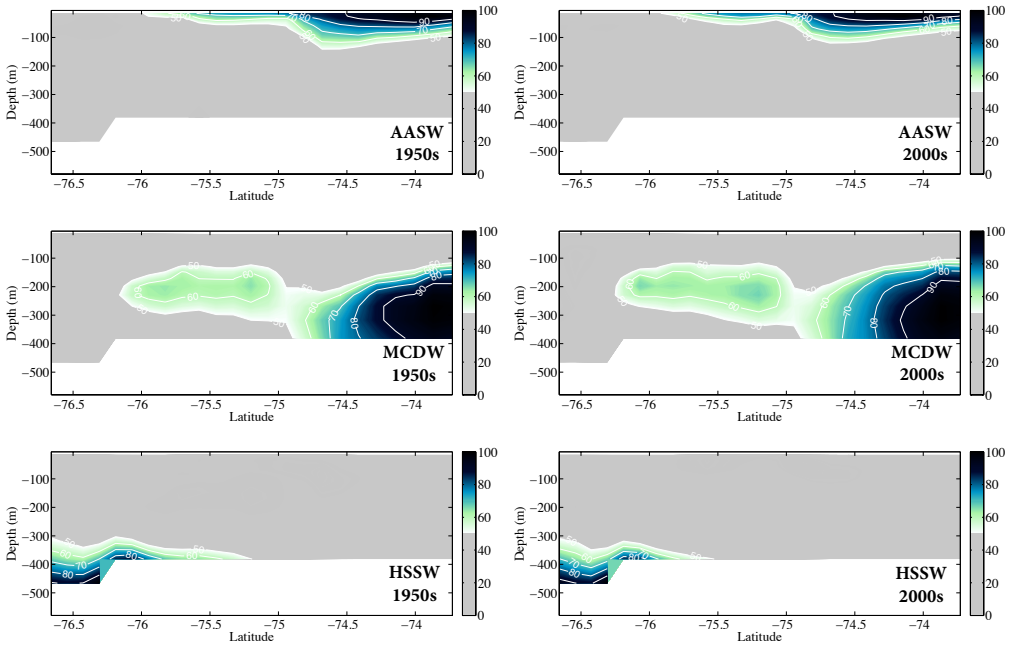

Figure 25: Water masses contribution (%) along the S2 section. The left panels refer to the 1950s and the right panels refer to the 2000s. Top panels display the AASW contribution, mid panels display the MCDW contribution, and bottom panels display the HSSW contribution.

The MCDW shelf intrusion is also observed at the shelf break vicinity. Since GCT is placed further east compared to GT and JT, MCDW is relatively warmer along S3 ($\theta \sim$ -0.2°C) but also slightly fresher (S ~ 34.62). Throughout the simulation period, the local variety of MCDW gets warmer (~ 0.5°C) due to the increased heat influx from CDW, and ~ 0.12 fresher.

Finally, there is the supercooled ISW ($\theta \sim$ -1.9°C) spreading along the continental shelf bottom under the ice shelf. The GCT is the primary export path for ISW towards the shelf slope (Dinniman et al., 2007; Orsi and Wiederwohl, 2009), which has direct bearing with its massive contribution along S3. As reported in previous studies (e.g. Budillon et al. (2002); Jacobs et al. (1985); Smethie Jr and Jacobs

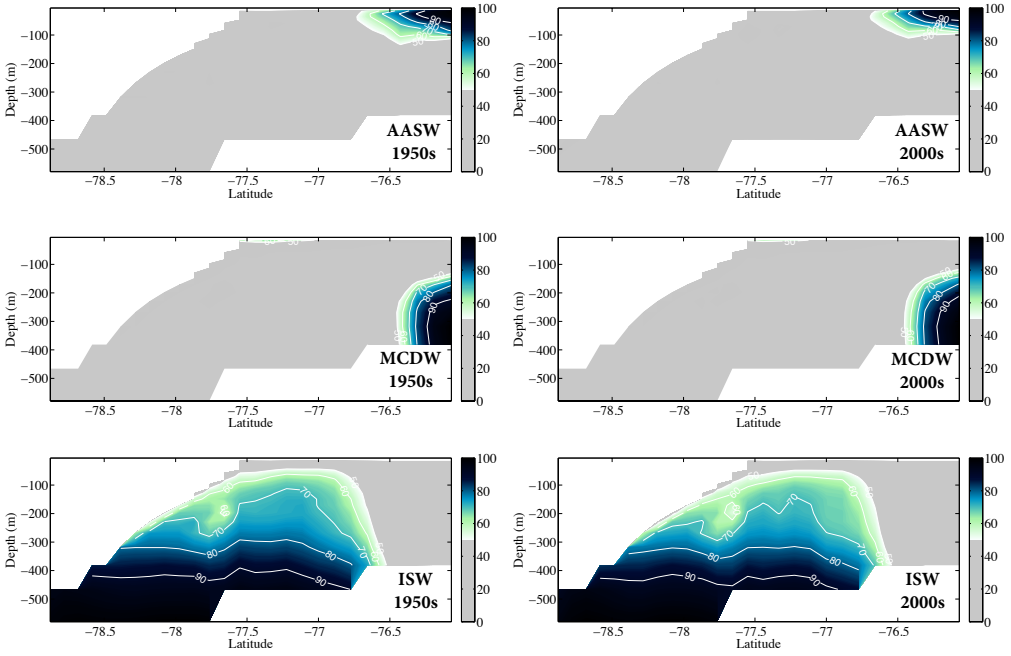

Figure 26: Water masses contribution (%) along the southern segment of the S3 section. The left panels refer to the 1950s and the right panels refer to the 2000s. Top panels display the AASW contribution, mid panels display the MCDW contribution, and bottom panels display the ISW contribution.

(2005); Budillon et al. (2011)) the ice cavity is dominated by the ISW that is formed by means of basal melting of the RIS. Although the ice shelf parameterization applied does not reproduce the basal melting mass exchange, which results in a very salty ISW (S ~ 34.85), the ice shelf thermodynamics allows the HSSW to become colder and to produce the densest ISW. During the simulation period the ISW maintains the very cold signature, but exhibits the freshening trend, dropping from S ~ 34.85 to S ~ 34.70.

Since the OMP results did not show clear variability trends for the water masses within the shelf regime, we have computed the sea water density (ρ) difference between the 2000s and the 1950s data for the S1, S2 and S3 southern cross–sections (Figure 27). Along the three cross–section a negative trend is observed. Along the S1 cross–section, which follows the Drygalsky Trough, the HSSW domain displays the most significant negative trend with a density decrease of about ~ 0.15 kg.m^{-3}. The surface also experienced an important density reduction ~ 0.12 kg.m^{-3}. The MCDW region displays the weaker negative trend of about ~ 0.05 kg.m^{-3} at the subsurface and ~ 0.09 kg.m^{-3} at 500 m depth. The S2 cross–section displays a very similar pattern to the S1. The main difference is related to the HSSW, whose density decrease of ~ 0.16 kg.m^{-3} suggests that water mass has become lighter. As for the S3 cross–section, which follows the export path of the ISW along the Glomar–Challenger Trough, the overall negative trend seems slightly less intense. The ISW decreased about ~ 0.13 kg.m^{-3} during the 6 decades.

As the shelf waters tend to become lighter, the bottom water production at the shelf slope can be directly influenced, resulting in a lessened dense waters formation rate and/or the production of a lighter bottom water (Bergamasco et al., 2002b;

Nicholls et al., 2009).

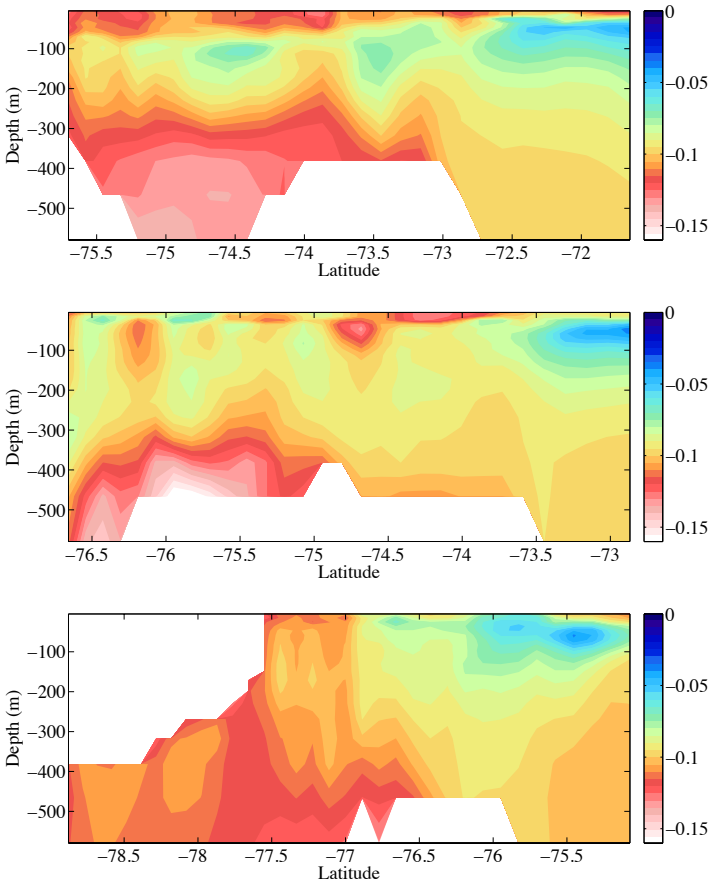

Figure 27: Sea water density ($kg.m^{-3}$) difference between the first (1950) and last (2000) decades of the simulation period. The upper panel represent the S1 cross–section, the mid panel represents the S2 cross–section, and the bottom panel represents the S3 southern cross–section.

The northern segment of the S3 cross–section also displays very interesting OMP results (Figure 28). As expected, AASW occupies the very surface layers and is barely seen, due to the greater depth of the section. The AASW changes little between the 1950s (θ ~ -0.5°C and S ~ 34.30) and the 2000s (θ ~ -0.3°C and S ~ 34.25). The CDW appears as a thick salty warm water layer under the AASW reaching down to 1500 m depth. Reported typical properties are $\theta > 1.5$ °C and S > 34.7 (Orsi and Wiederwohl, 2009). Here, CDW spreads along almost the entire section intermediate layers with θ ~ 2.5°C and S ~ 34.9, which is consistent with the observations. Throughout the simulation period the CDW gets warmer (θ ~ 3.3°C) and slightly less salty S ~ 34.85, which resulted in the shallowing observed in Figure 28 mid panels.

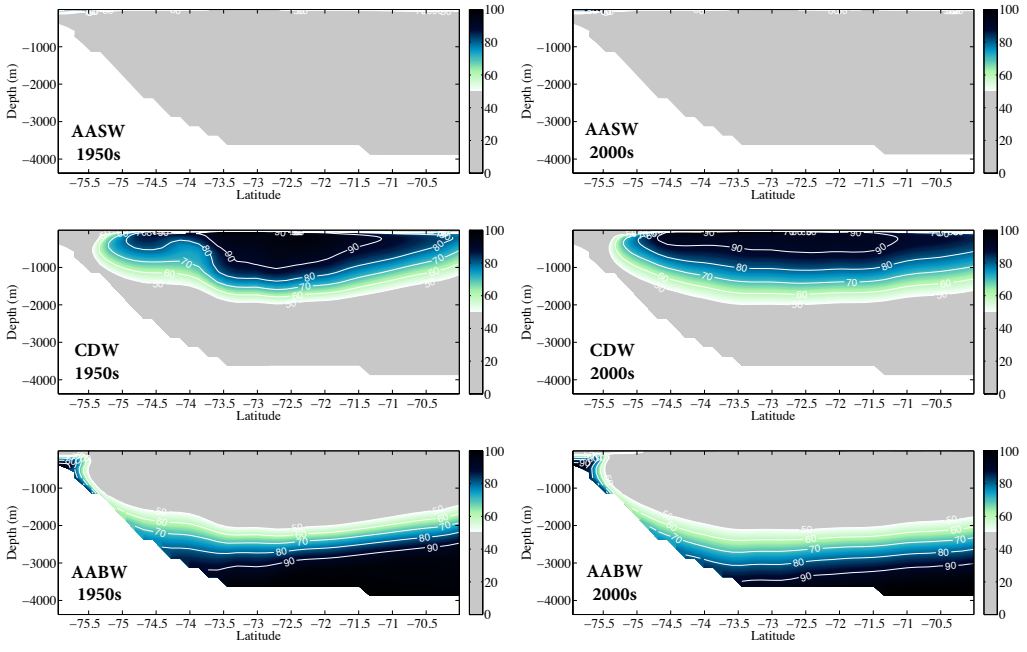

Figure 28: Water masses contribution (%) along the northern segment of the S3 section. The left panels refer to the 1950s and the right panels refer to the 2000s. Top panels display the AASW contribution, mid panels display the CDW contribution, and bottom panels display the AABW contribution.

The bottom layers are occupied by the globally important AABW, responsible to link the upper and lower limbs of the MOC (Orsi et al., 2001, 2002). Important contribution of AABW near the shelf slope can be observed. This is related to the shelf waters mixing responsible for the AABW formation (Bergamasco et al., 2002b). The AABW is the water mass whose OMP results reveal the most clear changes. Between the 1950s and the 2000s the bottom contribution of the AABW has waned suggesting a decrease in the water mass volume. The salinity/density decline on sinking waters near Antarctica has been reported in previous studies (e.g. Jacobs (2004, 2006); Aoki et al. (2005); Rintoul (2007)) as well as the export of warmer AABW (Johnson and Doney, 2006). In the same line, the AABW temperature has risen during the simulation period from $\theta \sim$ -0.4°C in the 1950s to $\theta \sim$ -0.3°C in the 2000s, while the salinity has lessened from 34.80 to 34.63. This salinity decrease may be related to the freshening and/or reduced production of the AABW, as reported by Azaneu et al. (2013).

To investigate the variability of the AABW, we have computed the neutral density (γ^n) for the S3 cross–section (Figure 29). Similar to Orsi and Wiederwohl (2009), we have defined the upper limit of the AABW as the neutral density layer γ^n= 28.3 kg.m^{-3}. Orsi and Wiederwohl (2009) used the γ^n= 28.27 kg.m^{-3} for observational data. We opted to use γ^n= 28.3 kg.m^{-3} to make sure it was within the AABW domain since the vertical resolution of the model is rather sparse at the deep and bottom layers. The first important thing is the extent of the γ^n= 28.3 kg.m^{-3} line tracing the origin of the AABW up to the continental shelf, in line with the formation process suggested by many authors (e.g. Bergamasco et al. (2002b,a); Orsi et al. (2001, 2002). Moreover, we must look at the evolution of the γ^n= 28.3 kg.m^{-3} layer.

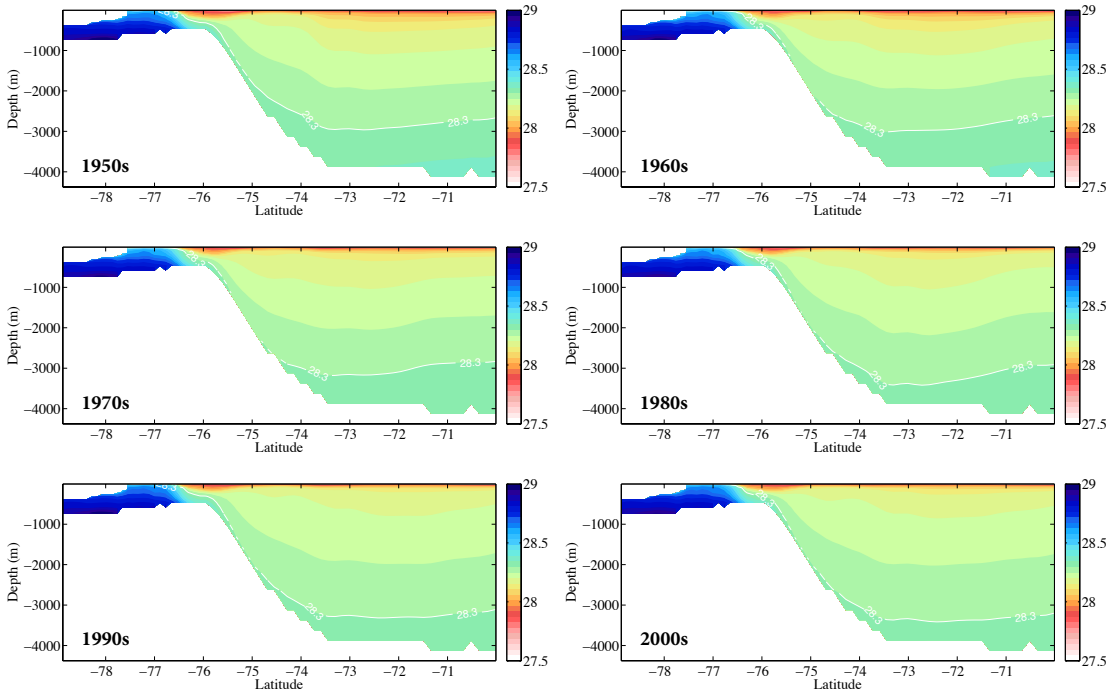

Figure 29: Neutral density (γ^n) vertical map for the S3 cross–section. The top left panel refers to the 1950s and the bottom right panel refers to the 2000s. The white line marks the γ^n= 28.3 kg.m^{-3} layer as the upper limit of the AABW.

To its northern extent, the γ^n= 28.3 kg.m^{-3} layer has deepened from approximately 2700 m depth to 3200 m. This suggests that either the AABW is becoming less dense and/or the formation rates have waned throughout the second half of the XXth century due to the increase in the heat transport to the Southern Ocean.

Although this work was aimed at the water masses in the Ross Sea, this intriguing finds regarding the AABW evolution motivated us to take a quick glance at the neutral density evolution along the 40 °W cross–section in the Weddell Sea (Figure 30). Using the same γ^n= 28.3 kg.m^{-3} reference layer for the AABW upper limit we found in the Weddell Sea similar trends as for the Ross Sea. Here, AABW origin is easily traced to the shelf waters, as reported by many authors (Naveira Garabato et al., 2002; Nicholls et al., 2009; Fahrbach et al., 2011; Hellmer et al., 2012). As for the evolution of the AABW, Figure 30 shows that the γ^n= 28.3 kg.m^{-3} layer has deepened during the simulation period. In the 1950s no $\gamma^n <$ 28.3 kg.m^{-3} is found under the 3000 m depth as a thick bottom layer is dominated by AABW. In the 2000s, however, no $\gamma^n >$ 28.3 kg.m^{-3} is found above the 3000 m depth. This suggests that a the export of the AABW from the Weddell Sea has also lessened during the second half of the XXth or that a lighter AABW is being produced. This is consistent with Azaneu et al. (2013), who analyzed hydrographic data to investigate the AABW production between 1958 and 2010, and reported a negative volume anomaly associated with the density decrease of the water mass.

Either way, the long–term results of this new energy adjustment are yet to be seen. From the oceanographic perspective, this may lead to a weakening of the MOC that will eventually wane the global poleward energy redistribution and reshape the Earth's climate.

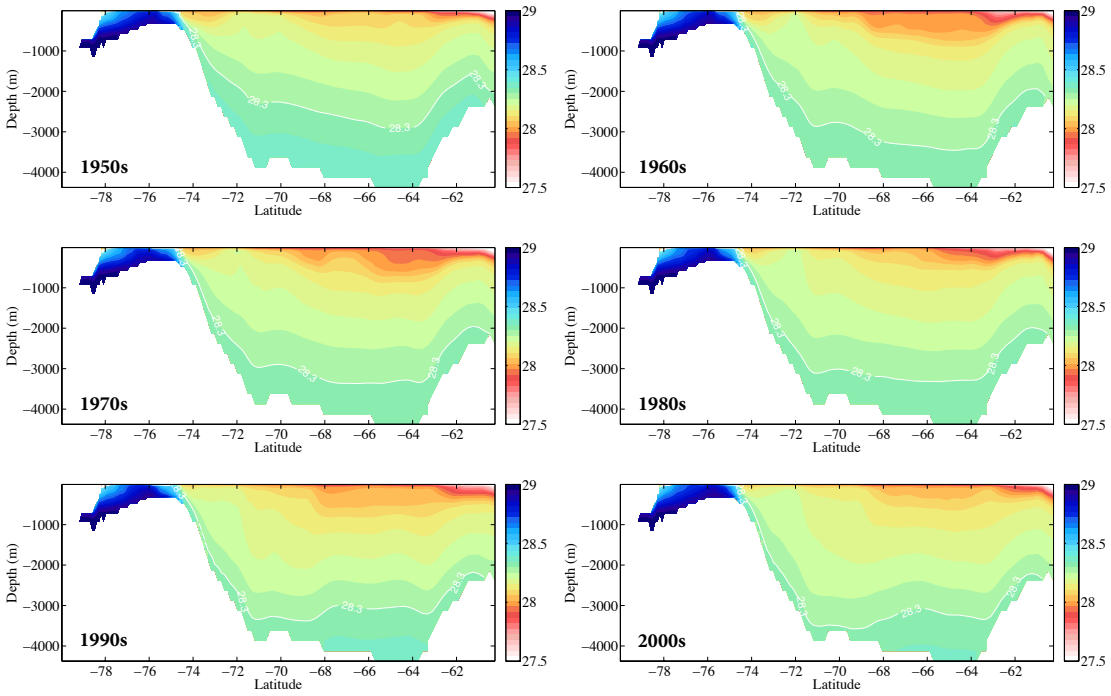

Figure 30: Neutral density (γ^n) vertical map for the 40°W cross–section in the Weddell Sea. The top left panel refers to the 1950s and the bottom right panel refers to the 2000s. The white line marks the γ^n= 28.3 kg.m^{-3} layer as the upper limit of the AABW.

7 Conclusions

In this work a thermodynamically active sea ice/ice shelf parameterization implemented in the regional ocean model ROMS was used to investigate changes in the Ross and Weddell Sea relative to water mass formation. ROMS was applied in a periodic circumpolar mid–to–high resolution domain. It has been shown by Meccia et al. (2013) that an ocean model alone is not able to reproduce the observed hydrography and circulation in the Southern Ocean. For the Ross Sea, we could show that, since sea–ice acts as a temperature and salinity regulator through sea–ice formation and melting, it must be considered for more realistic representations of Antarctic shelf processes. Along with the sea–ice, we were able to show that ice shelves surrounding Antarctica play an important role in the formation of the shelf water masses and that they also have to be prescribed in a realistic numerical way to improve the representation of the role of the Southern Ocean dynamics in global circulation and climate. Considering that poleward of the shelf break, 40% of the sea surface is covered by floating ice shelves, the interaction between the ice shelves and the ocean is a fundamental element of the climate system.

We have applied these two cryosphere components modules on our simulations and the results showed a realistic representation of the Ross Sea water masses. Although model solutions underneath the ice shelves are difficult to validate due to the scarcity of observations, our results suggest that the thermodynamic fluxes between the sea ice/ice shelf and the ocean must be considered in order to obtain representative hydrographic values under the ice shelves. Results suggest that the

numerical investigations of such an isolated environment as the cavity beneath the ice shelves is not only feasible but much useful to understand the oceanographic processes related to water transformation under the ice shelves.

The model setup used was able to reproduce the formation of the main water masses in the Ross Sea water: Antarctic Surface Water (AASW), Circumpolar Deep Water (CDW), Antarctic Bottom Water (AABW) and Shelf Water (SW), further separated into Ice Shelf Water (ISW) and High Salinity Shelf Water (HSSW) in agreement with the observations of Orsi and Wiederwohl (2009). The OMP water masses separating scheme allowed the investigations of the spacial distribution of theses water masses along the 3 cross–sections analyzed.

Regarding the interannual experiment, although little variability could be verified from the OMP results from the 1950s to the 2000s, the shelf waters presented an overall freshening trend apparently linked to the increased heat influx from the CDW and its modified form MCDW. The investigation of the AABW suggests that the water mass is becoming less dense (as reported by Johnson and Doney (2006)), which could lead to the waning of the MOC strength and, therefore, lessen the poleward heat redistribution.

The model capability to reproduce the cryosphere–linked processes directly related to the ISW and HSSW formation and the AABW formation, must be credited to the sea ice/ice shelf parameterization. Even though the ice shelf is static in time, the lack of mass exchange would not inhibit the ISW formation, as the heat exchange would produce the supercooled water under the Ross Sea Ice Shelf. In the same fashion, the absence of polynias in the ice shelf parameterization did not suppress the HSSW formation by means of sea ice production. Since these two shelf

waters were reproduced in the simulation, the model was also able to represent the formation and variability of the AABW.

The model represents a relevant contribution to climate studies and there is a lot more to be done. The future directions comprise the investigation of the Weddell Sea water masses variability and the AABW formation around the entire Antarctic Continent.

8 References

References

Aoki, S., Bindoff, N. L., and Church, J. A.: Interdecadal water mass changes in the Southern Ocean between 30 E and 160 E, Geophysical Research Letters, 32, 2005.

Assmann, K., Hellmer, H., and Beckmann, A.: Seasonal variation in circulation and water mass distribution on the Ross Sea continental shelf, Antarctic Science, 15, 3–11, 2003.

Azaneu, M., Kerr, R., Mata, M. M., and Garcia, C. A.: Trends in the deep Southern Ocean (1958–2010): Implications for Antarctic Bottom Water properties and volume export, Journal of Geophysical Research: Oceans, 118, 4213–4227, 2013.

Baines, P. and Condie, S.: Observations and modelling of Antarctic downslope flows: a review, Ocean, ice and atmosphere: interactions at the Antarctic continental margin, pp. 29–49, 1998.

Ball, F.: The katabatic winds of Adelie Land and King George V Land, Tellus, 9, 201–208, 1957.

Barber, M. and Crane, D.: Current flow in the north-west Weddell Sea, Antarctic Science, 7, 39–50, 1995.

Bergamasco, A., Defendi, V., and Meloni, R.: Some dynamics of water outflow from

beneath the Ross Ice Shelf during 1995 and 1996, Antarctic Science, 14, 74–82, 2002a.

Bergamasco, A., Defendi, V., Zambianchi, E., and Spezie, G.: Evidence of dense water overflow on the Ross Sea shelf-break, Antarctic Science, 14, 271–277, 2002b.

Bergamasco, A., Budillon, G., Carniel, S., Defendi, V., Meloni, R., Paschini, E., Sclavo, M., and Spezie, G.: Downslope flow across the Ross Sea shelf break (Antarctica), AGU Fall Meeting Abstracts, pp. C414+, 2003.

Bergamasco, A., Defendi, V., Budillon, G., and Spezie, G.: Downslope flow observations near Cape Adare shelf-break, Antarctic Science, 16, 199–204, 2004.

Bindoff, N., Rosenberg, M., and Warner, M.: On the circulation and water masses over the Antarctic continental slope and rise between 80 and 150E, Deep Sea Research Part II: Topical Studies in Oceanography, 47, 2299–2326, doi:10.1016/S0967-0645(00)00038-2, 2000.

Böning, C. W., Dispert, A., Visbeck, M., Rintoul, S., and Schwarzkopf, F. U.: The response of the Antarctic Circumpolar Current to recent climate change, Nature Geoscience, 1, 864–869, 2008.

Broecker, W. S.: Unpleasant surprises in the greenhouse?, nature, 328, 123–126, doi:10.1038/328123a0, 1987.

Bromwich, D. and Kurtz, D.: Katabatic wind forcing of the Terra Nova Bay polynya, Journal of Geophysical Research, 89, 3561–3572, 1984.

Bryan, K., Manabe, S., and Pacanowski, R. C.: A global ocean-atmosphere climate

model. Part II. The oceanic circulation, Journal of Physical Oceanography, 5, 30–46, 1975.

Budgell, W.: Numerical simulation of ice-ocean variability in the Barents Sea region, Ocean Dynamics, 55, 370–387, 2005.

Budillon, G. and Spezie, G.: Thermohaline structure and variability in the Terra Nova Bay polynya (Ross Sea) between 1995–98, Antarctic Science, 12, 501–516, 2000.

Budillon, G., Tucci, S., Artegiani, A., and Spezie, G.: Water masses and suspended matter characteristics of the western Ross Sea, Ross Sea ecology. Berlin: Springer, pp. 63–81, 1999.

Budillon, G., Gremes Cordero, S., and Salusti, E.: On The Dense Water Spreading Off The Ross Sea Shelf (antarctica), EGS XXVII General Assembly, Nice, 21-26 April 2002, abstract #944, 27, 944–+, 2002.

Budillon, G., Pacciaroni, M., Cozzi, S., Rivaro, P., Catalano, G., Ianni, C., and Cantoni, C.: An optimum multiparameter mixing analysis of the shelf waters in the Ross Sea, Antarctic Science, 15, 105–118, 2003.

Budillon, G., Castagno, P., Aliani, S., Spezie, G., and Padman, L.: Thermohaline variability and Antarctic bottom water formation at the Ross Sea shelf break, Deep Sea Research Part I: Oceanographic Research Papers, 58, 1002–1018, 2011.

Butler, J. H., King, D. B., Lobert, J. M., Montzka, S. A., Yvon-Lewis, S. A., Hall, B. D., Warwick, N. J., Mondeel, D. J., Aydin, M., and Elkins, J. W.: Oceanic dis-

tributions and emissions of short-lived halocarbons, Global biogeochemical cycles, 21, 2007.

Carmack, E.: Water characteristics of the Southern Ocean south of the Polar Front, A voyage of Discovery, pp. 15–41, 1977.

Carmack, E.: Large-scale physical oceanography of polar oceans, 1990.

Carmack, E. and Foster, T.: On the flow of water out of the Weddell Sea, Deep Sea Research and Oceanographic Abstracts, 22, 711–724, doi:10.1016/0011--7471(75)90077--7, 1975.

Cenedese, C., Whitehead, J., Ascarelli, T., and Ohiwa, M.: A dense current flowing down a sloping bottom in a rotating fluid, Journal of Physical Oceanography, 34, 188–203, 2004.

Chelton, D. B., Deszoeke, R. A., Schlax, M. G., El Naggar, K., and Siwertz, N.: Geographical variability of the first baroclinic Rossby radius of deformation, Journal of Physical Oceanography, 28, 433–460, 1998.

Colling, A.: Ocean circulation, Elsevier, 2001.

Convey, P., Stevens, M. I., Hodgson, D. A., Smellie, J. L., Hillenbrand, C.-D., Barnes, D. K., Clarke, A., Pugh, P. J., Linse, K., and Cary, S. C.: Exploring biological constraints on the glacial history of Antarctica, Quaternary Science Reviews, 28, 3035–3048, 2009.

Coward, A. and De Cuevas, B.: The OCCAM 66 level model: Model description, physics, initial conditions and external forcing, 2005.

Cubillos, J., Wright, S., Nash, G., De Salas, M., Griffiths, B., Tilbrook, B., Poisson, A., and Hallegraeff, G.: Calcification morphotypes of the coccolithophorid Emiliania huxleyi in the Southern Ocean: changes in 2001 to 2006 compared to historical data, Marine Ecology-Progress Series, 348, 47–54, 2007.

Cunningham, S. A., Alderson, S. G., King, B. A., and Brandon, M. A.: Transport and variability of the Antarctic Circumpolar Current in Drake Passage, Journal of Geophysical Research (Oceans), 108, 8084–+, doi:10.1029/2001JC001147, 2003.

Curry, R., Dickson, B., and Yashayaev, I.: A change in the freshwater balance of the Atlantic Ocean over the past four decades, Nature, 426, 826–829, 2003.

Deacon, G.: The hydrology of the Southern Ocean, vol. 15, Cambridge University Press, 1937.

Deacon, G.: The Weddell Gyre, Deep Sea Research Part A. Oceanographic Research Papers, 26, 981–995, 1979.

Deacon, G.: Physical and biological zonation in the Southern Ocean, Deep Sea Research Part A. Oceanographic Research Papers, 29, 1–15, 1982.

Deacon, G.: The antartic circumpolar océan, 1984.

Dinniman, M., Klinck, J., and Smith Jr, W.: Influence of sea ice cover and icebergs on circulation and water mass formation in a numerical circulation model of the Ross Sea, Antarctica, Journal of Geophysical Research, 112, C11 013, doi:10.1029/2006JC004036, 2007.

Dong, B., Sutton, R. T., and Scaife, A. A.: Multidecadal modulation of El Nino–

Southern Oscillation (ENSO) variance by Atlantic Ocean sea surface temperatures, Geophysical Research Letters, 33, 2006.

Ducklow, H. W., Baker, K., Martinson, D. G., Quetin, L. B., Ross, R. M., Smith, R. C., Stammerjohn, S. E., Vernet, M., and Fraser, W.: Marine pelagic ecosystems: the west Antarctic Peninsula, Philosophical Transactions of the Royal Society B: Biological Sciences, 362, 67–94, 2007.

Emery, W. and Thomson, R.: Data analysis methods in physical oceanography, 634 pp, 1998.

Fahrbach, E., Rohardt, G., Schröder, M., and Strass, V.: Transport and structure of the Weddell Gyre, Annales Geophysicae, 12, 840–855, doi:10.1007/s005850050109, 1994.

Fahrbach, E., Rohardt, G., Scheele, N., Schroder, M., Strass, V., and Wisotzki, A.: Formation and discharge of deep and bottom water in the northwestern Weddell Sea, Journal of Marine Research, 53, 515–538, 1995.

Fahrbach, E., Hoppema, M., Rohardt, G., Boebel, O., Klatt, O., and Wisotzki, A.: Warming of deep and abyssal water masses along the Greenwich meridian on decadal time scales: The Weddell gyre as a heat buffer, Deep Sea Research Part II: Topical Studies in Oceanography, 58, 2509–2523, 2011.

Fairall, C. W., Bradley, E. F., et al.: Bulk Parameterization of Air–Sea Fluxes: Updates and Verification for the COARE Algorithm, J. Climate, 16, 571–591, 2003.

Foldvik, A., Gammelsrød, T., Østerhus, S., Fahrbach, E., Rohardt, G., Schröder,

M., Nicholls, K. W., Padman, L., and Woodgate, R. A.: Ice shelf water overflow and bottom water formation in the southern Weddell Sea, Journal of Geophysical Research (Oceans), 109, 2015–+, doi:10.1029/2003JC002008, 2004.

Foster, T. D. and Carmack, E. C.: Frontal zone mixing and Antarctic Bottom Water formation in the southern Weddell Sea, in: Deep Sea Research and Oceanographic Abstracts, vol. 23, pp. 301–317, Elsevier, 1976.

Fusco, G., Flocco, D., Budillon, G., Spezie, G., and Zambianchi, E.: Dynamics and Variability of Terra Nova Bay Polynya, Marine Ecology, 23, 201–209, 2002.

Fyfe, J. C. and Saenko, O. A.: Simulated changes in the extratropical Southern Hemisphere winds and currents, Geophysical Research Letters, 33, 2006.

Fyfe, J. C., Saenko, O. A., Zickfeld, K., Eby, M., and Weaver, A. J.: The role of poleward-intensifying winds on Southern Ocean warming., Journal of Climate, 20, 2007.

Gill, A.: Circulation and bottom water production in the Weddell Sea, Deep Sea Research and Oceanographic Abstracts, 20, 111–140, doi:10.1016/0011-7471(73)90048-X, 1973.

Gille, S. T.: Meridional Displacement of the Antarctic Circumpolar Current.

Gille, S. T.: Warming of the Southern Ocean Since the 1950s, Science, 295, 1275–1278, doi:10.1126/science.1065863, 2002.

Gille, S. T.: Decadal-scale temperature trends in the Southern Hemisphere ocean., Journal of Climate, 21, 2008.

Gong, D. and Wang, S.: Definition of Antarctic oscillation index, grl, 26, 459–462, doi:10.1029/1999GL900003, 1999.

Gordon, A.: Western Weddell Sea thermohaline stratification, Ocean, Ice and Atmosphere: Interactions at the Antarctic Continental Margin, Antarct. Res. Ser, 75, 215–240, 1998.

GORDON, A. and COMISO, J.: Polynyas in the southern ocean, Scientific American, 258, 90–97, 1988.

Gordon, A. and Tchernia, P.: Waters of the continental margin off Adelie Coast, Antarctica, Antarctic oceanology, 2, 59–69, 1972.

Gordon, A. L., Zambianchi, E., Orsi, A., Visbeck, M., Giulivi, C. F., Whitworth, T., and Spezie, G.: Energetic plumes over the western Ross Sea continental slope, grl, 31, 21 302–+, doi:10.1029/2004GL020785, 2004.

Gordon, A. L., Visbeck, M., and Comiso, J. C.: A Possible Link between the Weddell Polynya and the Southern Annular Mode., Journal of Climate, 20, 2007.

Gouretski, V.: Deep water property comparison for the WOCE global hydrographic data set, Bundesamt f

"ur Seeschiffahrt und Hydrographie Tech. Rep, 1999.

Griffies, S. M., Biastoch, A., Böning, C., Bryan, F., Danabasoglu, G., Chassignet, E. P., England, M. H., Gerdes, R., Haak, H., Hallberg, R. W., et al.: Coordinated ocean-ice reference experiments (COREs), Ocean Modelling, 26, 1–46, 2009.

Grotti, M., Soggia, F., Abelmoschi, M. L., Rivaro, P., Magi, E., and Frache, R.:

Temporal distribution of trace metals in Antarctic coastal waters, Marine Chemistry, 76, 189–209, 2001.

Haidvogel, D., Wilkin, J., and Young, R.: A semi-spectral primitive equation ocean circulation model using vertical sigma and orthogonal curvilinear horizontal coordinates, Journal of Computational Physics, 94, 151–185, 1991.

Haidvogel, D. B., Arango, H., et al.: Ocean forecasting in terrain-following coordinates: Formulation and skill assessment of the Regional Ocean Modeling System, Journal of Computational Physics, 227, 3595–3624, 2008.

Hall, A. and Visbeck, M.: Synchronous Variability in the Southern Hemisphere Atmosphere, Sea Ice, and Ocean Resulting from the Annular Mode(., Journal of Climate, 15, 3043–3057, doi:10.1175/1520-0442(2002)015, 2002.

Hallberg, R. and Gnanadesikan, A.: The role of eddies in determining the structure and response of the wind-driven Southern Hemisphere overturning: Results from the Modeling Eddies in the Southern Ocean (MESO) project., Journal of Physical Oceanography, 36, 2006.

Hellmer, H.: Impact of Antarctic ice shelf basal melting on sea ice and deep ocean properties, Geophysical Research Letters, 31, 2004.

Hellmer, H. H. and Beckmann, A.: The Southern Ocean: A ventilation contributor with multiple sources, Geophysical Research Letters, 28, 2927–2930, 2001.

Hellmer, H. H., Kauker, F., Timmermann, R., Determann, J., and Rae, J.: Twenty-first-century warming of a large Antarctic ice-shelf cavity by a redirected coastal current, Nature, 485, 225–228, 2012.

Heywood, K. J., Locarnini, R. A., Frew, R. D., Dennis, P. F., and King, B. A.: Transport and water masses of the Antarctic Slope Front system in the eastern Weddell Sea, Antarctic Research Series, 75, 203–214, 1998.

Heywood, K. J., Naveira Garabato, A. C., Stevens, D. P., and Muench, R. D.: On the fate of the Antarctic Slope Front and the origin of the Weddell Front, Journal of Geophysical Research: Oceans (1978–2012), 109, 2004.

Hinrichsen, H. and Tomczak, M.: Optimum multiparameter analysis of the water mass structure in the western North Atlantic Ocean, Journal of Geophysical Research-Oceans, 98, 1993.

Hogg, A. M., Meredith, M. P., Blundell, J. R., and Wilson, C.: Eddy heat flux in the Southern Ocean: Response to variable wind forcing., Journal of Climate, 21, 2008.

Holland, D. and Jenkins, A.: Modeling thermodynamic ice-ocean interactions at the base of an ice shelf, Journal of Physical Oceanography, 29, 1787–1800, 1999.

Holland, D., Jacobs, S., and Jenkins, A.: Modelling the ocean circulation beneath the Ross Ice Shelf, Antarctic Science, 15, 13–23, 2003.

Hughes, T. J., Mazzei, L., Oberai, A. A., and Wray, A. A.: The multiscale formulation of large eddy simulation: Decay of homogeneous isotropic turbulence, Physics of Fluids (1994-present), 13, 505–512, 2001.

Hughes, T. P., Baird, A. H., Bellwood, D. R., Card, M., Connolly, S. R., Folke, C., Grosberg, R., Hoegh-Guldberg, O., Jackson, J., Kleypas, J., et al.: Climate

change, human impacts, and the resilience of coral reefs, science, 301, 929–933, 2003.

Hunke, E.: Viscous–plastic sea ice dynamics with the EVP model: Linearization issues, Journal of Computational Physics, 170, 18–38, doi:10.1006/jcph.2001.6710, 2001.

Huthnance, J.: Circulation, exchange and water masses at the ocean margin: the role of physical processes at the shelf edge, Progress in Oceanography, 35, 353–431, doi:10.1016/0079-6611(95)00012-6, 1995.

Ivanov, V. V., Shapiro, G. I., Huthnance, J. M., Aleynik, D. L., and Golovin, P. N.: Cascades of dense water around the world ocean [review article], Progress in Oceanography, 60, 47–98, doi:10.1016/j.pocean.2003.12.002, 2004.

Jacobs, S.: Bottom water production and its links with the thermohaline circulation, Antarctic Science, 16, 427–437, 2004.

Jacobs, S.: Observations of change in the Southern Ocean, Royal Society of London Philosophical Transactions Series A, 364, 1657–1681, doi:10.1098/rsta.2006.1794, 2006.

Jacobs, S. and Giulivi, C.: Interannual ocean and sea ice variability in the Ross Sea, Antarctic Research Series, 75, 135–150, 1998.

Jacobs, S. and Giulivi, C.: Thermohaline data and ocean circulation on the Ross Sea continental shelf, Oceanography of the Ross Sea, Antarctica, p. 3, 1999.

Jacobs, S., Amos, A., and Bruchhausen, P.: Ross Sea oceanography and Antarctic bottom water formation, Deep-Sea Research, 17, 935–62, 1970.

Jacobs, S., Fairbanks, R., and Horibe, Y.: Origin and evolution of water masses near the Antarctic continental margin: evidence from H 2 18 O/H 2 16 O ratios in seawater, Oceanology of the Antarctic Continental Shelf, 43, 59–85, 1985.

Jacobs, S. S. and Comiso, J. C.: Sea ice and oceanic process on the Ross Sea continental shelf, jgr, 94, 18 195–18 211, doi:10.1029/JC094iC12p18195, 1989.

Jacobs, S. S., Giulivi, C. F., and Mele, P. A.: Freshening of the Ross Sea During the Late 20th Century, Science, 297, 386–389, doi:10.1126/science.1069574, 2002.

Johnson, G.: Quantifying Antarctic bottom water and North Atlantic deep water volumes, Journal of Geophysical Research-Oceans, 113, C05 027, 2008.

Johnson, G. C. and Doney, S. C.: Recent western South Atlantic bottom water warming, Geophysical Research Letters, 33, 2006.

Karsten, R., Jones, H., and Marshall, J.: The Role of Eddy Transfer in Setting the Stratification and Transport of a Circumpolar Current, Journal of Physical Oceanography, 32, 39–54, doi:10.1175/1520-0485(2002)032, 2002.

Karstensen, J. and Tomczak, M.: Ventilation processes and water mass ages in the thermocline of the southeast Indian Ocean, grl, 24, 2777–2780, doi:10.1029/97GL02708, 1997.

Karstensen, J. and Tomczak, M.: Age determination of mixed water masses using CFC and oxygen data, jgr, 103, 18 599–18 610, doi:10.1029/98JC00889, 1998.

Kerr, R., Wainer, I., and Mata, M.: Representation of the Weddell Sea deep water masses in the ocean component of the NCAR–CCSM model, Antarctic Science, 21, 301–312, doi:10.1017/S0954102009001825, 2009.

Kerr, R., Heywood, K., Mata, M., and Garcia, C.: On the outflow of dense water from the Weddell and Ross Seas in OCCAM model., Ocean Science, 8, 2012.

Killworth, P. D.: Mixing of the Weddell Sea continental slope, Deep Sea Research, 24, 427–448, 1977.

Klatt, O., Fahrbach, E., Hoppema, M., and Rohardt, G.: The transport of the Weddell Gyre across the Prime Meridian, Deep Sea Research Part II: Topical Studies in Oceanography, 52, 513–528, 2005.

Kurtz, D. and Bromwich, D.: A recurring, atmospherically forced polynya in Terra Nova Bay, Oceanology of the Antarctic continental shelf, p. 177, 1985.

Kurtz, D. D. and Bromwich, D. H.: Satellite observed behavior of the Terra Nova Bay polynya, Journal of Geophysical Research: Oceans (1978–2012), 88, 9717–9722, 1983.

Large, W. and Yeager, S.: The global climatology of an interannually varying air–sea flux data set, Climate Dynamics, 33, 341–364, 2009.

Le Quéré, C., Rödenbeck, C., Buitenhuis, E. T., Conway, T. J., Langenfelds, R., Gomez, A., Labuschagne, C., Ramonet, M., Nakazawa, T., Metzl, N., et al.: Saturation of the Southern Ocean CO2 sink due to recent climate change, science, 316, 1735–1738, 2007.

Lenton, A. and Matear, R. J.: Role of the Southern Annular Mode (SAM) in southern ocean CO2 uptake, Global Biogeochemical Cycles, 21, 2007.

Levitus, S., Antonov, J., and Boyer, T.: Warming of the world ocean, 1955–2003, Geophysical Research Letters, 32, 2005.

Locarnini, R.: Water masses and circulation in the Ross Gyre and environs, Texas A & M University, Office of Graduate Studies, 1994.

Lovenduski, N. S., Gruber, N., Doney, S. C., and Lima, I. D.: Enhanced CO2 outgassing in the Southern Ocean from a positive phase of the Southern Annular Mode, Global Biogeochemical Cycles, 21, 2007.

Lumpkin, R. and Speer, K.: Global ocean meridional overturning., Journal of Physical Oceanography, 37, 2007.

Lythe, M., Vaughan, D., and the BEDMAP Consortium: BEDMAP: A new ice thickness and subglacial topographic model of Antarctica, Journal of Geophysical Research, 106, 11 335–11 351, 2001a.

Lythe, M., Vaughan, D., et al.: BEDMAP: A new ice thickness and subglacial topographic model of Antarctica, Journal of Geophysical Research, 106, 11 335–11, 2001b.

Mackas, D. L., Denman, K. L., and Bennett, A. F.: Least squares multiple tracer analysis of water mass composition, jgr, 92, 2907–2918, doi:10.1029/JC092iC03p02907, 1987.

Manabe, S. and Bryan, K.: Climate calculations with a combined ocean-atmosphere model, Journal of the Atmospheric Sciences, 26, 786–789, 1969.

Marshall, G. J.: Trends in the southern annular mode from observations and reanalyses., Journal of Climate, 16, 2003.

Marshall, G. J.: Half-century seasonal relationships between the Southern Annular

mode and Antarctic temperatures, International Journal of Climatology, 27, 373–383, 2007.

Marshall, G. J., Orr, A., van Lipzig, N. P., and King, J. C.: The impact of a changing Southern Hemisphere annular mode on Antarctic Peninsula summer temperatures., Journal of Climate, 19, 2006.

McCartney, M. S. and Donohue, K. A.: A deep cyclonic gyre in the Australian–Antarctic Basin, Progress in Oceanography, 75, 675–750, 2007.

Meccia, V., Wainer, I., Tonelli, M., and Curchitser, E.: Coupling a thermodynamically active ice shelf to a regional simulation of the Weddell Sea., Geoscientific Model Development, 6, 2013.

Mellor, G. and Kantha, L.: An ice-ocean coupled model, Journal of Geophysical Research, 94, 937–10, 1989.

Meredith, M. P. and Hogg, A. M.: Circumpolar response of Southern Ocean eddy activity to a change in the Southern Annular Mode, Geophysical Research Letters, 33, 2006.

Meredith, M. P. and King, J. C.: Rapid climate change in the ocean west of the Antarctic Peninsula during the second half of the 20th century, Geophysical Research Letters, 32, 2005.

Montes-Hugo, M., Doney, S. C., Ducklow, H. W., Fraser, W., Martinson, D., Stammerjohn, S. E., and Schofield, O.: Recent changes in phytoplankton communities associated with rapid regional climate change along the western Antarctic Peninsula, Science, 323, 1470–1473, 2009.

Morrow, R., Valladeau, G., and Sallee, J.-B.: Observed subsurface signature of Southern Ocean sea level rise, Progress in Oceanography, 77, 351–366, 2008.

Muench, R., Padman, L., Gordon, A., and Orsi, A.: A dense water outflow from the Ross Sea, Antarctica: Mixing and the contribution of tides, Journal of Marine Systems, 77, 369–387, 2009.

Naveira Garabato, A. C., McDonagh, E. L., Stevens, D. P., Heywood, K. J., and Sanders, R. J.: On the export of Antarctic bottom water from the Weddell Sea, Deep Sea Research Part II: Topical Studies in Oceanography, 49, 4715–4742, 2002.

NGDC: Data Announcement 88–MGG–02, Digital relief of the Surface of the Earth, NOAA, National Geophysical Data Center – NGDC, Boulder, Colorado, 1988.

Nicholls, K., Østerhus, S., Makinson, K., Gammelsrød, T., and Fahrbach, E.: Ice-ocean processes over the continental shelf of the southern Weddell Sea, Antarctica: A review, Reviews of Geophysics, 47, RG3003, 2009.

Oke, P. R. and England, M. H.: Oceanic response to changes in the latitude of the Southern Hemisphere subpolar westerly winds., Journal of Climate, 17, 2004.

Olbers, D., Borowski, D., VOeLKER, C., and WOeLFF, J.: The dynamical balance, transport and circulation of the Antarctic Circumpolar Current, Antarctic science, 16, 439–470, 2004.

O'Neill, L. W., Chelton, D. B., Esbensen, S. K., and Wentz, F. J.: High-resolution satellite measurements of the atmospheric boundary layer response to SST variations along the Agulhas Return Current., Journal of climate, 18, 2005.

Orsi, A.: Circulation, mixing, and production of Antarctic Bottom Water, Progress in Oceanography, 43, 55–109, doi:10.1016/S0079-6611(99)00004-X, 1999.

Orsi, A. and Wiederwohl, C.: A recount of Ross Sea waters, Deep Sea Research Part II: Topical Studies in Oceanography, 56, 778–795, 2009.

Orsi, A., Nowlin, W., and Whitworth, T.: On the circulation and stratification of the Weddell Gyre, Deep–sea research. Part A. Oceanographic research papers, 40, 169–203, 1993.

Orsi, A., Whitworth, T., and Nowlin, W.: On the meridional extent and fronts of the Antarctic Circumpolar Current, Deep Sea Research Part I: Oceanographic Research, 42, 641–673, doi:10.1016/0967-0637(95)00021-W, 1995.

Orsi, A., Jacobs, S., Gordon, A., and Visbeck, M.: Cooling and ventilating the abyssal ocean, Geophys. Res. Lett, 28, 2923–2926, 2001.

Orsi, A., Smethie Jr, W., and Bullister, J.: On the total input of Antarctic waters to the deep ocean: A preliminary estimate from chlorofluorocarbon measurements, J. Geophys. Res, 107, 3122, 2002.

Parkinson, C. L.: Southern Ocean sea ice and its wider linkages: insights revealed from models and observations, Antarctic Science, 16, 387–400, 2004.

Poole, R. and Tomczak, M.: Optimum multiparameter analysis of the water mass structure in the Atlantic Ocean thermocline, Deep Sea Research Part I: Oceanographic Research, 46, 1895–1921, doi:10.1016/S0967-0637(99)00025-4, 1999.

Pritchard, H. D. and Vaughan, D. G.: Widespread acceleration of tidewater glaciers

on the Antarctic Peninsula, Journal of Geophysical Research: Earth Surface (2003–2012), 112, 2007.

Raphael, M.: Impact of observed sea-ice concentration on the Southern Hemisphere extratropical atmospheric circulation in summer, Journal of Geophysical Research: Atmospheres (1984–2012), 108, 2003.

Redfield, A., Ketchum, B., and Richards, F.: The influence of organisms on the composition of sea-water, 1963.

Reid, J. L.: On the total geostrophic circulation of the Pacific Ocean: Flow patterns, tracers, and transports, Progress in Oceanography, 39, 263–352, 1997.

Rignot, E. and Jacobs, S. S.: Rapid bottom melting widespread near Antarctic ice sheet grounding lines, Science, 296, 2020–2023, 2002.

Rignot, E., Casassa, G., Gogineni, P., Krabill, W., Rivera, A. u., and Thomas, R.: Accelerated ice discharge from the Antarctic Peninsula following the collapse of Larsen B ice shelf, Geophysical Research Letters, 31, 2004.

Rignot, E., Bamber, J. L., Van Den Broeke, M. R., Davis, C., Li, Y., Van De Berg, W. J., and Van Meijgaard, E.: Recent Antarctic ice mass loss from radar interferometry and regional climate modelling, Nature Geoscience, 1, 106–110, 2008.

Rintoul, S.: On the origin and influence of Adelie Land Bottom Water, Ocean, Ice and Atmosphere: Interactions at the Antarctic continental margin, pp. 151–171, 1998.

Rintoul, S., Sparrow, M., Meredith, M., Wadley, V., Speer, K., Hofmann, E., Sum-

merhayes, C., Urban, E., and Bellerby, R.: The Southern Ocean Observing System, Oceanography, 25, 74, 2012a.

Rintoul, S. R.: Rapid freshening of Antarctic Bottom Water formed in the Indian and Pacific oceans, Geophysical Research Letters, 34, 2007.

Rintoul, S. R. and Sokolov, S.: Baroclinic transport variability of the Antarctic Circumpolar Current south of Australia (WOCE repeat section SR3), jgr, 106, 2795–2814, doi:10.1029/2000JC900107, 2001.

Rintoul, S. R., Sparrow, M., Meredith, M. P., Wadley, V., Speer, K., Hofmann, E., Summerhayes, C., Urban, E., Bellerby, R., Ackley, S., et al.: The Southern Ocean observing system: initial science and implementation strategy, SCAR and SCOR, 2012b.

Rodman, M. and Gordon, A.: Southern Ocean bottom water of the Australian-New Zealand sector, Journal of Geophysical Research, 87, 1982.

Russo, A., Artegiani, A., Budillon, G., Paschini, E., and Spezie, G.: Upper ocean thermal structure and fronts between New Zealand and the Ross Sea (Austral summer 1994–1995 and 1995–1996), in: Oceanography of the Ross Sea Antarctica, pp. 67–75, Springer, 1999.

Sabine, C. L., Feely, R. A., Gruber, N., Key, R. M., Lee, K., Bullister, J. L., Wanninkhof, R., Wong, C., Wallace, D. W., Tilbrook, B., et al.: The oceanic sink for anthropogenic CO2, science, 305, 367–371, 2004.

Saenko, O. A., Fyfe, J. C., and England, M. H.: On the response of the oceanic wind-

driven circulation to atmospheric CO2 increase, Climate dynamics, 25, 415–426, 2005.

Sallée, J., Speer, K., Morrow, R., and Lumpkin, R.: An estimate of Lagrangian eddy statistics and diffusion in the mixed layer of the Southern Ocean, Journal of Marine Research, 66, 441–463, 2008.

Sarmiento, J. L., Slater, R., Barber, R., Bopp, L., Doney, S. C., Hirst, A., Kleypas, J., Matear, R., Mikolajewicz, U., Monfray, P., et al.: Response of ocean ecosystems to climate warming, Global Biogeochemical Cycles, 18, 2004.

Schmitz, W. J.: On the eddy field in the Agulhas Retroflection, with some global considerations, jgr, 101, 16 259–16 272, doi:10.1029/96JC01143, 1996.

Schmitz, W. J. and McCartney, M. S.: On the North Atlantic circulation, Reviews of Geophysics, 31, 29–50, doi:10.1029/92RG02583, 1993.

Schodlok, M. P., Hellmer, H. H., and Beckmann, A.: On the transport, variability and origin of dense water masses crossing the South Scotia Ridge, Deep Sea Research Part II: Topical Studies in Oceanography, 49, 4807–4825, 2002.

Shapiro, G. I. and Hill, A. E.: Dynamics of Dense Water Cascades at the Shelf Edge, Journal of Physical Oceanography, 27, 2381–2394, doi:10.1175/1520-0485(1997)027, 1997.

Shchepetkin, A. F. and McWilliams, J. C.: The regional oceanic modeling system (ROMS): a split-explicit, free-surface, topography-following-coordinate oceanic model, Ocean Modelling, 9, 347–404, 2005.

Shepherd, A., Wingham, D., and Rignot, E.: Warm ocean is eroding West Antarctic ice sheet, Geophysical Research Letters, 31, 2004.

Shindell, D. T., Rind, D., and Lonergan, P.: Increased polar stratospheric ozone losses and delayed eventual recovery owing to increasing greenhouse-gas concentrations, Nature, 392, 589–592, 1998.

Simmonds, I.: Modes of atmospheric variability over the Southern Ocean, Journal of Geophysical Research: Oceans (1978–2012), 108, SOV–5, 2003.

Smethie, W. and Jacobs, S.: Circulation and melting under the Ross Ice Shelf: estimates from evolving CFC, salinity and temperature fields in the Ross Sea, Deep Sea Research Part I: Oceanographic Research Papers, 52, 959–978, 2005.

Smethie Jr, W. and Jacobs, S.: Melting and water mass transformation under the Ross Ice Shelf: estimates from evolving CFC, salinity and temperature fields in the Ross Sea, Deep-Sea Research, 2005.

Smith, W. and Sandwell, D.: Global sea floor topography from satellite altimetry and ship depth soundings, Science, 277, 1956–1962, 1997.

Sokolov, S. and Rintoul, S. R.: On the relationship between fronts of the Antarctic Circumpolar Current and surface chlorophyll concentrations in the Southern Ocean, Journal of Geophysical Research: Oceans (1978–2012), 112, 2007.

Sokolov, S. and Rintoul, S. R.: Circumpolar structure and distribution of the Antarctic Circumpolar Current fronts: 2. Variability and relationship to sea surface height, Journal of Geophysical Research: Oceans (1978–2012), 114, 2009.

Song, Y. and Haidvogel, D.: A semi–implicit ocean circulation model using a generalized topography–following coordinate system, Journal of Computational Physics, 115, 228–244, 1994.

Speer, K., Rintoul, S. R., and Sloyan, B.: The Diabatic Deacon Cell*, Journal of physical oceanography, 30, 3212–3222, 2000.

Sprintall, J.: Seasonal to interannual upper-ocean variability in the Drake Passage, Journal of Marine Research, 61, 27–57, 2003.

Stammerjohn, S., Martinson, D., Smith, R., Yuan, X., and Rind, D.: Trends in Antarctic annual sea ice retreat and advance and their relation to El Niño–Southern Oscillation and Southern Annular Mode variability, Journal of Geophysical Research: Oceans (1978–2012), 113, 2008.

Stover, C. L.: A new account of Ross Sea waters: characteristics, volumetrics, and variability, Ph.D. thesis, Texas A&M University, 2006.

Sulman, F.: Short-and long-term changes in climate, 1982.

Summerhayes, C., Thorpe, S., and Brewer, P.: Oceanography: an illustrated guide, Manson, 1996.

Sverdrup, H.: On conditions for the vernal blooming of phytoplankton, Journal du Conseil, 18, 287–295, 1953.

Swart, N. and Fyfe, J.: Observed and simulated changes in the Southern Hemisphere surface westerly wind-stress, Geophysical Research Letters, 39, 2012.

Talley, L. D., Pickard, G. L., Emery, W. J., and Swift, J. H.: Descriptive physical oceanography: an introduction, Academic Press, 2011.

Tchernia, P. and Jeannin, P. F.: Circulation in Antarctic waters as revealed by iceberg tracks 1972–1983, Polar Record, 22, 263–269, 1984.

Thomas, R. H.: The creep of ice shelves: theory, J. Glaciol, 12, 45–53, 1973.

Thompson, D. and Solomon, S.: Interpretation of recent Southern Hemisphere climate change, 2002.

Toggweiler, J. and Samuels, B.: On the ocean's large-scale circulation near the limit of no vertical mixing, Journal of Physical Oceanography, 28, 1832–1852, 1998.

Tomczak, M.: A multi-parameter extension of temperature/salinity diagram techniques for the analysis of non-isopycnal mixing, Progress in Oceanography, 10, 147–171, doi:10.1016/0079-6611(81)90010-0, 1981.

Tomczak, M.: Some historical, theoretical and applied aspects of quantitative water mass analysis, Journal of marine research, 57, 275–303, 1999.

Tomczak, M. and Large, D.: Optimum multiparameter analysis of mixing in the thermocline of the eastern Indian Ocean, Journal of Geophysical Research, 94, 16 141–16, 1989.

Tomczak, M., Large, D. G. B., and Nancarrow, N.: Identification of diapycnal mixing through optimum multiparameter analysis. 1. Test of feasibility and sensitivity, jgr, 99, 25 267–25 274, doi:10.1029/94JC01947, 1994.

Tonelli, M., Wainer, I., and Curchitser, E.: A modelling study of the hydrographic structure of the Ross Sea., Ocean Science Discussions, 9, 2012.

Tréguer, P. and Jacques, G.: Review Dynamics of nutrients and phytoplankton,

and fluxes of carbon, nitrogen and silicon in the Antarctic Ocean, in: Weddell Sea Ecology, pp. 149–162, Springer, 1993.

Trenberth, K. E., Large, W. G., and Olson, J. G.: The mean annual cycle in global ocean wind stress, Journal of Physical Oceanography, 20, 1742–1760, 1990.

Turner, J.: The Melting of Ice in the Arctic Ocean: The Influence of Double-Diffusive Transport of Heat from Below., Journal of Physical Oceanography, 40, 2010.

Turner, J., Colwell, S. R., Marshall, G. J., Lachlan-Cope, T. A., Carleton, A. M., Jones, P. D., Lagun, V., Reid, P. A., and Iagovkina, S.: Antarctic climate change during the last 50 years, International journal of Climatology, 25, 279–294, 2005.

Turner, J., Comiso, J. C., Marshall, G. J., Lachlan-Cope, T. A., Bracegirdle, T., Maksym, T., Meredith, M. P., Wang, Z., and Orr, A.: Non-annular atmospheric circulation change induced by stratospheric ozone depletion and its role in the recent increase of Antarctic sea ice extent, Geophysical Research Letters, 36, 2009.

Van Woert, M. L.: Wintertime dynamics of the Terra Nova Bay polynya, jgr, 104, 7753–7770, doi:10.1029/1999JC900003, 1999.

Venegas, S. A. and Drinkwater, M. R.: Sea ice, atmosphere and upper ocean variability in the Weddell Sea, Antarctica, Journal of Geophysical Research: Oceans (1978–2012), 106, 16 747–16 765, 2001.

Verdy, A., Dutkiewicz, S., Follows, M., Marshall, J., and Czaja, A.: Carbon dioxide and oxygen fluxes in the Southern Ocean: Mechanisms of interannual variability, Global Biogeochemical Cycles, 21, 2007.

Wallace, J. M. and Hobbs, P. V.: Atmosphere science - an introductory survey., 1977.

Whitworth, T. and Nowlin, W. D.: Water masses and currents of the Southern Ocean at the Greenwich Meridian, Journal of Geophysical Research: Oceans (1978–2012), 92, 6462–6476, 1987.

Whitworth III, T.: Zonation and geostrophic flow of the Antarctic Circumpolar Current at Drake Passage, Deep Sea Research Part A. Oceanographic Research Papers, 27, 497–507, 1980.

Whitworth III, T.: Monitoring the transport of the Antarctic circumpolar current at Drake Passage, Journal of Physical Oceanography, 13, 2045–2057, 1983.

Whitworth III, T., Orsi, A., Kim, S., Nowlin Jr, W., and Locarnini, R.: Water masses and mixing near the Antarctic Slope Front, Antarctic Research Series, 75, 1–27, 1998.

Wilchinsky, A. V., Feltham, D. L., and Hopkins, M. A.: Effect of shear rupture on aggregate scale formation in sea ice, Journal of Geophysical Research: Oceans (1978–2012), 115, 2010.

Wilkin, J. and Hedstrom, K.: User's manual for an orthogonal curvilinear grid-generation package, Institute of Marine and Coastal Sciences, Rutgers University http://www. marine. rutgers. edu/po/tools/gridpak/grid_manual. ps. gz, 1998.

Williams, G. D., Bindoff, N. L., Marsland, S. J., and Rintoul, S. R.: Formation and export of dense shelf water from the Adélie Depression, East Antarctica, Journal of Geophysical Research (Oceans), 113, 4039–+, doi:10.1029/2007JC004346, 2008.

Wilson, P. A. and Norris, R. D.: Warm tropical ocean surface and global anoxia during the mid-Cretaceous period, Nature, 412, 425–429, 2001.

Worthington, L.: The water masses of the World Ocean: Some results of a fine-scale census, Evolution of physical oceanography, pp. 42–69, 1981.

Yin, J. H.: A consistent poleward shift of the storm tracks in simulations of 21st century climate, Geophysical Research Letters, 32, 2005.

You, Y. and Tomczak, M.: Thermocline circulation and ventilation in the Indian Ocean derived from water mass analysis, Deep-sea research. Part A. Oceanographic research papers, 40, 13–56, 1993.

Zwally, H. J. and Gloersen, P.: Passive microwave images of the polar regions and research applications, Polar Record, 18, 431–450, 1977.

Zwally, H. J., Comiso, J. C., Parkinson, C. L., Cavalieri, D. J., and Gloersen, P.: Variability of Antarctic sea ice 1979–1998, Journal of Geophysical Research: Oceans (1978–2012), 107, 9–1, 2002.